Witnessing the process of bacterial cell death: novel antimicrobials and their mechanisms of action

Ouyang, X.

Witnessing the Process of Bacterial Cell Death

NOVEL ANTIMICROBIALS AND THEIR MECHANISMS OF ACTION

XUDONG OUYANG

Witnessing the Process of Bacterial Cell Death:

Novel Antimicrobials and Their Mechanisms of Action

Xudong Ouyang

ISBN: 978-94-6423-508-1

Cover: designed by Xudong Ouyang; cover images are micrographs of *Bacillus subtilis* strain 168 taken by Xudong Ouyang

Lay-out by Xudong Ouyang
Printed by ProefschriftMaken

Witnessing the Process of Bacterial Cell Death:

Novel Antimicrobials and Their Mechanisms of Action

Het verloop van bacteriële celdood waarnemen:
Nieuwe antimicrobiële middelen en hun werkingsmechanismen

proefschrift

ter verkrijging van
de graad van doctor aan de Universiteit Leiden,
op gezag van rector magnificus prof.dr.ir. H. Bijl,
volgens besluit van het college voor promoties
te verdedigen op 23 november 2021
klokke 15.00 uur

door

Xudong Ouyang
geboren te Jinan, China
in 1991

Promotores:

Prof. Dr. J. den Hertog

Prof. Dr. H.P. Spaink

Promotiecommissie:

Prof. Dr. G.P. van Wezel

Prof. Dr. N.I. Martin

Prof. Dr. D. Claessen

Prof. Dr. L.W. Hamoen — University of Amsterdam, Amsterdam, the Netherlands

Prof. Dr. S.H.M. Rooijakkers — University Medical Center Utrecht, Utrecht, the Netherlands

Printing of this thesis was (partly) financially supported by the Netherlands Society of Medical Microbiology (NVMM) and the Royal Netherlands Society for Microbiology (KNVM)

Table of Contents

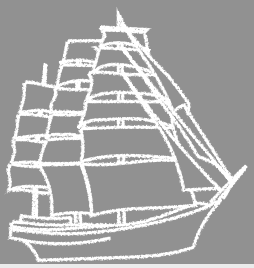

General Introduction

CHAPTER 1

Xudong Ouyang[1,2] and Jeroen den Hertog[1,2]

1. Hubrecht Institute-KNAW and University Medical Center Utrecht,
Utrecht, the Netherlands
2. Institute Biology Leiden, Leiden University,
Leiden, the Netherlands

ANTIMICROBIAL DISCOVERY

Antimicrobial resistance

The average life expectancy was around 47 years in the pre-antibiotic era, partly due to the high mortality as a result of infectious diseases [1]. The discovery of penicillin in 1928 has written a new chapter in the book of medicine and was marked as the beginning of the antibiotic era [2]. The worldwide use of penicillin started in the year 1945, since when antimicrobials have been essential drugs to modern healthcare. After penicillin, many more antimicrobials were discovered, especially between the 1950s and 1970s. In this period, more than half of the antibiotic classes in use today was isolated; therefore, it was named "the golden era" in antibiotic discovery [3,4]. As a result, the leading medical reason causing death has shifted from infectious diseases to non-infectious diseases such as cancer and stroke, and the average life expectancy has risen [1]. In addition, the application of antimicrobials is expanded, from only for treating bacterial infections, to a large variety of uses such as protecting patients with compromised immune systems or cancers, and even to preventing infections in agriculture and livestock.

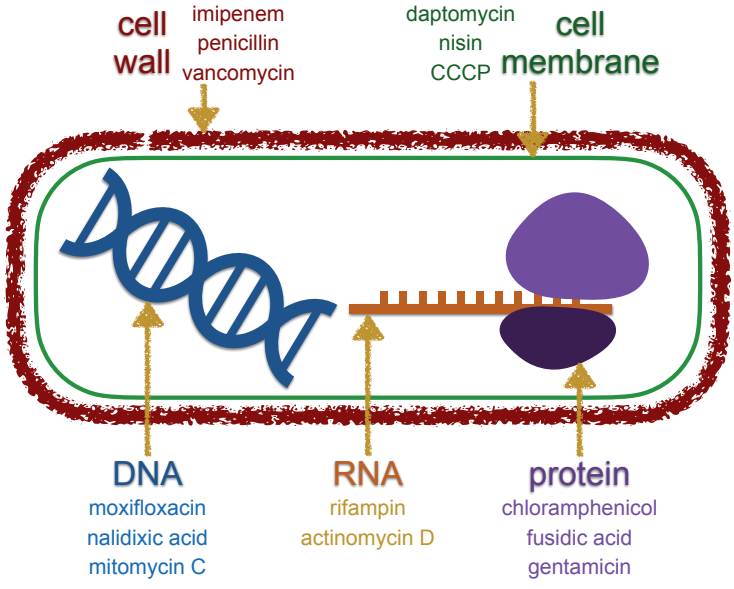

Fig. 1. Most common classes of antimicrobials. Antimicrobials can be classified based on their target. Examples of antimicrobials of each class are listed.

Nevertheless, with the abuse of antimicrobials, an issue has developed, which is antimicrobial resistance [5–7]. Actually, the emergence of antimicrobial resistance is due to the natural evolutionary response of bacterial strains to antimicrobials that are naturally produced by microorganisms. For example, in 1940, an *Escherichia coli* strain was reported to produce penicillinase, which inactivates penicillin [8]. This was even one year before the clinical use of penicillin [9]. However, large scale applications of antimicrobials in health care and agriculture have driven bacterial selection, resulting in spreading of antimicrobial resistance into human society [10]. Despite the discovery of a variety of antimicrobial classes with different targets (Fig. 1), no antimicrobial could avoid development of resistance against it in hospitals. Fig. 2 exhibits a timeline for some antimicrobials, depicting the year of their first clinical application and the year when resistance was identified. Because of the emerging antimicrobial resistance issue, bacterial infections have become a serious threat again, requiring a more complicated therapy to be cured [11]. The resistant bacteria, especially the multidrug resistant "superbugs", have led to higher patient mortality and rising costs [12,13]. Therefore, we are in a strong need for new antimicrobials with novel mechanism of action (MoA) to combat the continuously emerging antimicrobial resistance.

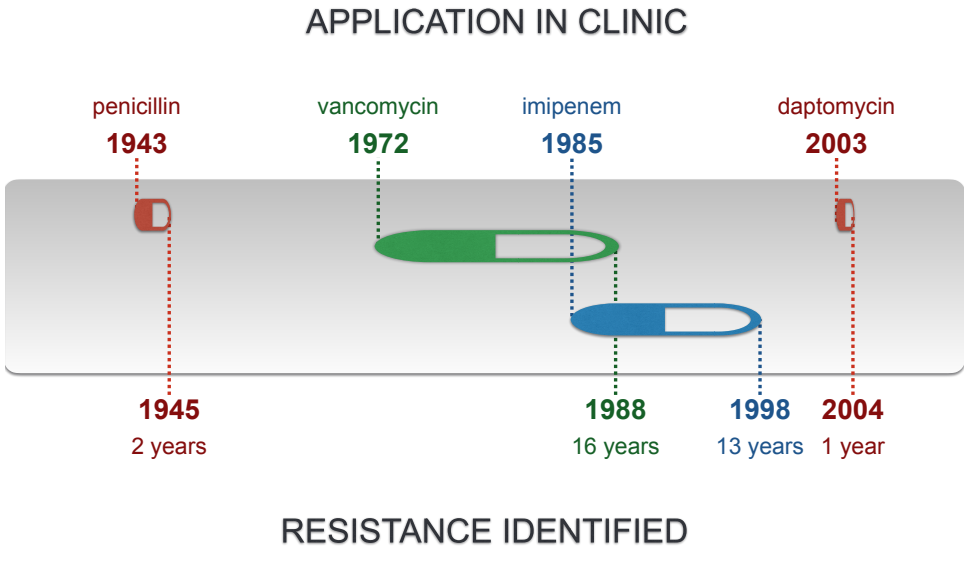

Fig. 2. Antimicrobial usage and resistance. The timeline of antimicrobials is depicted, indicating when they were first used in the clinic and when resistance was identified. Four examples of antimicrobials are shown.

Fungal natural products

To compete with other species or to survive a harsh environment, organisms have good reasons to produce functional compounds, otherwise known as natural products [14]. These compounds have played important roles in medical application through history, and will undoubtedly continue to open up the unknown medical spaces and provide pharmacological benefits [15,16], especially in the field of antimicrobial drug discovery and development [17]. In the Food and Drug Administration (FDA) of the U.S., approximately 59% approved antimicrobials were derived from nature [18], and natural products from microbial origin are privileged in this sphere [17]. The kingdom of fungi contains countless and diverse fungal species, which produce a large variety of bio-active compounds as secondary metabolites [19]. These metabolites are not essential for the growth of fungi, and are different from the metabolites of the primary metabolic pathways [20]. In general, secondary metabolites are small bioactive compounds that are produced at specific stages of fungal growth to alter fungal development or communicate with their environment [21,22]. One example is melanin, a special pigment found in most organisms, including fungi. It provides fungi the ability to defend against environmental stresses like ultraviolet light or oxidizing agents [23]. Another example is variegatic acid, which is a pigment from the rot fungus *Serpula lacrymans* that is induced by bacterial encounters. It has the function to inhibit the biofilm formation of *Bacillus subtilis* [24]. Fungal natural product research is aimed at transferring the natural ecological functions of secondary metabolites to medical application for the benefit of human society.

Fungal natural products have been effectively used in Chinese medicine through the ages, without knowing the identity of the compounds themselves. The study of fungal natural products as we know it, started in 1922 by Harold Raistrick and bloomed after the successful discovery of penicillin. Since then, it has led to the identification of thousands of metabolites containing antimicrobial, antifungal or antitumor activities [19,25]. However, in spite of the successful application of β-lactams in the clinic, which accounts for up to 60% of all clinical antimicrobials, fungal natural products are not the main source of compounds in the antimicrobial discovery process [17]. Instead, actinomycetes and bacteria are the main source of newly identified compounds with antimicrobial activity. Nevertheless, genomic approaches have identified several gene clusters encoding biosynthetic enzymes producing natural products per fungal genome, just like actinomycetes, suggesting that fungal natural products are an excellent source of compounds for the antimicrobial discovery field [17].

GRAM-POSITIVE BACTERIA

Gram-positive pathogens

Traditionally, the first procedure to identify an unknown bacterial strain is to perform Gram-staining and evaluate using a microscope. This approach generates the first-sight information of a bacterium: cell size, cell shape and the distinction between Gram-positive bacteria or Gram-negative bacteria [26]. The name of the Gram-staining comes from Hans Christian Gram, a Danish bacteriologist who found that some bacterial cells are not able to achieve decolorization of gentian violet, later known as Gram-positive bacteria [27]. These have a thick peptidoglycan cell wall topped by teichoic acid and lipoteichoic acid as the outside of their cell envelope, together with a single cytoplasmic membrane [27,28]. Their thick peptidoglycan cell wall retains the violet stain. Gram-negative bacteria have a thin peptidoglycan layer as their cell wall, in between the cytoplasmic membrane and the outer membrane [27,28]. It is easier to decolorize the violet stain from the thin peptidoglycan layer. The different cell envelopes between Gram-positive and Gram-negative bacteria are visualized in Fig. 3.

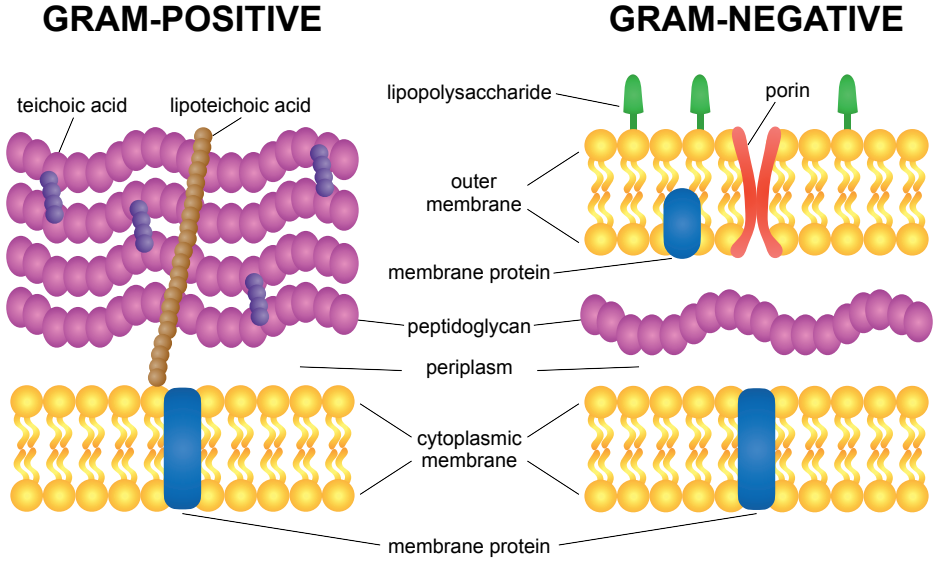

Fig. 3. The most striking difference between Gram-positive and Gram-negative bacteria is the presence of an outer membrane in the cell envelope. The structure of a fraction of the cell envelope of Gram-positive and Gram-negative bacteria is shown.

There are pathogenic bacteria among both the Gram-positive and Gram-negative bacteria. With the development of antimicrobial resistance, multidrug resistant Gram-positive pathogens have become one of the major therapeutic challenges [29]. Three Gram-positive strains were present on the list of global priority pathogens by the World Health Organization (WHO) in 2017: vancomycin-resistant *Enterococcus faecium* (VRE), Methicillin-resistant *Staphylococcus aureus* (MRSA) and penicillin-non-susceptible *Streptococcus pneumonia* [30]. These bacteria cause both community-acquired infections and healthcare-associated infections, forming serious clinical problems. The mechanism underlying resistance is generally acquisition of the ability to degrade antimicrobials, modification of the antimicrobial targets, or overexpression of efflux pumps [31]. For example, *S. aureus* is one of the major human pathogens, which was initially treated with penicillin. Only a few years after the clinical use of penicillin, a penicillin-resistant *S. aureus* strain emerged, which produced a plasmid-encoded penicillinase [32]. Later, a more dangerous methicillin-resistant strain, MRSA, was identified to produce an additional penicillin binding protein PBP2a, which has a reduced affinity to almost all β-lactam antimicrobials [33] and allows bacteria to grow in the presence of these antimicrobials. The outbreaks of MRSA have led to severe problems both in healthcare systems and communities. Another example is VRE that acquired vancomycin-resistance gene clusters through transposons, resulting in the replacement of D-alanyl-D-alanine with D-alanyl-D-lactate termini in the cell wall to lower the binding affinity of vancomycin [29]. Several attempts have been made to deal with multidrug resistant pathogens by modification of existing antimicrobials, but with little success [31]. Searching for innovative antimicrobial classes with novel targets or even antibiotic alternatives, like bacteriophages and probiotics, holds more promise for the future.

Bacillus subtilis

B. subtilis is a strain of rod-shaped Gram-positive bacteria, with cells that are 4–10 μm long and 0.25–1.0 μm in diameter. It is ubiquitous in nature with large habitats, ranging from soil to aquatic environments [34] and therefore is also simple to be cultured in the lab. Hence, *B. subtilis* is the model of choice for many labs studying Gram-positive bacteria, especially the *B. subtilis* strain 168. When culturing this strain, the addition of tryptophan is essential even if the medium contains acid-hydrolyzed proteins, because this strain is a tryptophan auxotroph (trpC2) [35]. Upon nutrient limitation, *B. subtilis* enters the self-protective process of sporulation. Actually, only a portion (typically 10%) of the population differentiates into

endospores. The rest of the cells use a bet-hedging strategy to lyse themselves and provide nutrients for sporulation [36,37]. Unlike the pathogenic organism *Bacillus anthracis* [38], *B. subtilis* is a Generally Regarded as Safe (GRAS) strain by FDA, and thus is used in a wide range of biotechnology industries, including food and medicine [39]. The popularity in bioindustries has helped this strain to attract attention in the studies of physiology and genetics.

The *B. subtilis* genome was sequenced more than two decades ago [40]. The accumulation of detailed knowledge at the level of DNA has generated a library of gene functions. In addition, with the development of transcriptomics and proteomics, the profiles of gene expression in *B. subtilis* have put another dimension to this important strain [39]. All the benefits suggest *B. subtilis* to be a highly amenable model for studying the antimicrobial MoA [41].

SCOPE OF THIS THESIS

The work described in this thesis aims to search for new classes of antimicrobials that interfere with novel cellular targets of Gram-positive bacteria. The den Hertog lab at the Hubrecht Institute has a library of fungal secondary metabolites from 10,207 strains of fungi. This library was successfully applied to screen for novel bioactive compounds using a zebrafish model [42]. Here, we used this library as a source to screen for novel antimicrobials. To this end, we screened and identified the antimicrobial activity using a working pipeline containing library screening, fungal culture optimization, activity purification and compound identification. Finally, we successfully identified several compounds with antimicrobial activity. Next, to further assess the antimicrobial property of the identified compounds, we developed a novel MoA identification strategy named Dynamic Bacterial Cytological Profiling (DBCP). This strategy distinguished antimicrobials from different classes using time-lapse imaging, and was used to determine the MoA of a poorly studied antimicrobial, harzianic acid (HA). In addition, we further described the MoAs of two promising antimicrobials, Berkchaetoazaphilone B (BAB) and HA. We provide evidence that BAB might affect energy metabolism. HA was found to be a multi-targeting antimicrobial that generated pores in the cell membrane when used at high concentration.

OUTLINE OF THIS THESIS

Chapter 2 provides a review of the advances in MoA identification strategies that were commonly used over the years. We first focused on some classic approaches that were established several decades ago and are still in use today with the implementation of novel techniques. Then we discussed the modern approaches that bring high hopes to the antimicrobial field, including omics approaches and imaging-based strategies.

Chapter 3 describes the strategy we used to screen fungal natural antimicrobial compounds. We screened for antimicrobial activity using a fungal secondary metabolites library against seven pathogenic bacteria and tried to identify the active compounds using ethyl acetate extraction, HPLC fractionation together with chemical analysis. The identified metabolites consist of both known antimicrobial compounds as well as relatively unexplored compounds. We also studied the antimicrobial property of BAB, an anti-cancer compound identified in 2015 [43], which was identified to contain antimicrobial activity in this screen.

Chapter 4 describes a novel strategy of antimicrobial MoA identification. An important bottleneck in antimicrobial discovery is the time-consuming analysis of the antimicrobial working mechanism. To facilitate breaking the bottleneck, we tried to develop a method to rapidly distinguish the effect of anti-Gram-positive bacterial compounds from different classes. To achieve this, we developed a novel imaging strategy using time-lapse imaging to record dynamic bacterial cytological changes. We improved the imaging protocol to make it simple and functional for bacterial long-term imaging. Using this method, dubbed DBCP, we observed bacteria over time and established fluorescence intensities qualitatively and quantitatively. It allowed to rapidly distinguish antimicrobials from all of the five main classes. Finally, we used DBCP to establish the MoA of HA, a poorly described secondary metabolite purified from the fungal culture of *Oidiodendron flavum*. Taken together, DBCP is proven to be an excellent tool for the first approach of antimicrobial MoA classification.

Chapter 5 unravels details about the antimicrobial MoA of HA. HA was first isolated as a novel antimicrobial agent from a fungal strain *Trichoderma harzianum* in 1994 [44], but not much data is available regarding its antimicrobial activity yet. In **Chapter 4**, we predicted HA to target the cell envelope using DBCP. Here, we applied several assays to confirm this prediction. In addition, we isolated HA-resistant bacteria and identified four mutated genes, which provides further insight into its MoA.

Chapter 6 summarizes the discussions of the thesis with future perspectives. We have provided a pipeline of antimicrobial discovery with detailed strategies from the upstream of screening fungal natural products to the downstream of MoA identification. Hopefully it will contribute some new insights into antimicrobial research.

REFERENCES

[1] WA A. The Treasure Called Antibiotics. Ann Ibadan Postgrad Med 2016;14:56–7.

[2] Stone MRL, Butler MS, Phetsang W, Cooper MA, Blaskovich MAT. Fluorescent Antibiotics: New Research Tools to Fight Antibiotic Resistance. Trends Biotechnol 2018;36:523–36. https://doi.org/10.1016/j.tibtech.2018.01.004.

[3] Aminov RI. A brief history of the antibiotic era: Lessons learned and challenges for the future. Front Microbiol 2010;1:1–7. https://doi.org/10.3389/fmicb.2010.00134.

[4] Marston HD, Dixon DM, Knisely JM, Palmore TN, Fauci AS. Antimicrobial resistance. JAMA - J Am Med Assoc 2016;316:1193–204. https://doi.org/10.1001/jama.2016.11764.

[5] Dcosta VM, King CE, Kalan L, Morar M, Sung WWL, Schwarz C, et al. Antibiotic resistance is ancient. Nature 2011;477:457–61. https://doi.org/10.1038/nature10388.

[6] Ling LL, Schneider T, Peoples AJ, Spoering AL, Engels I, Conlon BP, et al. A new antibiotic kills pathogens without detectable resistance. Nature 2015;517:455–9. https://doi.org/10.1038/nature14098.

[7] Park AJ, Krieger JR, Khursigara CM. Survival proteomes: The emerging proteotype of antimicrobial resistance. FEMS Microbiol Rev 2016;40w:323–42. https://doi.org/10.1093/femsre/fuv051.

[8] Abraham EP, Chain E. An Enzyme from Bacteria able to. Nature 1940;146:837.

[9] Lobanovska M, Pilla G. Penicillin's discovery and antibiotic resistance: Lessons for the future? Yale J Biol Med 2017;90:135–45.

[10] Holmes AH, Moore LSP, Sundsfjord A, Steinbakk M, Regmi S, Karkey A, et al. Understanding the mechanisms and drivers of antimicrobial resistance. Lancet 2016;387:176–87. https://doi.org/10.1016/S0140-6736(15)00473-0.

[11] Hancock REW. Mechanisms of action of newer antibiotics for Gram-positive pathogens. Lancet Infect Dis 2005;5:209–18. https://doi.org/10.1016/S1473-3099(05)70051-7.

[12] Gelband H, Miller-Petrie M, Pant S, Gandra S, Levinson J, Barter D, et al. The state of the world's antibiotics 2015. Wound Heal South Africa 2015;8:30–4.

[13] Butler MS, Buss AD. Natural products - The future scaffolds for novel antibiotics? Biochem Pharmacol 2006;71:919–29. https://doi.org/10.1016/j.bcp.2005.10.012.

[14] Bajaj S, Ong ST, Chandy KG. Contributions of natural products to ion channel pharmacology. Nat Prod Rep 2020;37:703–16. https://doi.org/10.1039/c9np00056a.

[15] Nishimura S, Matsumori N. Chemical diversity and mode of action of natural products targeting lipids in the eukaryotic cell membrane. Nat Prod Rep 2020;37:677–702. https://doi.org/10.1039/c9np00059c.

[16] Harvey AL, Edrada-Ebel R, Quinn RJ. The re-emergence of natural products for drug discovery in the genomics era. Nat Rev Drug Discov 2015;14:111–29. https://doi.org/10.1038/nrd4510.

[17] Wright GD. Opportunities for natural products in 21st century antibiotic discovery. Nat Prod Rep 2017;34:694–701. https://doi.org/10.1039/c7np00019g.

[18] Zhang DD, Chapman E. The role of natural products in revealing NRF2 function. Nat Prod Rep 2020;37:797–826. https://doi.org/10.1039/c9np00061e.

[19] Keller NP, Turner G, Bennett JW. Fungal secondary metabolism - From biochemistry to genomics.

Nat Rev Microbiol 2005;3:937–47. https://doi.org/10.1038/nrmicro1286.

[20] Bennett JW, Bentley R. What's in a Name?-Microbial Secondary Metabolism. Adv Appl Microbiol 1989;34:1–28. https://doi.org/10.1016/S0065-2164(08)70316-2.

[21] Brakhage AA. Regulation of fungal secondary metabolism. Nat Rev Microbiol 2013;11:21–32. https://doi.org/10.1038/nrmicro2916.

[22] Keller NP. Fungal secondary metabolism: regulation, function and drug discovery. Nat Rev Microbiol 2019;17:167–80. https://doi.org/10.1038/s41579-018-0121-1.

[23] Eisenman HC, Casadevall A. Synthesis and assembly of fungal melanin. Appl Microbiol Biotechnol 2012;93:931–40. https://doi.org/10.1007/s00253-011-3777-2.

[24] Tauber JP, Gallegos-Monterrosa R, Kovács ÁT, Shelest E, Hoffmeister D. Dissimilar pigment regulation in Serpula lacrymans and Paxillus involutus during inter-kingdom interactions. Microbiol (United Kingdom) 2018;164:65–77. https://doi.org/10.1099/mic.0.000582.

[25] RAISTRICK H. A region of biosynthesis. Proc R Soc Lond B Biol Sci 1950;136. https://doi.org/10.1142/9789812795984_0035.

[26] Gregersen T. Rapid method for distinction of gram-negative from gram-positive bacteria. vol. 5. 1978. https://doi.org/10.1007/BF00498806.

[27] Megrian D, Taib N, Witwinowski J, Beloin C, Gribaldo S. One or two membranes? Diderm Firmicutes challenge the Gram-positive/Gram-negative divide. Mol Microbiol 2020;113:659–71. https://doi.org/10.1111/mmi.14469.

[28] Cremin K, Jones BA, Teahan J, Meloni GN, Perry D, Zerfass C, et al. Scanning Ion Conductance Microscopy Reveals Differences in the Ionic Environments of Gram-Positive and Negative Bacteria. Anal Chem 2020;92:16024–32. https://doi.org/10.1021/acs.analchem.0c03653.

[29] Cornaglia G. Fighting infections due to multidrug-resistant Gram-positive pathogens. Clin Microbiol Infect 2009;15:209–11. https://doi.org/10.1111/j.1469-0691.2009.02737.x.

[30] Tacconelli E, Magrini N. Global priority list of antibiotic-resistant bacteria to guide research, discovery, and development of new antibiotics. 2017.

[31] Jubeh B, Breijyeh Z, Karaman R. Resistance of gram-positive bacteria to current antibacterial agents and overcoming approaches. Molecules 2020;25:2888. https://doi.org/10.3390/molecules25122888.

[32] Chambers HF, DeLeo FR. Waves of resistance: Staphylococcus aureus in the antibiotic era. Nat Rev Microbiol 2009;7:629–41. https://doi.org/10.1038/nrmicro2200.

[33] Dweba CC, Zishiri OT, El Zowalaty ME. Methicillin-resistant staphylococcus aureus: Livestock-associated, antimicrobial, and heavy metal resistance. Infect Drug Resist 2018;11:2497–509. https://doi.org/10.2147/IDR.S175967.

[34] Harwood CR, Pohl S, Smith W, Wipat A. Bacillus subtilis. Model Gram-Positive Synthetic Biology Chassis. Methods Microbiol., vol. 40, Academic Press Inc.; 2013, p. 87–117. https://doi.org/10.1016/B978-0-12-417029-2.00004-2.

[35] Zeigler DR, Prágai Z, Rodriguez S, Chevreux B, Muffler A, Albert T, et al. The origins of 168, W23, and other Bacillus subtilis legacy strains. J Bacteriol 2008;190:6983–95. https://doi.org/10.1128/JB.00722-08.

[36] Veening JW, Stewart EJ, Berngruber TW, Taddei F, Kuipers OP, Hamoen LW. Bet-hedging and epigenetic inheritance in bacterial cell development. vol. 105. 2008. https://doi.org/10.1073/

pnas.0700463105.

[37] González-Pastor JE, Hobbs EC, Losick R. Cannibalism by sporulating bacteria. vol. 301. 2003. https://doi.org/10.1126/science.1086462.

[38] Rasko DA, Altherr MR, Han CS, Ravel J. Genomics of the Bacillus cereus group of organisms. FEMS Microbiol Rev 2005;29:303–29. https://doi.org/10.1016/j.femsre.2004.12.005.

[39] Martinez RM. Bacillus subtilis. vol. 1. Elsevier Inc.; 2013. https://doi.org/10.1016/B978-0-12-374984-0.00125-X.

[40] Kocabaş P, Çalik P, Çalik G, Özdamar TH. Microarray studies in Bacillus subtilis. Biotechnol J 2009;4:1012–27. https://doi.org/10.1002/biot.200800330.

[41] Van Duy N, Mäder U, Tran NP, Cavin JF, Tam LT, Albrecht D, et al. The proteome and transcriptome analysis of Bacillus subtilis in response to salicylic acid. Proteomics 2007;7:698–710. https://doi.org/10.1002/pmic.200600706.

[42] Hoeksma J, Misset T, Wever C, Kemmink J, Kruijtzer J, Versluis K, et al. A new perspective on fungal metabolites: identification of bioactive compounds from fungi using zebrafish embryogenesis as read-out. Sci Rep 2019;9:1–16. https://doi.org/10.1038/s41598-019-54127-9.

[43] Stierle AA, Stierle DB, Girtsman T, Mou TC, Antczak C, Djaballah H. Azaphilones from an Acid Mine Extremophile Strain of a Pleurostomophora sp. J Nat Prod 2015;78:2917–23. https://doi.org/10.1021/acs.jnatprod.5b00519.

[44] Sawa R, Mori Y, Iinuma H, Naganawa H, Hamada M, Yoshida S, et al. Harzianic acid, a new antimicrobial antibiotic from a fungus. J Antibiot (Tokyo) 1994;47:731–2. https://doi.org/10.7164/antibiotics.47.731.

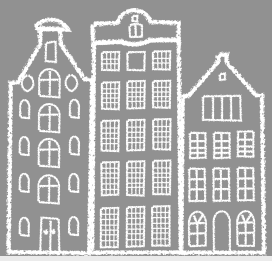

Strategies for Identification of the Mechanism of Action of Antimicrobial Agents

CHAPTER 2

Xudong Ouyang[1,2] and Jeroen den Hertog[1,2]

1. Hubrecht Institute-KNAW and University Medical Center Utrecht, Utrecht, the Netherlands
2. Institute Biology Leiden, Leiden University, Leiden, the Netherlands

ABSTRACT

Identification of the mechanism of action (MoA) of an antimicrobial agent is one of the vital parts in antimicrobial discovery and development, because MoA provides information about the biochemical process through which an antimicrobial produces its pharmacological effect on bacteria. However, the MoA identification process is tedious and has become one of the bottlenecks in antimicrobial discovery. Here, we provide an overview of the strategies that were developed successfully over the years. This overview describes both classic approaches, which were established several decades ago but have been renovated using the advances of novel techniques, and modern approaches, which were developed recently taking advantage of high-tech solutions. This review will provide insight into the selection of MoA identification strategies, valuable for antimicrobial research.

INTRODUCTION

Antimicrobial agents kill bacteria or inhibit bacterial growth and thus antagonize bacterial infections, which has a huge impact on human health and animal welfare. The mechanism of action (MoA) of antimicrobial agents describes the biochemical process through which an antimicrobial produces its pharmacological effect on bacteria [1]. An antimicrobial agent may achieve its effects on inhibition of any of the macromolecular synthesis pathways, or destruction of the sub-cellular structures. To elucidate the MoA of an antimicrobial agent is one of the vital parts in antimicrobial discovery and development [2,3]. Nowadays, MoA information of a drug has become more important than ever. As a consequence of increasing cases of antimicrobial resistance, development of alternative anti-infective therapies, such as the combination of different antimicrobials, is important for saving human lives. These therapies require more accurate elucidation of the interaction between antimicrobials and microbes. Therefore, understanding antimicrobial MoA is fundamental to optimize patient care, including antimicrobial selection, infection control and resistance prevention [4]. However, the target candidates in bacterial cells are very broad, including not only proteins, but also DNA and lipids. Whereas many new MoA identification strategies have been discovered by development of new techniques, the process of identifying antimicrobial targets remains complex and laborious [3], which makes it a bottleneck in the discovery of novel antimicrobial agents, including those from nature products.

Natural products have played important roles in yielding compounds with novel structures and novel bio-activities [5]. They are impacting the world by their unique chemical and biological properties that were gained by evolutionary processes to survive in harsh environments and would not be simply achieved using synthetic chemistry. Approximately two-thirds of the antimicrobials in clinical application are derived from natural products [6]. However, over the last few decades, the natural product antimicrobial research has attracted less attention at many pharmaceutical companies, due to the low yield of useful compounds [7]. Despite remarkable achievements in the discovery of active natural product antimicrobials, the procedure of turning these compounds into clinical application is relatively time-consuming. For a significant part, this can be attributed to the difficulty in identification of the MoA of natural products [8]. Unfortunately, there is no universal method that will accurately facilitate identification of the MoA of all antimicrobials. Thus, it is essential to select an approach or to combine multiple approaches for a faster and more accurate MoA identification.

The purpose of this review is to provide some insight into MoA identification with an overview of both traditional and modern strategies that were developed successfully over the past 20 years. We will first focus on some classic approaches that were established several decades ago but are still in use today. Some of the old methods are renovated using the advances of novel techniques. Next, we will review modern omics approaches, which are considered as the "high hopes" in the field of antimicrobial discovery [9]. Finally, we will discuss some novel imaging-based strategies, which were initially developed for eukaryotic cells, and then developed further for bacterial cells. This review will not include all MoA identification strategies available in the antimicrobial research area, but rather provides a first peek into the realm of MoA identification strategies.

CLASSIC APPROACHES

In order to determine the targets of specific antimicrobial agents, several classic strategies are available, including target-based screenings, in which the direct interaction between the antimicrobial agent and its target is expected to be assessed, and phenotype-based screenings, where the pathway that an antimicrobial agent affects is explored by phenotypic read-out [3]. In the following section, we will discuss three kinds of widely used classic approaches: macromolecular synthesis (MMS) assays, genetic approaches and affinity approaches.

MMS assays

An important way to determine the pathway of inhibition is to measure the effect of test compounds on MMS. These types of assays are indirect approaches that have been applied for almost 50 years [10]. MMS assays monitor the incorporation of radiolabeled tracers of the major biosynthetic pathways. Inhibition of DNA, RNA, protein, and cell wall synthesis will lead to a lower incorporation of radio-activity at a certain time of incubation (Fig. 1) [11–13]. Originally, MMS assays were laborious with large volumes of culture, trichloroacetic acid (TCA) precipitation, followed by washing and drying steps [13]. In addition, the incubation time with radiolabeled tracers sometimes had to be long (1-2 h) to be detected, and this could affect more than one pathway and thus confound the results [14]. If performed properly, the results of MMS still are informative. For example, Crumplin and Smith tried to identify the MoA of nalidixic acid using MMS approaches in 1975 [13]. Initially, all the tested pathways including DNA, RNA and protein synthesis were affected, although

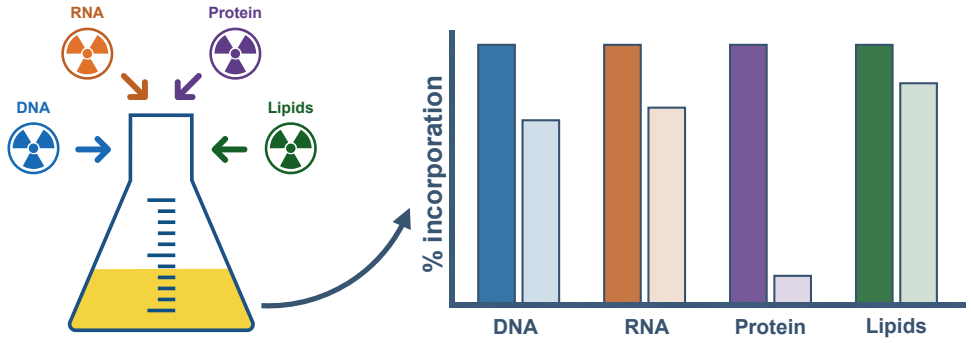

Fig. 1. Schematic representation of MMS assay. This assay monitors the incorporation of radiolabeled tracers of the major biosynthetic pathways. Inhibition of DNA, RNA, protein, or lipid synthesis will lead to a lower incorporation of radio-activity.

to a different extent. Afterwards, they adjusted the concentration of nalidixic acid to lower levels and performed these assays on different bacterial strains, and finally identified DNA synthesis to be the initial target. However, they also assumed RNA synthesis to be a secondary target, which was not proven in later studies [15,16]. Yet, their research still provides valuable information about the MoA of nalidixic acid.

Over the years, improvements have been achieved to shorten the period of incubation and increase the throughput. Cunningham et al. successfully developed a modified MMS assay in microplate format with shorter duration by optimizing the bacterial growth rates and precursor concentrations, and establishing simultaneous determination of all the pathways in adequate signal-to-noise ratios [10]. The modified assay is completed within half the bacterial generation time and therefore limits unexpected changes and facilitates the assessment of almost 100 compounds per week against four pathways.

Whereas MMS assays are informative and widely used in antimicrobial research, they have drawbacks. For antimicrobials that specifically target one of the MMS pathways, incorporation of radiolabeled tracers will provide direct information about the inhibition of that specific pathway [17,18]. However, if a nonspecific mechanism of inhibition occurs, like for instance in the case of nisin, all pathways are inhibited within a narrow concentration range, making it difficult to distinguish between them. In addition, for an antimicrobial with novel MoA, MMS assays may also fail to generate useful information [7]. Nevertheless, despite all these disadvantages, MMS assays are still considered to be a good prediction tool at an early stage of research. For example, at the start stage of the analysis of the MoA of daptomycin,

MMS assays successfully suggested a cell wall defect. A strong disruption of cell wall synthesis was observed, whereas less effects were evident on the synthesis of DNA, RNA, and protein [18]. Together with a series of subsequent assays including 2D SDS/PAGE, membrane property and protein delocalization measurements, Müller et al. have added new perspective onto the interaction between daptomycin and the cell envelope.

Genetic approaches

Genetic approaches are direct approaches to identify antimicrobial targets. Normally, genetic approaches are being used to confirm or reject hypotheses of the MoA, which are based on prior information. One of the approaches is to regulate the expression level of the candidate target protein (Fig. 2). Overexpression of a target gene may lead to drug-resistance and may be achieved using an inducible promoter [19]. The overexpressed putative target protein may bind the antimicrobial agent, and therefore lower its working concentration, resulting in increased tolerance to that antimicrobial. However, whereas the overexpressed protein may interact with the antimicrobial, it is not definitive proof that this causes growth inhibition [8]. For instance, overproduction of efflux pumps may lead to resistance to a large variety of unrelated antimicrobials, but these are certainly not the targets of these antimicrobials [20]. Downregulation of the putative target may sensitize the bacteria to an inhibitor, providing evidence that the gene is involved in the antibacterial activity of the compound. To downregulate gene expression, one method is to upregulate the production of antisense RNA, which may reduce target protein expression [21]. However, interpretation of these experiments is often challenging. If multiple genes/proteins act in parallel, inactivation of each of these may sensitize the other proteins, which leads to the identification of multiple targets including potential false positive hits. For example, β-lactam antibiotics specifically target PBPs. It has been reported that if peptidoglycan biosynthesis proteins other than PBPs are under-expressed, bacteria may also become sensitive to β-lactam antibiotics [22]. This may provide evidence for the function of β-lactam antibiotics to affect cell wall synthesis. Interestingly, genetic downregulation of the target protein sometimes may reduce the sensitivity. In a study of quinolones, it was suggested that decreased expression of one of their targets, topoisomerase IV, generates low-level quinolone resistance [23]. This is due to the reduced amount of quinolone-topoisomerase complex, which is the real “poison” that inhibits bacterial growth. In those cases, further work is required to elucidate the MoA.

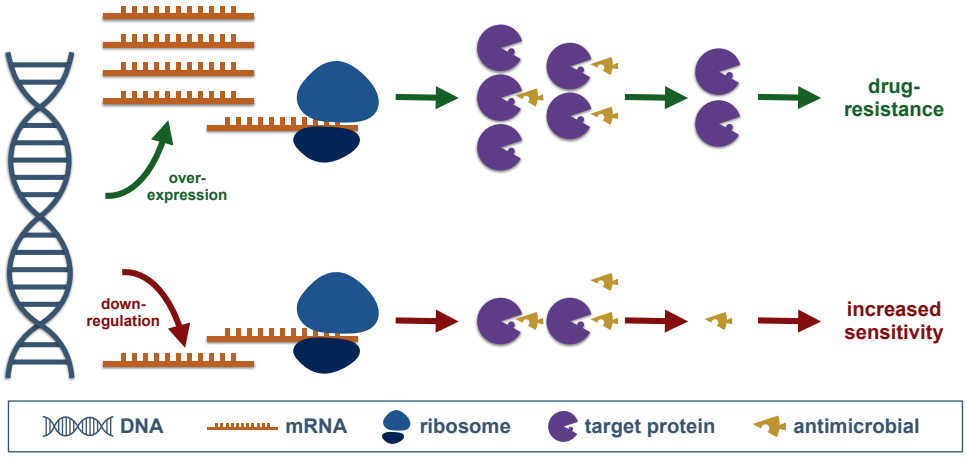

Fig. 2. Schematic representation of genetic approaches. Overexpression of putative target protein may bind the antimicrobial agent, and therefore lower its working concentration, resulting in increased resistance to that antimicrobial. In contrast, downregulation of the putative target may sensitize the bacteria to an inhibitor, providing evidence that the gene is involved in the antibacterial activity of the compound.

Whereas most genetic approaches are considered to be verifying prior hypotheses, there are also genetic approaches that are applied for initial screening. These make use of a mutant library of bacteria with a panel of inactivated genes. A drawback is that only non-essential genes are inactivated in these libraries and hence this approach is not feasible for antimicrobials targeting essential genes. By using higher or lower concentrations of an antimicrobial, more resistant or more sensitive strains are selected from the mutant library. Studying the gene functions of these hits will generate a first impression of the antimicrobial mechanism. An example of a *Staphylococcus aureus* mutant library is the Nebraska Transposon Mutant Library (NTML), which consists of 1,920 unique transposon mutants with inactivated non-essential genes [24]. In a recent study, low concentrations of oxacillin were tested against the NTML to search for mutants with increased susceptibility, which led to identification of *mecA* as one of the hits. The *mecA* gene encodes the alternative penicillin binding protein 2a (PBP2a), which is in line with oxacillin's MoA of binding to penicillin-binding proteins (PBPs) [25]. In the same study of oxacillin [25], daptomycin failed to provide any informative hits. The development of CRISPR or antisense RNA may complement the use of mutant libraries. Instead of complete gene inactivation by knock-out, the use of CRISPR technology or antisense RNA to

knockdown essential genes may facilitate investigation of essential gene functions [21,26], and thus benefits the antimicrobial research area.

Another genetic approach is to select drug resistant colonies by growing bacteria in antimicrobial agents for a long time. Identification of mutated genes that cause resistance in bacteria may provide insight into the underlying mechanism. Whereas evolving drug resistant colonies is not very complicated in the lab, traditionally, the identification of mutations in resistant colonies was time-consuming. However, due to the development of next-generation sequencing, the task of mapping resistant mutations became rapid and affordable [27]. Although there are several traits to develop bacterial resistance to a drug, and some of them may not be associated with the drug's MoA, this method has proven powerful for a variety of well-known antimicrobials [7].

Overall, genetic approaches are useful tools for identification of antimicrobial targets, but they also have limitations. If an antimicrobial binds to DNA or lipids, which are also proven targets for compounds [3,28], genetic approaches might be invalid. Whereas genetic approaches alone might not be definitive in demonstrating antimicrobial MoA, they definitely help to provide insight into the targets of antimicrobial agents.

Affinity approaches

Affinity chromatography is another direct approach with a rather simple workflow (Fig. 3). Traditionally, the tested antimicrobial is immobilized onto a solid matrix and then exposed to bacterial cell lysates. After multiple washing steps to remove non-binding proteins, the matrix-bound proteins are eluted for identity analysis using N-terminal amino acid sequencing [29,30]. An alternative approach for affinity binding is to attach the tested antimicrobial covalently to a cell-permeable analytical tag, which is then allowed to bind the target protein in live bacterial cells [31].

In principle, affinity chromatography is applicable for the identification of any antimicrobial binding protein, but actually, to select the appropriate modification site on the antimicrobial without affecting its original target-binding property is not an easy task. Over the years, several improvements have been made to address this issue [32–36]. One interesting method is the non-selective universal labeling method, which is able to attach structurally different molecules using a photo-crosslinking reaction [32]. This reaction produces a mixture of differently modified ligands, some of which are assumed to still bind the target. Other promising methods are label-free strategies, such as "pulse proteolysis" [37], "stability of proteins from rates of

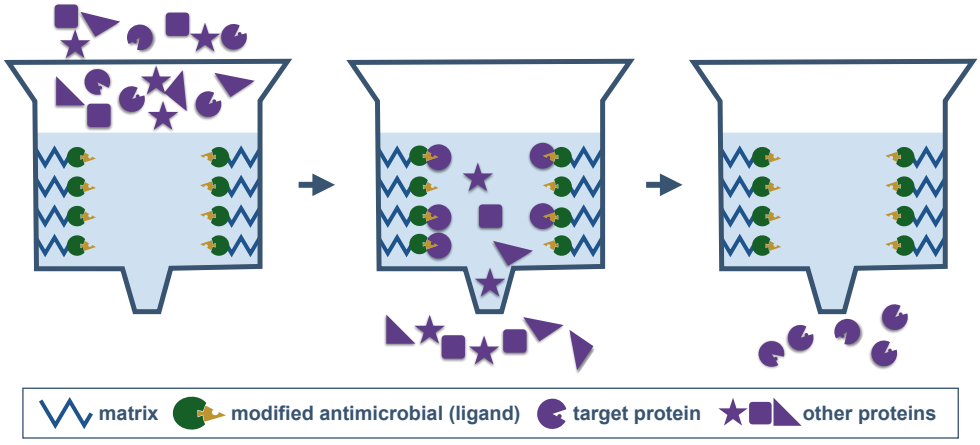

Fig. 3. Schematic representation of affinity chromatography. The tested antimicrobial is modified as a ligand, immobilized onto a solid matrix and then exposed to bacterial cell lysates. After multiple washing steps to remove non-binding proteins, the matrix-bound protein (target protein) is eluted for identification.

oxidation" (SPROX) [38] and "drug affinity responsive target stability" (DARTS) [39]. The underlying concept of these strategies is that the thermodynamic stability of the target protein will change when binding to ligand. These strategies have nice perspective because of their intrinsic advantage of being "label-free".

The development of mass spectrometry (MS) has greatly improved the identification of eluted proteins and straightforward workflows now include gel electrophoresis, protein band extraction and MS analysis [31]. The resolution, sensitivity, and throughput of MS-based methods has reached another level compared to the traditional N-terminal amino acid sequencing using Edman degradation. In addition, MS-based methods also benefit the affinity purification process. For example, Ong et al. labeled their cell lysates for negative control or positive probe with light or heavy isotopes using a quantitative proteomics method named SILAC, separately, and then MS was applied to identify the target proteins in combined protein samples without separation by gel electrophoresis [40]. But MS mediated approaches also have limitations. One of which is the requirement of specialized researchers and sophisticated instruments, which may not be available for all labs.

Lately, affinity approaches have contributed much to the MoA research of vancomycin [41–44]. However, they have not been broadly used in MoA identification of natural antimicrobials [7]. An intrinsic drawback is that these approaches require high-affinity interactions. There is a variety of interacting traits between

antimicrobials and their targets, and the interactions are not always high-affinity. Otherwise, affinity approaches are excellent tools for direct target identification of antimicrobials.

Above, we have compared the advantages and drawbacks of three classic approaches and have discussed their improvements over the years. Whereas these methods were established several decades ago, there is a reason why they are still in use today. These approaches do provide insight into the MoA of antimicrobials. The combination of classic approaches with continuously developing novel high-tech methodology may give the old methods a second and modern life.

OMICS APPROACHES

Next to classic approaches, several modern approaches, including omics technologies, have been developed and used extensively in recent years. The 'age of omics' has shed light onto the discovery of new antimicrobial compounds by developing global analysis tools such as genomics, transcriptomics and proteomics [9]. Genomics has been applied not only to explore silent antimicrobial biosynthetic pathways, but also to search for novel antibiotic targets. Transcriptomic and proteomic analyses generate information about the expression of genes in response to antimicrobials at the RNA and protein level, respectively, and changes in response to antimicrobial treatment provide insight into the working mechanism of these antimicrobial agents [45–47]. Here, we will focus on the impact of the global analysis studies and provide insight into each of these promising approaches. A brief schematic of introductions and major applications of these approaches can be found in Fig. 4.

Genomic approaches

Genomic methods are applied to explore the hidden property of bacterial genomes, such as searching for essential bacterial genes as the potential targets for novel antimicrobials, searching for genes that contribute to drug resistance or searching for potential antimicrobial synthetic gene clusters [48,49]. These approaches enable rapid antimicrobial target, resistance or synthesis prediction and therefore facilitate the search for antimicrobials with novel MoA. Unlike the other approaches reviewed here, genomic methods will not provide direct targets for antimicrobial compounds. Nevertheless, given the bright perspective of genomic methods to contribute to antimicrobial discovery, it is still interesting to discuss those here.

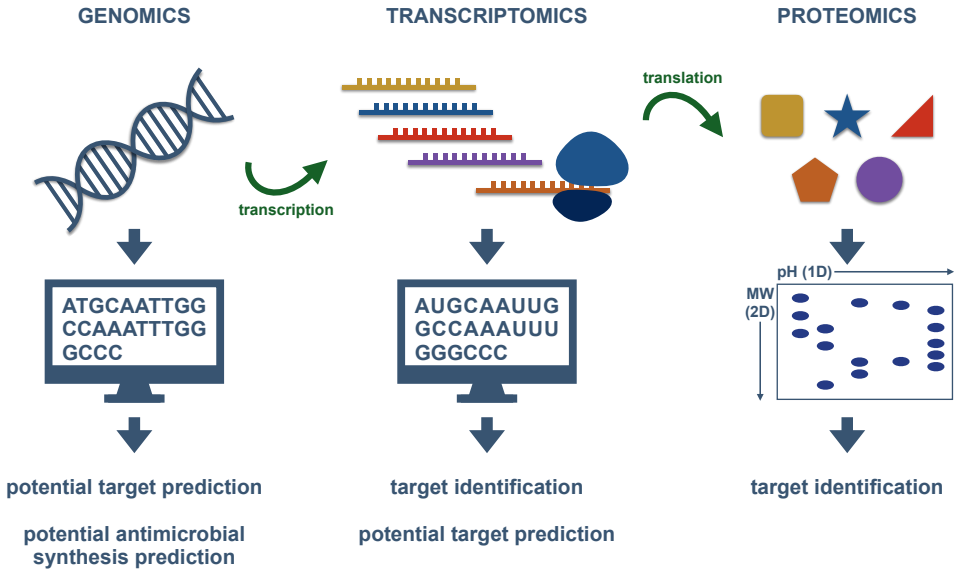

Fig. 4. Concepts and applications of omics approaches. The concept of genomics, transcriptomics and proteomics are schematically represented. Next-generation sequencing is performed to analyze genome and transcriptome, whereas 2D SDS-PAGE is the most common method for proteome analysis. Their application in antimicrobial discovery are listed below each approach.

Two commonly used genomic methods for antimicrobial discovery are genome mining and comparative genomics. The former one has achieved some goals by successfully characterizing several antimicrobial biosynthesis loci, including cyclic lipopeptide antimicrobials from *Pseudomonas aeruginosa*, polymyxin from *Paenibacillus polymyxa*, and polyketides from *Bacillus amyloliquefaciens* [9,50–52].

The focus of comparative genomics is on the identification of potential antimicrobial targets [53–55]. It is believed that conserved genes in different bacterial genomes often turn out to be essential, and therefore have the potential to become targets of broad-spectrum antimicrobials. Subtractive genome analysis is a method to search for conserved bacterial genes that are not present in eukaryotes. Admittedly, little of these efforts have arrived at clinical stages. One limitation to this approach may be the lack of distant gene relationships [48]. Essential bacterial functions are generally encoded by gene pairs [56], and these distant gene relationships are essential for target identification. Another obstacle is that the “essential gene” is relative rather than absolute, because this is dependent on the growth conditions. A study found pyrimidine–imidazole compounds to be novel anti-tuberculosis drugs

in vitro, but had no effects in an infected mouse model *in vivo* [57]. The reason for this discrepancy is that pyrimidine-imidazole inhibits glycerol metabolism, which is required for bacterial growth, but not for *Mycobacterium tuberculosis* during infection.

Lately, comparative genomics has also contributed to the identification of antimicrobial resistance gene clusters [58–60]. These studies illustrate the more complex mechanism of resistance than what was assumed previously. Comparative genomics suggests that antimicrobial resistance is not only due to mutations in the targets, but also to mutations in genes in charge of DNA repair, energy metabolism or transmembrane transporters. In addition, some studies reveal that many mutations encoding unannotated proteins may also contribute to antimicrobial resistance [61,62]. This provides leads for genetic studies in the future.

Different from genomic approaches, transcriptomic and proteomic approaches provide insight into the global response of bacterial cells to antimicrobials, which in turn provides insight into the MoA of certain compounds. In the following paragraphs, we will discuss their recent applications.

Transcriptomics approaches

The transcriptome is the signature of bacterial gene expression, which may be established under different environmental conditions and/or at specific growth stages. Categorizing the transcriptome is fundamental to investigate the functional elements of the genome and can therefore lead to a better understanding of bacterial status. One of the key purposes of transcriptomics is to quantify the changes in each transcript under different conditions [63]. This may benefit antimicrobial research, because an antimicrobial may influence many cellular pathways [64] and analysis of differential gene expression may help to predict the MoA of antimicrobial agents.

Traditional quantification techniques of RNA expression levels, such as real-time PCR and northern blotting, were widely used to characterize cellular transcriptomes in the 1990s [45]. However, these techniques do not allow analysis of the expression levels of all genes in one go. Therefore, multiple replicates need to be performed, which hampers interpretation of the results. Recently, with the development of next-generation sequencing, whole-cell analysis approaches have attracted more interest. One approved approach is RNA-Seq, which is developed to profile the transcriptome using deep-sequencing technologies. Compared to the traditional approaches, RNA-Seq has several advantages: it provides a far more precise resolution with high throughput and low background noise; it offers a high dynamic range for quantifying

the level of gene expression; it requires low amount of input RNA, and the cost for mapping transcriptomes is relatively low [63].

RNA-Seq has successfully been used for antimicrobial MoA elucidation. In a MoA study of two natural products, transcriptomic analysis of methicillin-resistant *Staphylococcus aureus* was performed by RNA-seq following treatment with ursolic acid and resveratrol [65]. The results illustrate the reduction of amino acid metabolism and adhesin expression in response to ursolic acid. Resveratrol causes disruption of surface proteins and capsular polysaccharides synthesis. RNA-Seq is also used to show the mechanism how one drug improves the efficiency of another drug. In this study, *Acinetobacter baumannii* was treated with sub-MIC of tigecycline, a drug that inhibits the initial codon recognition step of tRNA accommodation [66]. Transcriptomic analysis clearly shows the downregulation of β-Lactamases, such as OXA-23 and AmpC, by tigecycline, which results in a decrease of the MIC of ceftazidime, an antimicrobial targeting the cell wall.

Another aspect of transcriptomics in the antimicrobial field is that RNA-seq may predict potential antimicrobial targets, similar to comparative genomics [45]. For instance, biofilm formation is an important virulence trait of infection [67]. Instead of growth inhibition, the inhibition of biofilm formation of pathogenic bacteria may be an alternative approach to treat infections. RNA-seq analysis of *A. baumannii* shows huge differences in gene expression between biofilm cells and planktonic cells, with overexpression of 1621 genes and new expression of 55 genes [68]. These differentially expressed genes are involved in a variety of biological processes including transcriptional regulation, motility, amino acid metabolism, quorum sensing as well as other important pathways. Disruption of some of the differentially expressed genes results in a considerable decrease in biofilm formation. This suggests that this large panel of genes contains potential targets of novel antimicrobials or biofilm inhibitors.

Whereas transcriptomics is technically relatively easy to perform, the analysis of the outcome may be challenging. The lack of a “golden standard” protocol makes it complicated to compare the results between individual studies [9]. The growth status of cells, the culture media, the antimicrobial concentration and even the antimicrobial incubation time may all greatly affect the outcome of gene expression patterns. However, as a first step in MoA identification, transcriptomics may still provide much valuable information.

Proteomics approaches

The bacterial proteome responds quickly to changes in the surrounding environment. Antimicrobial treatment of bacteria results in direct and specific responses in their proteome. The goal of proteomics approaches is to globally analyze protein changes over time by identifying and quantifying proteins. This may help to formulate a hypothesis of the antibiotic target and MoA [69]. An additional advantage of proteomics is the quantification of post-translational modifications (PTM), which are not detectable by transcriptomic approaches.

In most cases, proteomic analysis is performed using two-dimensional electrophoresis (2-DE) and MS. With 2-DE, proteins are separated by gels on the basis of their isoelectric points in the first dimension and of their molecular weights in the second dimension. This results in a proteome map showing a variety of spots, each corresponding to a different protein. This method is routinely performed to study bacterial protein expression under given conditions. In a study using *Bacillus subtilis*, such proteome maps demonstrate the complex cellular responses to 30 distinct antimicrobial compounds [70]. Each of the antimicrobials induces a complex and unique protein expression profile. However, overlaps are evident in the expression of some proteins in response to distinct antimicrobials with similar MoAs. Analysis of the similarities results in identification of 122 marker proteins with at least two-fold overexpression compared to the untreated control. These markers are excellent references for the MoA study of novel antimicrobials. The marker protein concept was successfully applied to a novel compound, BAY 50-2369, and it is classified as a protein synthesis inhibitor. A recent MoA study of daptomycin, mentioned above in the "*MMS assay*" part [18], is also a successful example of 2-DE. The proteome map of daptomycin-treated bacteria was compared with maps from previous studies [70,71], resulting in identification of matching marker proteins of bacteria treated with cell membrane-active antimicrobials, which provides evidence for the membrane defects induced by daptomycin. However, the gel-based separation system has limitations. For example, it has low throughput and high inter-gel variability. More importantly, it can only be applied to proteins with certain properties, because it has poor recovery of very small and very large proteins as well as hydrophobic proteins.

Recently, with the improvements in liquid chromatography (LC) and tandem MS (MS/MS) technology, several gel-free proteomics methods have been established. These methods facilitate identification and quantification of complex peptide mixtures containing proteins digested by proteolytic enzymes. Subsequently, computational

approaches are being used to assemble these peptides back to proteins [72]. As a consequence of the LC separation process, gel-free methods are more sensitive and less laborious, compared to the gel-based methods. However, the popularity of gel-free approaches is less than gel-based methods in the antimicrobial fields. The greatest challenge in gel-free approaches is the computational approach, which is not as accurate as one would like for high-resolution data, although significant advances in analysis programs have been made over the years [72,73]. With the continuous improvement of bioinformatic analysis tools, gel-free approaches may become the superior application in the future. However, for now, gel-based methods are still dominant in proteomic analysis of antimicrobial MoA. Considering the limitations of the gels, transcriptomics data may be useful supplements. The combination of the two omics approaches may provide an interesting perspective for antimicrobial MoA identification.

Similar to the omics approaches above, other omics methods, like metabolomics and lipidomics, are also widely used to generate bacterial signatures in antimicrobial research [45]. Whereas all of these omics methods provide valuable information about antimicrobial targets, they are indirect approaches and therefore do not necessarily provide information about the direct target(s) of antimicrobials. These methods are developed for the initial stages of target identification. Despite that these approaches are modern and fascinating, they do not have significant advantages for MoA identification by themselves. Since the time spent and cost involved in the omics approaches is relatively high, it is wise for each application to choose the most appropriate approach.

MORPHOLOGICAL PROFILING

Inhibition of a specific pathway in a cell may result in specific changes in the cell phenotype, including changes of molecular signatures (e.g. transcriptome or proteome) and cellular morphology [74]. Above, we have illustrated the application of omics approaches that use molecular signatures in identification of antimicrobial MoAs. Assessment of cellular morphology is also an important way to generate information about pathway defects and antimicrobials generating similar phenotypes may target the same pathways. With the advances in microscopy, cellular morphological profiling is another attractive way to hypothesize about the MoA of antimicrobials by reflecting the global cellular effects. For eukaryotic cells, many aspects of cellular morphological changes are easily observed under a microscope, followed by automated computational analysis [75,76].

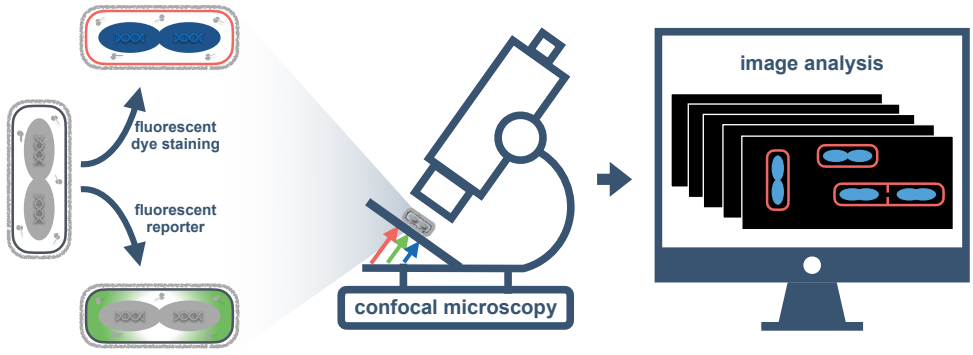

Fig. 5. Concepts of BCP. Fluorescent bacterial cells (by fluorescent dye staining or fluorescent protein expression) are imaged by confocal microscopy. Images are then analyzed using specific programs.

However, to apply this strategy onto antimicrobial MoA identification, i.e. to profile the cellular changes in prokaryotic cells, is a more challenging task. This is mainly due to the smaller size of bacterial cells, high phototoxicity and enhanced movement of bacterial cells. With the development of microscopy, high resolution images reflecting bacterial sub-cellular structures are gradually achievable. In this part, we will discuss the advances of imaging-based strategies in antimicrobial MoA identification.

Bacterial cytological profiling (BCP)

The concept of BCP was initially validated in 2013 by Nonejuie and colleagues [77]. With micrographs of Gram-negative bacteria, *Escherichia coli*, treated with different antimicrobials, they successfully classified 41 antimicrobials into five groups, based on the five major pathways, including DNA synthesis, RNA synthesis, protein synthesis, lipid synthesis and peptidoglycan synthesis. In addition, the small differences within each group may also be target related, and may therefore allow further distinguishing. For this approach, *E. coli* cells are visualized by staining with DAPI (cell permeable nucleoid dye with blue fluorescence), FM4-64 (membrane dye with far red fluorescence) and SYTOX-Green (cell impermeable nucleoid dye with green fluorescence), immobilized by agarose pads and magnified by a 100× objective. Cell morphological differences are distinguished based on the features both from the shape parameters and the intensity of each of the dyes. As a proof-of-principle, the MoA of a natural antimicrobial, spirohexenolide A, was predicted to be active on the cell membrane.

Compared to the classic and omics approaches, BCP provides reliable MoA information, but with a less tedious workflow (Fig. 5) and lower amount of compound required. But it also has limitations. Whereas it provides information which pathway is affected, this phenotype-based indirect approach does not provide information about the molecular targets. Another limitation is that the hypothesis can only be derived from the reference set, which is based on profiling of control-treated antimicrobials with defined MoA. If an antimicrobial has a MoA that has not been described before, BCP cannot provide information. Last, but not least is the limitation that whereas BCP can be used on Gram-negative bacteria [77,78], the application of BCP on Gram-positive bacteria seems to be more complicated. Due to the strong cell wall, the shape of Gram-positive cells normally does not change significantly. Fortunately, some efforts have been made to improve these limitations.

To address these limitations, several improvements were made. To visualize potential new target defects, Lamsa et al. established a method, dubbed Rapid inhibition profiling (RIP) [79,80], which demonstrates that degradation of essential proteins in some of the major pathways, for example DNA synthesis, RNA synthesis, fatty acid synthesis, and peptidoglycan synthesis, matches the profiles of antimicrobials inhibiting the same pathways. This suggests that RIP has the potential to generate a library of profiles by inactivating each of the pathways, including the ones that are not known to be targeted by antimicrobials and thus reflect novel MoAs.

To apply BCP to Gram-positive bacteria, several avenues were developed. The first possible solution is to generate a panel of GFP-reporters covering many pathways. This panel has been successfully applied for several in-depth analyses of antimicrobial targets [18,81,82]. However, no single reporter was generated covering more than two main antimicrobial classes. This suggests that for classification of unknown antimicrobial candidates, at least five reporters will be needed each time. This approach is rather laborious, because for each reporter an accurate minimum inhibitory concentration (MIC) of the antimicrobial has to be established. Another possible solution is to add a new dimension to BCP, i.e. time, by taking advantage of time-lapse imaging and perform dynamic bacterial cytological profiling (DBCP). We have just developed this strategy and have acquired several benefits from it.

DBCP

DBCP is a method to record bacterial changes before, during and after antimicrobial treatment using time-lapse imaging. The term dynamic is added ahead of BCP because the same cell is imaged over time, which is fundamentally different from

individual images of distinct cells or cultures at different time points. Bacterial long-term imaging was facilitated by an improved imaging protocol, which is based on a previously described technique [83]. The technique we developed contains several improvements, including the advantage to add antimicrobials at any time, which is less time consuming and less laborious (**Chapter 4**). In addition, several adjustments have been made to reduce the chance of being affected by environmental factors, such as staining toxicity and phototoxicity. Finally, DBCP has been successfully performed on a Gram-positive bacterium *B. subtilis* and allows to rapidly distinguish between anti-Gram-positive drugs from all of the five different pathways. As a proof-of-concept, a naturally occurring antimicrobial was identified to target the cell envelope. DBCP has several benefits. It allows to record the direct response from single cells to specific antimicrobial agents over time and to provide a first glance of timepoints at which a certain antimicrobial starts to have effects, cell growth starts to be inhibited and/or cells to be killed. These parameters are all important to establish antimicrobial MoA.

DBCP has its limitations. This imaging-based strategy results in the 'most similar' signatures, and thereby has an intrinsic danger of false positive matches. Therefore, subsequent validation experiments are fundamental to this approach. Nevertheless, considering the ease of accessibility and the affordability, DBCP is an excellent approach for the initial stage of MoA identification.

CONCLUSION AND OUTLOOK

Antimicrobial resistance is one of the major threats to human health. Although many classes of antimicrobials are available on the market, none of them escapes emerging resistance. We have a strong need for new classes of antimicrobials with novel MoA to resolve the infections that are caused by the so-called "superbugs", which are pathogens that are resistant to multiple antimicrobials. MoA identification of newly screened antimicrobials has become more important than ever before. However, this process remains to be the bottleneck in drug discovery.

Here, we have reviewed various approaches that are developed for MoA identification. It will be smart to choose the most appropriate strategy depending on the expertise of the lab and the properties of the antimicrobial agent. Classic approaches were developed for slow processes decades ago, but two approaches from it, genetic approaches and affinity chromatography, are the only methods to directly identify the real targets at the molecular level. Even though they are relatively laborious and time-consuming, an appropriate and accurate hypothesis about the

pathway of the antimicrobial target might significantly shorten the process. All the modern approaches (omics, imaging-based methods etc.) as well as the improved MMS assay are actually designed for generating the hypothesis in a fast and accurate process. Although the "high hopes from omics" is not yet fulfilled, the global profiling methods of omics are definitely shedding light on future antibacterial discovery. They are high throughput and easily performed. The MMS assay and the imaging-based methods also contribute to some aspects of antimicrobial research and provide more options for researchers in the field. But they all have specific limitations.

It is important to note that no perfect method has been established for antimicrobial MoA identification yet, at least until now. However, due to the development of methodologies and technologies, it will be interesting to see how these approaches will influence the antimicrobial research in the future. There might be new ideas and new hopes coming in and old strategies dying out. But overall, until the emergence of the next "penicillin", we will never have the chance to take a short break from the battle with the kingdom of microorganisms.

REFERENCES

[1] Ariëns EJ. Molecular Pharmacology V3: The Model of Action of Biology Active Compounds. vol. 1. Elsevier; 2012.

[2] Schenone M, Dančík V, Wagner BK, Clemons PA. Target identification and mechanism of action in chemical biology and drug discovery. Nat Chem Biol 2013;9:232–40. https://doi.org/10.1038/nchembio.1199.

[3] Muroi M, Futamura Y, Osada H. Integrated profiling methods for identifying the targets of bioactive compounds: MorphoBase and ChemProteoBase. Nat Prod Rep 2016;33:621–5. https://doi.org/10.1039/c5np00106d.

[4] Hancock REW. Mechanisms of action of newer antibiotics for Gram-positive pathogens. Lancet Infect Dis 2005;5:209–18. https://doi.org/10.1016/S1473-3099(05)70051-7.

[5] Romo D, Liu JO. Editorial: Strategies for cellular target identification of natural products. Nat Prod Rep 2016;33:592–4. https://doi.org/10.1039/c6np90016j.

[6] Newman DJ, Cragg GM. Natural products as sources of new drugs over the 30 years from 1981 to 2010. J Nat Prod 2012;75:311–35. https://doi.org/10.1021/np200906s.

[7] Farha MA, Brown ED. Strategies for target identification of antimicrobial natural products. Nat Prod Rep 2016;33:668–80. https://doi.org/10.1039/c5np00127g.

[8] Silver LL. Challenges of antibacterial discovery. Clin Microbiol Rev 2011;24:71–109. https://doi.org/10.1128/CMR.00030-10.

[9] Wecke T, Mascher T. Antibiotic research in the age of omics: From expression profiles to interspecies communication. J Antimicrob Chemother 2011;66:2689–704. https://doi.org/10.1093/jac/dkr373.

[10] Cunningham ML, Kwan BP, Nelson KJ, Bensen DC, Shaw KJ. Distinguishing on-target versus off-target activity in early antibacterial drug discovery using a macromolecular synthesis assay. J Biomol Screen 2013;18:1018–26. https://doi.org/10.1177/1087057113487208.

[11] Daly JS, Eliopoulos GM, Willey S, Moellering RC. Mechanism of action and in vitro and in vivo activities of S-6123, a new oxazolidinone compound. vol. 32. 1988. https://doi.org/10.1128/AAC.32.9.1341.

[12] Canepari P, Boaretti M, Del Mar Lleo M, Satta G. Lipoteichoic acid as a new target for activity of antibiotics: Mode of action of daptomycin (LY146032). vol. 34. 1990. https://doi.org/10.1128/AAC.34.6.1220.

[13] Crumplin GC, Smith JT. Nalidixic acid: an antibacterial paradox. vol. 8. 1975. https://doi.org/10.1128/AAC.8.3.251.

[14] Smith DH, Davis BD. Mode of action of novobiocin in Escherichia coli. vol. 93. 1967. https://doi.org/10.1128/jb.93.1.71-79.1967.

[15] Sugino A, Peebles CL, Kreuzer KN, Cozzarelli NR. Mechanism of action of nalidixic acid: Purification of Escherichia coli nalA gene product and its relationship to DNA gyrase and a novel nicking-closing enzyme. Proc Natl Acad Sci U S A 1977;74:4767–71. https://doi.org/10.1073/pnas.74.11.4767.

[16] Drlica K, Zhao X. DNA gyrase, topoisomerase IV, and the 4-quinolones. Microbiol Mol Biol Rev 1997;61:377–92. https://doi.org/10.1128/.61.3.377-392.1997.

[17] Wang J, Soisson SM, Young K, Shoop W, Kodali S, Galgoci A, et al. Platensimycin is a selective FabF inhibitor with potent antibiotic properties. Nature 2006;441:358–61. https://doi.org/10.1038/nature04784.

[18] Müller A, Wenzel M, Strahl H, Grein F, Saaki TNV, Kohl B, et al. Daptomycin inhibits cell envelope synthesis by interfering with fluid membrane microdomains. Proc Natl Acad Sci U S A 2016;113:E7077–86. https://doi.org/10.1073/pnas.1611173113.

[19] Li X, Zolli-Juran M, Cechetto JD, Daigle DM, Wright GD, Brown ED. Multicopy suppressors for novel antibacterial compounds reveal targets and drug efflux susceptibility. Chem Biol 2004;11:1423–30. https://doi.org/10.1016/j.chembiol.2004.08.014.

[20] Lomovskaya O, Warren MS, Lee A, Galazzo J, Fronko R, Lee M, et al. Identification and characterization of inhibitors of multidrug resistance efflux pumps in Pseudomonas aeruginosa: Novel agents for combination therapy. Antimicrob Agents Chemother 2001;45:105–16. https://doi.org/10.1128/AAC.45.1.105-116.2001.

[21] Yin D, Fox B, Lonetto ML, Etherton MR, Payne DJ, Holmes DJ, et al. Identification of antimicrobial targets using a comprehensive genomic approach. Pharmacogenomics 2004;5:101–13. https://doi.org/10.1517/phgs.5.1.101.25679.

[22] Donald RGK, Skwish S, Forsyth RA, Anderson JW, Zhong T, Burns C, et al. A Staphylococcus aureus Fitness Test Platform for Mechanism-Based Profiling of Antibacterial Compounds. Chem Biol 2009;16:826–36. https://doi.org/10.1016/j.chembiol.2009.07.004.

[23] Ince D, Hooper DC. Quinolone Resistance Due to Reduced Target Enzyme Expression. J Bacteriol 2003;185:6883–92. https://doi.org/10.1128/JB.185.23.6883-6892.2003.

[24] Fey PD, Endres JL, Yajjala VK, Widhelm TJ, Boissy RJ, Bose JL, et al. A genetic resource for rapid and comprehensive phenotype screening of nonessential Staphylococcus aureus genes. MBio 2013;4:537–49. https://doi.org/10.1128/mBio.00537-12.

[25] Vestergaard M, Leng B, Haaber J, Bojer MS, Vegge CS, Ingmer H. Genome-wide identification of antimicrobial intrinsic resistance determinants in staphylococcus aureus. Front Microbiol 2016;7:2018. https://doi.org/10.3389/fmicb.2016.02018.

[26] Peters JM, Colavin A, Shi H, Czarny TL, Larson MH, Wong S, et al. A comprehensive, CRISPR-based functional analysis of essential genes in bacteria. Cell 2016;165:1493–506. https://doi.org/10.1016/j.cell.2016.05.003.

[27] Metzker ML. Sequencing technologies the next generation. Nat Rev Genet 2010;11:31–46. https://doi.org/10.1038/nrg2626.

[28] Le Lay C, Dridi L, Bergeron MG, Ouellette M, Fliss I. Nisin is an effective inhibitor of Clostridium difficile vegetative cells and spore germination. J Med Microbiol 2016;65:169–75. https://doi.org/10.1099/jmm.0.000202.

[29] Futamura Y, Muroi M, Osada H. Target identification of small molecules based on chemical biology approaches. Mol Biosyst 2013;9:897–914. https://doi.org/10.1039/c2mb25468a.

[30] Ziegler S, Pries V, Hedberg C, Waldmann H. Target identification for small bioactive molecules: Finding the needle in the haystack. Angew Chemie - Int Ed 2013;52:2744–92. https://doi.org/10.1002/anie.201208749.

[31] Zheng W, Li G, Li X. Affinity purification in target identification: the specificity challenge. Arch Pharm Res 2015;38:1661–85. https://doi.org/10.1007/s12272-015-0635-2.

[32] Kanoh N, Honda K, Simizu S, Muroi M, Osada H. Photo-Cross-Linked Small-Molecule Affinity

Matrix for Facilitating Forward and Reverse Chemical Genetics. Angew Chemie 2005;117:3625–8. https://doi.org/10.1002/ange.200462370.

[33] Koshi Y, Nakata E, Miyagawa M, Tsukiji S, Ogawa T, Hamachi I. Target-specific chemical acylation of lectins by ligand-tethered DMAP catalysts. J Am Chem Soc 2008;130:245–51. https://doi.org/10.1021/ja075684q.

[34] Hosoya T, Hiramatsu T, Ikemoto T, Nakanishi M, Aoyama H, Hosoya A, et al. Novel bifunctional probe for radioisotope-free photoaffinity labeling: Compact structure comprised of photospecific ligand ligation and detectable tag anchoring units. Org Biomol Chem 2004;2:637–41. https://doi.org/10.1039/b316221d.

[35] Cisar JS, Cravatt BF. Fully functionalized small-molecule probes for integrated phenotypic screening and target identification. J Am Chem Soc 2012;134:10385–8. https://doi.org/10.1021/ja304213w.

[36] Chang Y, Schlebach JP, VerHeul RA, Park C. Simplified proteomics approach to discover protein-ligand interactions. Protein Sci 2012;21:1280–7. https://doi.org/10.1002/pro.2112.

[37] Park C, Marqusee S. Pulse proteolysis: A simple method for quantitative determination of protein stability and ligand binding. Nat Methods 2005;2:207–12. https://doi.org/10.1038/nmeth740.

[38] West GM, Tang L, Fitzgerald MC. Thermodynamic analysis of protein stability and ligand binding using a chemical modification- and mass spectrometry-based strategy. Anal Chem 2008;80:4175–85. https://doi.org/10.1021/ac702610a.

[39] Pai MY, Lomenick B, Hwang H, Schiestl R, McBride W, Loo JA, et al. Drug affinity responsive target stability (DARTS) for small-molecule target identification. Methods Mol Biol 2015;1263:287–98. https://doi.org/10.1007/978-1-4939-2269-7_22.

[40] Ong SE, Schenone M, Margolin AA, Li X, Do K, Doud MK, et al. Identifying the proteins to which small-molecule probes and drugs bind in cells. Proc Natl Acad Sci U S A 2009;106:4617–22. https://doi.org/10.1073/pnas.0900191106.

[41] Koteva K, Hong HJ, Wang XD, Nazi I, Hughes D, Naldrett MJ, et al. A vancomycin photoprobe identifies the histidine kinase VanSsc as a vancomycin receptor. Nat Chem Biol 2010;6:327–9. https://doi.org/10.1038/nchembio.350.

[42] Sinha Roy R, Yang P, Kodali S, Xiong Y, Kim RM, Griffin PR, et al. Direct interaction of a vancomycin derivative with bacterial enzymes involved in cell wall biosynthesis. Chem Biol 2001;8:1095–106. https://doi.org/10.1016/S1074-5521(01)00075-8.

[43] Chen L, Walker D, Sun B, Hu Y, Walker S, Kahne D. Vancomycin analogues active against vanA-resistant strains inhibit bacterial transglycosylase without binding substrate. Proc Natl Acad Sci U S A 2003;100:5658–63. https://doi.org/10.1073/pnas.0931492100.

[44] Eirich J, Orth R, Sieber SA. Unraveling the protein targets of vancomycin in living S. aureus and E. faecalis cells. J Am Chem Soc 2011;133:12144–53. https://doi.org/10.1021/ja2039979.

[45] Pulido MR, García-Quintanilla M, Gil-Marqués ML, McConnell MJ. Identifying targets for antibiotic development using omics technologies. Drug Discov Today 2016;21:465–72. https://doi.org/10.1016/j.drudis.2015.11.014.

[46] Armengaud J. Microbiology and proteomics, getting the best of both worlds! Environ Microbiol 2013;15:12–23. https://doi.org/10.1111/j.1462-2920.2012.02811.x.

[47] Brötz-Oesterhelt H, Bandow JE, Labischinski H. Bacterial proteomics and its role in antibacterial drug discovery. Mass Spectrom Rev 2005;24:549–65. https://doi.org/10.1002/mas.20030.

[48] Sakharkar KR, Sakharkar MK, Chow VTK. Biocomputational strategies for microbial drug target identification. Methods Mol Med 2008;142:1–9. https://doi.org/10.1007/978-1-59745-246-5_1.

[49] Nes IF, Johnsborg O. Exploration of antimicrobial potential in LAB by genomics. Curr Opin Biotechnol 2004;15:100–4. https://doi.org/10.1016/j.copbio.2004.02.001.

[50] De Bruijn I, De Kock MJD, Yang M, De Waard P, Van Beek TA, Raaijmakers JM. Genome-based discovery, structure prediction and functional analysis of cyclic lipopeptide antibiotics in Pseudomonas species. Mol Microbiol 2007;63:417–28. https://doi.org/10.1111/j.1365-2958.2006.05525.x.

[51] Choi SK, Park SY, Kim R, Kim S Bin, Lee CH, Kim JF, et al. Identification of a polymyxin synthetase gene cluster of Paenibacillus polymyxa and heterologous expression of the gene in Bacillus subtilis. J Bacteriol 2009;191:3350–8. https://doi.org/10.1128/JB.01728-08.

[52] Chen XH, Vater J, Piel J, Franke P, Scholz R, Schneider K, et al. Structural and functional characterization of three polyketide synthase gene clusters in Bacillus amyloliquefaciens FZB 42. J Bacteriol 2006;188:4024–36. https://doi.org/10.1128/JB.00052-06.

[53] Lee DS, Burd H, Liu J, Almaas E, Wiest O, Barabási AL, et al. Comparative genome-scale metabolic reconstruction and flux balance analysis of multiple Staphylococcus aureus genomes identify novel antimicrobial drug targets. J Bacteriol 2009;191:4015–24. https://doi.org/10.1128/JB.01743-08.

[54] Sakharkar KR, Sakharkar MK, Chow VTK. Gene fusion in Helicobacter pylori: Making the ends meet. Antonie van Leeuwenhoek, Int J Gen Mol Microbiol 2006;89:169–80. https://doi.org/10.1007/s10482-005-9021-2.

[55] Galperin MY, Koonin E V. Searching for drug targets in microbial genomes. Curr Opin Biotechnol 1999;10:571–8. https://doi.org/10.1016/S0958-1669(99)00035-X.

[56] Thomaides HB, Davison EJ, Burston L, Johnson H, Brown DR, Hunt AC, et al. Essential bacterial functions encoded by gene pairs. J Bacteriol 2007;189:591–602. https://doi.org/10.1128/JB.01381-06.

[57] Pethe K, Sequeira PC, Agarwalla S, Rhee K, Kuhen K, Phong WY, et al. A chemical genetic screen in Mycobacterium tuberculosis identifies carbon-source-dependent growth inhibitors devoid of in vivo efficacy. Nat Commun 2010;1:1–8. https://doi.org/10.1038/ncomms1060.

[58] Lázár V, Nagy I, Spohn R, Csörgo ' B, Györkei Á, Nyerges Á, et al. Genome-wide analysis captures the determinants of the antibiotic cross-resistance interaction network. Nat Commun 2014;5:1–12. https://doi.org/10.1038/ncomms5352.

[59] Händel N, Schuurmans JM, Feng Y, Brul S, Ter Kuile BH. Interaction between mutations and regulation of gene expression during development of de novo antibiotic resistance. Antimicrob Agents Chemother 2014;58:4371–9. https://doi.org/10.1128/AAC.02892-14.

[60] Gallagher LA, Lee SA, Manoil C. Importance of core genome functions for an extreme antibiotic resistance trait. MBio 2017;8. https://doi.org/10.1128/mBio.01655-17.

[61] Su HC, Khatun J, Kanavy DM, Giddings MC. Comparative genome analysis of ciprofloxacin-resistant pseudomonas aeruginosa reveals genes within newly identified high variability regions associated with drug resistance development. Microb Drug Resist 2013;19:428–36. https://doi.org/10.1089/mdr.2012.0258.

[62] Chernov VM, Chernova OA, Mouzykantov AA, Lopukhov LL, Aminov RI. Omics of antimicrobials and antimicrobial resistance. Expert Opin Drug Discov 2019;14:455–68. https://doi.org/10.1080

/17460441.2019.1588880.

[63] Wang Z, Gerstein M, Snyder M. RNA-Seq: A revolutionary tool for transcriptomics. Nat Rev Genet 2009;10:57–63. https://doi.org/10.1038/nrg2484.

[64] Blair JMA, Webber MA, Baylay AJ, Ogbolu DO, Piddock LJV. Molecular mechanisms of antibiotic resistance. Nat Rev Microbiol 2015;13:42–51. https://doi.org/10.1038/nrmicro3380.

[65] Qin N, Tan X, Jiao Y, Liu L, Zhao W, Yang S, et al. RNA-Seq-based transcriptome analysis of methicillin-resistant staphylococcus aureus biofilm inhibition by ursolic acid and resveratrol. Sci Rep 2014;4:1–9. https://doi.org/10.1038/srep05467.

[66] Hua X, Chen Q, Li X, Yu Y. Global transcriptional response of Acinetobacter baumannii to a subinhibitory concentration of tigecycline. Int J Antimicrob Agents 2014;44:337–44. https://doi.org/10.1016/j.ijantimicag.2014.06.015.

[67] Hasan F, Xess I, Wang X, Jain N, Fries BC. Biofilm formation in clinical Candida isolates and its association with virulence. Microbes Infect 2009;11:753–61. https://doi.org/10.1016/j.micinf.2009.04.018.

[68] Rumbo-Feal S, Gómez MJ, Gayoso C, Álvarez-Fraga L, Cabral MP, Aransay AM, et al. Whole Transcriptome Analysis of Acinetobacter baumannii Assessed by RNA-Sequencing Reveals Different mRNA Expression Profiles in Biofilm Compared to Planktonic Cells. PLoS One 2013;8:e72968. https://doi.org/10.1371/journal.pone.0072968.

[69] Wenzel M, Bandow JE. Proteomic signatures in antibiotic research. Proteomics 2011;11:3256–68. https://doi.org/10.1002/pmic.201100046.

[70] Bandow JE, Brötz H, Leichert LIO, Labischinski H, Hecker M. Proteomic approach to understanding antibiotic action. Antimicrob Agents Chemother 2003;47:948–55. https://doi.org/10.1128/AAC.47.3.948-955.2003.

[71] Wenzel M, Kohl B, Münch D, Raatschen N, Albada HB, Hamoen L, et al. Proteomic response of Bacillus subtilis to lantibiotics reflects differences in interaction with the cytoplasmic membrane. Antimicrob Agents Chemother 2012;56:5749–57. https://doi.org/10.1128/AAC.01380-12.

[72] Park AJ, Krieger JR, Khursigara CM. Survival proteomes: The emerging proteotype of antimicrobial resistance. FEMS Microbiol Rev 2016;40:323–42. https://doi.org/10.1093/femsre/fuv051.

[73] Cox J, Mann M. MaxQuant enables high peptide identification rates, individualized p.p.b.-range mass accuracies and proteome-wide protein quantification. Nat Biotechnol 2008;26:1367–72. https://doi.org/10.1038/nbt.1511.

[74] Fetz V, Prochnow H, Brönstrup M, Sasse F. Target identification by image analysis. Nat Prod Rep 2016;33:655–67. https://doi.org/10.1039/c5np00113g.

[75] Perlman ZE, Slack MD, Feng Y, Mitchison TJ, Wu LF, Altschuler SJ. Multidimensional drug profiling by automated microscopy. Science (80-) 2004;306:1194–8. https://doi.org/10.1126/science.1100709.

[76] Mitchison TJ. Small-molecule screening and profiling by using automated microscopy. ChemBioChem 2005;6:33–9. https://doi.org/10.1002/cbic.200400272.

[77] Nonejuie P, Burkart M, Pogliano K, Pogliano J. Bacterial cytological profiling rapidly identifies the cellular pathways targeted by antibacterial molecules. Proc Natl Acad Sci U S A 2013;110:16169–74. https://doi.org/10.1073/pnas.1311066110.

[78] Sun Y, Heidary DK, Zhang Z, Richards CI, Glazer EC. Bacterial Cytological Profiling Reveals the Mechanism of Action of Anticancer Metal Complexes. Mol Pharm 2018;15:3404–16. https://doi.org/10.1021/acs.molpharmaceut.8b00407.

[79] Lamsa A, Lopez-Garrido J, Quach D, Riley EP, Pogliano J, Pogliano K. Rapid Inhibition Profiling in Bacillus subtilis to Identify the Mechanism of Action of New Antimicrobials. ACS Chem Biol 2016;11:2222–31. https://doi.org/10.1021/acschembio.5b01050.

[80] Peters CE, Lamsa A, Liu RB, Quach D, Sugie J, Brumage L, et al. Rapid Inhibition Profiling Identifies a Keystone Target in the Nucleotide Biosynthesis Pathway. ACS Chem Biol 2018;13:3251–8. https://doi.org/10.1021/acschembio.8b00273.

[81] Wenzel M, Rautenbach M, Vosloo JA, Siersma T, Aisenbrey CHM, Zaitseva E, et al. The multifaceted antibacterial mechanisms of the pioneering peptide antibiotics tyrocidine and gramicidin S. MBio 2018;9:1–20. https://doi.org/10.1128/mBio.00802-18.

[82] Zhu JH, Wang BW, Pan M, Zeng YN, Rego H, Javid B. Rifampicin can induce antibiotic tolerance in mycobacteria via paradoxical changes in rpoB transcription. Nat Commun 2018;9. https://doi.org/10.1038/s41467-018-06667-3.

[83] de Jong IG, Beilharz K, Kuipers OP, Veening JW. Live cell imaging of Bacillus subtilis and Streptococcus pneumoniae using automated time-lapse microscopy. J Vis Exp 2011:1–6. https://doi.org/10.3791/3145.

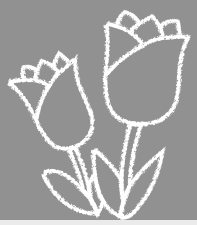

Berkchaetoazaphilone B, an Antimicrobial Agent Affecting Energy Metabolism from a Screen of 10,207 Fungi

CHAPTER 3

Xudong Ouyang[1,2], Jelmer Hoeksma[1], Gisela van der Velden[1], Wouter A.G. Beenker[1], Maria H. van Triest[3], Boudewijn M.T. Burgering[3] and Jeroen den Hertog[1,2]

1. Hubrecht Institute-KNAW and University Medical Center Utrecht, Utrecht, the Netherlands
2. Institute Biology Leiden, Leiden University, Leiden, the Netherlands
3. Molecular Cancer Research, Center Molecular Medicine, University Medical Center Utrecht, the Netherlands; Oncode Institute

Adapted from doi: 10.1038/s41598-021-98252-w

ABSTRACT

Antimicrobial resistance has become one of the major threats to human health. Therefore, there is a strong need for novel antimicrobials with new mechanisms of action. The kingdom of fungi is an excellent source of antimicrobials for this purpose because it encompasses countless fungal species that harbor unusual metabolic pathways. Previously, we have established a library of secondary metabolites from 10,207 strains of fungi. Here, we screened for antimicrobial activity of the library against seven pathogenic bacterial strains and investigated the identity of the active compounds using ethyl acetate extraction, activity-directed purification using HPLC fractionation and chemical analyses. We initially found 280 antimicrobial strains and subsequently identified 17 structurally distinct compounds from 26 strains upon further analysis. All but one of these compounds, berkchaetoazaphilone B (BAB), were known to have antimicrobial activity. Here, we studied the antimicrobial properties of BAB, and found that BAB affected energy metabolism in both prokaryotic and eukaryotic cells. We conclude that fungi are a rich source of chemically diverse secondary metabolites with antimicrobial activity.

INTRODUCTION

In the pre-antibiotic era, the average life expectancy was around 47 years, partly because of the high mortality due to infectious diseases [1]. This situation was changed by the discovery of penicillin in 1928, which innovated the course of medicine and was marked as the beginning of the antibiotic era [2]. However, an issue arose in connection to the use of antibiotics, antimicrobial resistance [3–5]. Although many classes of antimicrobials have been discovered, resistance to these antimicrobials developed shortly after their use in hospitals [6]. Bacterial infection has become a serious threat to humans again because of this emerging resistance, especially when the so-called "superbugs", which are pathogens that are resistant to multiple antibiotics, appear in hospitals [7]. The treatment of infections is becoming complex, resulting in rising costs and higher patient mortality. In Europe, around 25,000 deaths are associated with antimicrobial resistance annually, costing 1.5 billion euros each year [8,9]. Thus, discovering novel antimicrobials with a new mechanism of action (MoA) is an endless task to fight newly emerging resistance.

The kingdom of fungi provides a wealth of antimicrobial agents [10]. There are countless fungal species that harbor unusual metabolic pathways [11]. The chemical products of these pathways are termed secondary metabolites, which are not required for life and growth of fungi per se. Secondary metabolites are often secreted bioactive compounds with low-molecular-weight that are produced at specific stages of morphological differentiation to develop interactions with other organisms or the environment [12]. Over millions of years, fungi have evolved in part by production of metabolites to perform important functions, to survive in harsh environments, to fight off invaders or to alter fungal development [13–16]. Thus, the functionally distinct fungal secondary metabolites have formed a diverse pool of biologically active natural compounds, including ones that are harmful (e.g. toxins) or beneficial (e.g. antimicrobials) to human beings [14], which is promising for drug discovery.

The systematic study of fungal secondary metabolites started in 1922 when Harold Raistrick identified over 200 metabolites [17]. Unfortunately, it did not attract much attention from the public. This situation changed in 1928 with the discovery of penicillin. Since then, studies into fungal secondary metabolites have been conducted, and thousands of metabolites with antimicrobial, antifungal or antitumor activities have been discovered [11]. Compared to the number of existing fungal species [18], this was only the tip of the iceberg. Due to the recent development of genome sequencing and bioinformatic analysis, genome mining has become a popular technique to screen for biosynthetic gene clusters of fungal

secondary metabolites [19]. However, genome data are not always available for the less studied species, which have a high chance to produce metabolites that have not been described before. The traditional cultivation-based method facilitates analysis of these species.

Previously, a library of fungal secondary metabolites from 10,207 strains was established in our lab, and zebrafish (*Danio rerio*) embryos were used as read-out to screen for novel bioactive compounds that induced developmental defects [20]. Over 30 compounds including many relatively unexplored bioactive compounds were successfully identified from that screen. Here, we applied this library to screen for novel antimicrobial compounds. To this end, we screened antimicrobial activity against seven pathogenic bacterial strains. Next, we purified the active compounds using ethyl acetate extraction and HPLC fractionation and identified them using chemical analysis. The identified metabolites consist of both known antimicrobial compounds as well as relatively unexplored compounds. One of these compounds was berkchaetoazaphilone B (BAB), an anti-cancer compound found in 2015 [21], which was identified to contain antimicrobial activity in this screen.

MATERIALS AND METHODS

Strains, reagents and cultures

Pathogenic bacteria were obtained from University Medical Center Utrecht and are listed in Table S1. *Bacillus subtilis* strain 168 was used to test antimicrobial activity in this study [22]. Fungal strains were obtained from Westerdijk Fungal Biodiversity Institute and were inoculated for 7 days on Malt Extract Agar (MEA) plates. For liquid cultures, two cubes of agar with surface area of approximately 0.25 cm^2 from each fungal species were cut and transferred into a 100 mL bottle containing 50 mL culturing medium (3.5% Czapek Dox Broth (CDB) + 0.5% yeast extract (YE)). Cultures were incubated at 25 °C for 7-14 days (depending on their growth) and were then filtered using 0.22 μm Millipore filters. For plate cultures, two cubes of agar from each fungal species were cut and transferred onto new specific agar plates and incubated at 25 °C for 7-14 days, depending on their growth. Commercial antimicrobials and resazurin were purchased from Sigma Aldrich. FM4-64 and $DiSC_3(5)$ were purchased from Thermo Fisher Scientific.

Antimicrobial activity screening

Bacterial cultures of different strains were grown to early exponential-phase in Mueller Hinton Broth (MHB) from their overnight cultures. Then they were diluted 1:100 into MHB, distributed into 96-well plates and tested with 1:1 ratio of fungal supernatants. Inhibition of bacterial growth was checked based on visual inspection after an overnight incubation at 37 °C. Antimicrobial activities and maximum inhibitory dilution (MID) were determined by testing of a range of fungal supernatant dilutions in a broth microdilution assay [23]. MID was defined as the highest dilution at which bacteria did not grow, based on visual inspection after an overnight incubation at 37 °C.

Purification and identification of biologically active compounds

Liquid cultures or agar plates were extracted with ethyl acetate. The solvent was evaporated and the residue was dissolved in DMSO. Extracts were fractionated using a modular preparative high-performance liquid chromatography (HPLC) system (Shimadzu) using a C18 reversed phase Reprosil column (10 µm, 120 Å, 250 × 22 mm). The mobile phase was 0.1% trifluoroacetic acid in water (buffer A) and 0.1% trifluoroacetic acid in acetonitrile (buffer B) in a linear gradient. Fractions were collected, dried in an Eppendorf speedvac concentrator, dissolved in DMSO and tested for antimicrobial activities.

The identification procedure was performed as previously described [20] using preparative HPLC (Shimadzu) using a Shimadzu Shim-pack GISTC18-HP reversed phase column (3 µm, 4.6 × 100 mm) coupled to a LCMS-2020 mass spectrometer (Shimadzu). High resolution mass spectrometry (HRMS) was measured on either a µQTOF instrument (Micromass Ltd) or an LCT instrument (Micromass Ltd). Samples were dissolved in DMSO-d_6 or $CDCl_3$ for NMR spectroscopy. ^{1}H-NMR, HSQC, HMBC and COSY spectra were measured at either 300 MHz, 400 MHz, 500 MHz or 600 MHz using either a Mercury-300, an Agilent-400, an INOVA-500 or a Bruker-600 spectometer. ^{13}C-NMR was measured using the same instruments at either 100 MHz or in case the Bruker-600 instrument was used at 150 MHz.

Growth curves

The overnight cultures of *B. subtilis* were diluted 1:50 into fresh LB medium and incubated at 37 °C with shaking. OD_{600} of cultures were measured by a FLUOstar microplate reader (BMG Labtech) every 30 min for 24 h. At an OD_{600} of 0.3, different concentrations of BAB were added.

Confocal microscopy

Microscopy was performed using a Perkin Elmer UltraView VoX spinning disk microscope essentially as described [24] and analyzed using Volocity v6.3 software. Z-stack images were collected over a length of 3 μm with 0.2 μm intervals and analyzed using Fiji [25].

Sporulation inhibition assay

Sporulation was assayed as previously described with modifications [26]. Antimicrobials (5 × minimal inhibitory concentration, MIC) or DMSO (control) were added and incubated with rolling at 37 °C for 5 h. Cells were then stained with FM 4–64, immobilized and imaged.

Resazurin assay

This resazurin oxidation–reduction indicator [27] assay was done as previously described [24]. Freshly prepared early exponential-phase cell cultures with an OD_{600} of 0.3 in LB medium were treated with antimicrobials (5 × MIC) or DMSO (control) for 5, 20 or 60 min. Cells were then incubated with 30 μg/mL resazurin for 45 min at 37 °C. Cells without any agent and boiled cells (95°C for 10 min) were used to calculate the standard respiration and no respiration, respectively. Absorbance of different samples was measured using a 540 nm/590 nm filter.

Screen for hypersensitive S. aureus transposon mutants to BAB with Nebraska Transposon Mutant Library (NTML)

The NTML consists of 1920 *S. aureus* transposon mutants. The strains were inoculated with 100 μL MHB containing 5 μg/mL erythromycin in sterile round-bottom 96-wells plates at 37 °C with shaking overnight. On the second day, 5 μL overnight culture was transferred into 95 μL MHB containing 5 μg/mL erythromycin for 2 h to make the start culture. Next, 5 μL start culture was added into 95 μL fresh MHB containing an antimicrobial of interest. After incubation overnight at 37 °C with shaking, bacterial growth was inspected visually.

Cytotoxicity assay

HepG2 cells were seeded in 96-well plates and grown in DMEM low glucose medium (ThermoFisher) supplemented with 10% FBS. Test compounds were added in different concentrations, with a final concentration of 1% DMSO and cells were

incubated for 20 h at 37 °C with 5% CO_2. Next, resazurin (Sigma-Aldrich) was added to reach a final concentration of 0.1 mM. After 3 h incubation, the fluorescence was measured on a PHERAstar microplate reader (BMG Labtech). Experiments were conducted in biological triplicates. IC_{50} was calculated using nonlinear regression in GraphPad Prism.

Measuring bioenergetics using Seahorse

Seahorse Bioscience XFe24 Analyzer was used to measure extracellular acidification rates (ECAR) in mpH/minute and oxygen consumption rates (OCR) in pmol O_2/ minute essentially as described before [28]. Cells were seeded in XF24 polystyrene cell culture microplates (Seahorse Bioscience) at a density of 20,000 cells per well. One hour before the measurements, culture medium was replaced either with or without BAB and the plate was incubated for 60 minutes at 37 °C. For the mitochondrial stress test, culture medium was replaced by Seahorse XF Base medium (Seahorse Bioscience), supplemented with 20 mM glucose (Sigma-Aldrich), 2 mM L-glutamine (Sigma-Aldrich), 5 mM pyruvate (Sigma-Aldrich) and 0.56 µL NaOH (1 M). During the test 5 µM oligomycin, 2 µM FCCP and 1 µM of Rotenone and Antimycin A (all Sigma-Aldrich) were injected into each well after 18, 45 and 63 minutes respectively. For the glycolysis stress test, culture medium was replaced by Seahorse XF Base medium, supplemented with 2 mM L-glutamine and 0.52 µL/mL NaOH (1M). Sensor cartridges (pre-hydrated in XF calibrant solution overnight in a CO_2-free incubator) were loaded with glucose (Port A), oligomycin (Port B), and 2-deoxyglucose (2-DG, Port C) to achieve concentrations of 1 mM, 2 µM, and 50 mM, respectively, after injection. During the test 10 mM glucose, 5 µM oligomycin and 100 mM 2-deoxyglucose (2-DG) (Sigma-Aldrich) were injected into each well after 18, 36 and 65 minutes respectively. After injections, measurements of 2 minutes were performed in triplicate, preceded by 4 minutes of mixture time. The first measurements after oligomycin injections were preceded by 5 minutes mixture time, followed by 8 minutes waiting time for the mitochondrial stress test and 5 minutes mixture time followed by 10 minutes waiting time for the glycolysis stress test. Both ECAR and OCR were normalized to individual protein amount, and data were analysed using the XF Mito Stress Test Report Generator.

RESULTS

In search of antimicrobials from a fungal metabolites library

To assess the antimicrobial activity of the fungal metabolite library, an initial screen was done by testing all the 10,207 fungal supernatants on seven pathogenic bacteria, including three Gram-positive strains and four Gram-negative strains. To determine their activity, log-phase bacteria were grown overnight in the presence of fungal supernatant. Subsequently, the inhibitory effect was scored by visual inspection. A total inhibition was recorded as "1" and no inhibition as "0". For some of the hits against *Staphylococcus aureus* USA300, bacterial growth was affected but not 100% inhibited. For these, a number of "0.5" was recorded. In the end, 280 fungi

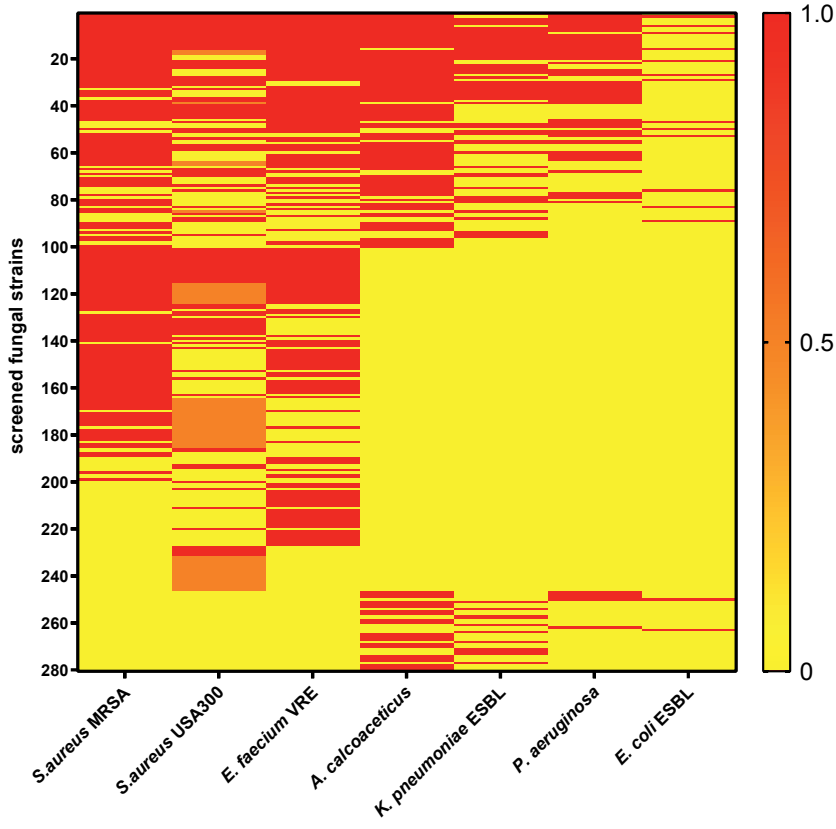

Fig. 1. Initial screen for antimicrobial activity from fungal secondary metabolites library. Each row of the map shows the activity of a single fungus against seven different bacteria. Active, half-active and inactive are indicated as "1" (red), "0.5" (orange) and "0" (yellow), respectively.

(2.7%) were defined as antimicrobial strains and listed in Fig. 1 as they showed antimicrobial activity against at least one of the bacterial strains. Among all tested pathogenic bacteria, the greatest number of hits was found to inhibit the growth of *S. aureus*. There were more than 140 hits against each of the two pathogenic *S. aureus* strains we tested. In contrast, the extended spectrum beta-lactamase (ESBL) producing *Escherichia coli* was the most difficult pathogen to target in our assays, as we found only 15 hits.

Of the 280 fungi with potential antimicrobial activity, 36% (100 strains) showed activity against both Gram-positive and Gram-negative bacteria. No fungus inhibited all seven pathogens but 39 fungi were able to affect the growth of five or six bacterial strains, including 28 fungi from the genera of *Aspergillus* and *Penicillium*. The species from these two genera are well studied producers of antimicrobial compounds, which provided proof-of-principle for the method we applied to uncover antimicrobial producing fungi. The other 180 strains showed activity only against Gram-positive or Gram-negative bacteria. In line with the notion that Gram-positive bacteria are more sensitive to antimicrobials than Gram-negative bacteria [29], 146 strains (52% of the total hits) only affected the growth of Gram-positive bacteria and 34 strains (12% of the total) only inhibited growth of Gram-negative bacteria.

As expected, there were multiple well-known producers of antimicrobial agents among the potential hits. To increase the chances to identify compounds that had not been described before, we focused on poorly studied fungi of which no information was available about secondary metabolites. We selected 56 fungal strains in this category and investigated their antimicrobial activities in detail.

Identification strategy of antimicrobial compounds

The secondary metabolites responsible for the observed antimicrobial activities were isolated and identified, using an activity-guided purification and identification procedure as outlined in Fig. 2 (Process A). First, to increase the yield of fungal compounds, we cultured 1 L of each fungus in liquid medium and extracted metabolites from the liquid culture with ethyl acetate. The extracts were dried using a rotary evaporator and dissolved in DMSO.

The widely used Gram-positive bacteria model, *B. subtilis* strain 168, was used as a read-out for further analysis of the antimicrobial activities and for analysis of the MoA of selected antimicrobial agents. The ethyl acetate extracts were tested on *B. subtilis* using microdilution assay until 320 × diluted and the maximum inhibitory dilution (MID) was recorded as the criterion of the activity. In the end, 47 extracts

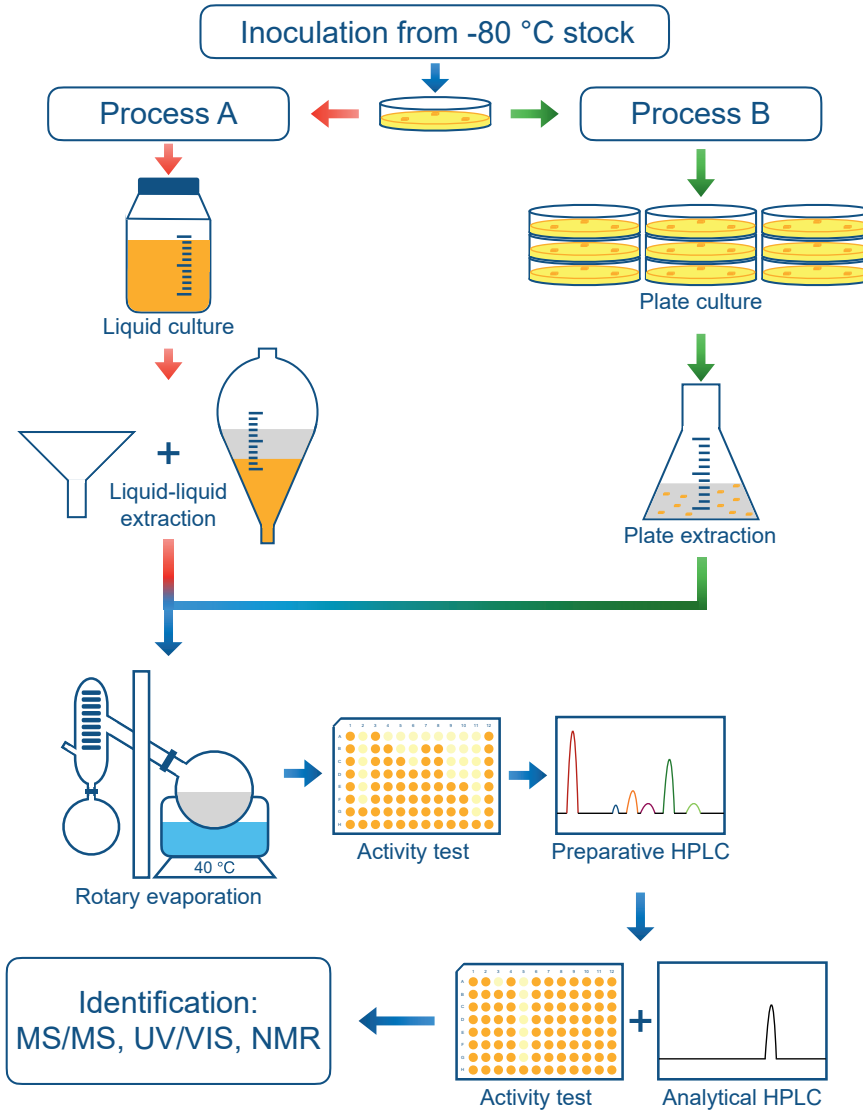

Fig. 2. Identification strategy of antimicrobial compounds from fungi. Fungi were inoculated on agar plates and subsequently cultured in liquid media, filtrated by 0.22 µm filter, and extracted with ethyl acetate as shown in Process A (red arrows). Next, samples were concentrated using a rotary evaporator and tested for their antimicrobial activity in 96-well plates. Active samples were fractionated by preparative-HPLC, followed by activity (96-well plates) and purity (analytical HPLC) check. Pure active fractions were then identified by a combination of several chemical analyses. If the yield of active compounds was not sufficient by culturing in liquid medium, plate extraction (Process B, green arrows) was applied by culturing fungi on agar plates and extracting compounds with ethyl acetate directly from cultures on agar.

Table 1. Fungal stains with identified metabolites. The 26 selected fungal strains with identified activities are listed. The initial activity of their fungal liquid-liquid extracts (in maximum inhibitory dilution, MID) and the identification process that was used (A1 means from Process A without culturing optimization; A2 means Process A with culturing optimization; and B means from Process B) were also present. The strains without CBS numbers were a gift from the Westerdijk fungal biodiversity institute.

CBS number	Species	MID	Process A or B	Metabolites
CBS 111.69	*Corynascus sepedonium*	320	A1	UCS-1025A
CBS 180.74	*Sarocladium oryzae*	320	A1	helvolic acid
CBS 194.67	*Ulocladium atrum*	160	A2	dehydrocurvularin
CBS 245.59	*Fusarium sacchari*	320	A1	fusaric acid
CBS 279.58	*Paecilomyces lilacinus*	80	A2	leucinostatins
CBS 305.72	*Trichophaea abundans*	80	A2	anthracobic acid A
CBS 316.67	*Eupenicillium senticosum*	320	A1	dehydrocurvularin
CBS 348.82	*Dactylaria lanosa*	80	A2	norlichexanthone
CBS 349.73	*Monochaetia lutea*	320	B	rugulosin A
CBS 366.71	*Oidiodendron flavum*	40	B	harzianic acid
CBS 399.73	*Sarocladium attenuatum*	320	A1	helvolic acid
CBS 417.64	*Mortierella globulifera*	320	A1	leucinostatins
CBS 438.86	*Arthroderma tuberculatum*	320	A1	fusidic acid
CBS 511.67	*Stilbella fimetaria*	320	A1	helvolic acid
CBS 573.67	*Pleurostomophora richardsiae*	320	B	berkchaetoazaphilone B
CBS 668.70	*Clonostachys compactiuscula*	160	B	TMC-154
CBS 114383	*Corynascus sepedonium*	320	A1	UCS-1025A
CBS 124389	*Cristaspora arxii*	160	B	gliotoxin
/	Unknown species 2121	320	B	asterric acid, 4'-chloroasterric acid, geodin hydrate
/	Unknown species 2172	320	A1	citrinin
/	Unknown species 2212	320	A1	citrinin
/	Unknown species 2239	80	A2	citrinin
/	Unknown species 2287	80	A2	citrinin
/	Unknown species 2288	320	A1	leucinostatins
/	Unknown species 2998	160	B	rugulosin A
/	Unknown species 9806	320	A1	helvolic acid

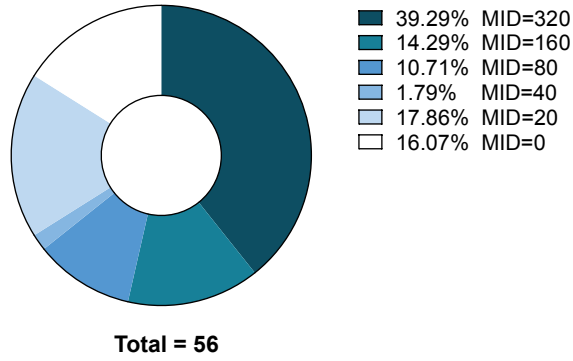

Fig. 3. Re-screen of antimicrobial activity from 56 hits. The extracts from 56 fungi were tested for their maximum inhibitory dilutions (MIDs) against *B. subtilis*. The MID of each fungus was plotted in a pie chart. Highest active dilution was 320 × diluted.

(around 84% of the strains, Fig. 3) showed antimicrobial activity. Of these, 22 strains showed MIDs greater or equal to 320, 8 showed MIDs equal to 160, and 17 showed MIDs less than 100. These 47 extracts were fractionated through preparative HPLC to obtain pure compounds. The resulting fractions, each containing a single HPLC peak were then tested on *B. subtilis*. For the chemical analysis, we first determined the purity, UV/ VIS spectra and nominal mass of the active fractions using analytical HPLC and LC-MS. Next, we compared the resulting data with available literature and databases [30,31], through which we were able to identify several compounds from active fractions as previously identified compounds. For the remaining unsolved fractions, accurate mass was determined through high resolution mass spectrometry (HRMS) and structural information was obtained using ^{1}H-NMR, ^{13}C-NMR and 2D-NMR.

Through activity-directed purification as described above, the antimicrobial agents from 13 fungi were successfully identified (A1 in Table 1). For the other strains, the amounts of active compound(s) were not sufficient for chemical analysis. Therefore, we sought to increase the yield of secondary metabolites through optimization.

Optimization for yield of fungal secondary metabolites

Environmental factors such as temperature, oxygen, humidity and nutrients are important for fungal metabolic pathways [32–34]. Here, we optimized four aspects of the culturing conditions: temperature, oxygen content, liquid growth medium and inoculating agar plates. Each of these aspects influenced the production of antimicrobial activity to a different extent in different fungi (examples in Table S2).

In the end, the antimicrobial compounds from six more fungi were identified (A2 in Table 1). Surprisingly, some fungal species, like the case of *Monochaetia lutea*, showed remarkable morphological differences on different inoculation plates (Fig. S1), but the activity of the respective liquid cultures did not differ much (Table S2). To study the differences further, we set up an alternative strategy to obtain secondary metabolites, which was to extract compounds directly from agar plates, as outlined in Fig. 2 (Process B). In practice, we compared agar-extracts from fungi grown on different plates using analytical HPLC and microdilution assay, to select the best conditions for large-scale cultures. Using the plate extraction strategy, the active compounds from seven fungi were successfully identified (Table 1).

Identification of BAB from Pleurostomophora richardsiae

The supernatant of *P. richardsiae* was shown to have antimicrobial activity in the initial screen and the active fraction was determined in the re-screen. However, the activity appeared to vary across different batches of liquid cultures (Fig. 4A). To optimize the production of the active fraction, we extracted the secondary metabolites from plate cultures (Fig. 4B). Analytical HPLC analysis of plate extracts from different agars showed that potato dextrose agar (PDA) plates induced the highest yield of the active compound (Fig. 4C). Subsequently, we cultured this fungus on 20 PDA plates and obtained sufficient amounts of the active fraction for its identification using chemical analyses.

First, the active fraction was measured on an LC-MS with diode array detection to assess the purity and meanwhile obtain a UV-Vis spectrum. The UV-Vis spectrum showed a distinct pattern with maximum absorption at 354 nm and lower peaks at 248 nm and 213 nm (Fig. 4D). The mass spectra revealed a M+H ion signal of 445.1 in the positive spectrum and a M-H ion signal of 443.1 in the negative spectrum (Fig. 4E), indicating a nominal mass of 444 for the main compound of the fraction. Next, HRMS was performed on the active compound and a mass of 467.2060 was found for the M+Na ion. Finally, nuclear magnetic resonance (NMR) spectra were collected using ^{1}H, ^{13}C, Heteronuclear Single-Quantum Correlation Spectroscopy (HSQC), Heteronuclear Multiple-Bond Correlation spectroscopy (HMBC) and homonuclear correlation (COSY) (Table S3, Fig. S2). All data combined indicated that this compound was BAB, previously published by Stierle et al [21].

Berkchaetoazaphilone B (Fig. 4F): $C_{25}H_{32}O_7$. HRMS: found 467.2060 (M+Na), calculated 467.2046 for $C_{25}H_{32}O_7Na$. NMR (400 MHz, DMSO-d_6): see Table S3. UV-Vis λ_{max}: 213 nm, 248 nm, 354 nm.

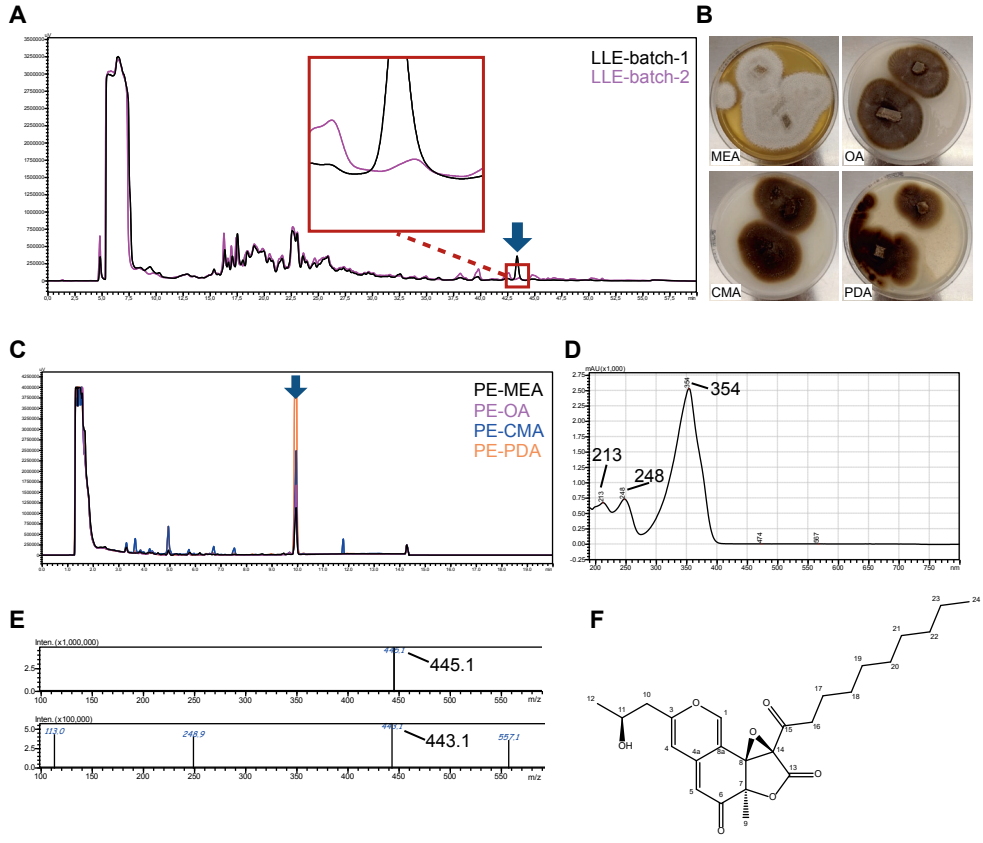

Fig. 4. Identification of the antimicrobial activity from fungus *Pleurostomophora richardsiae*. (A) Preparative HPLC profiles of extracts from two batches of liquid culture using liquid-liquid extraction (LLE). (B) *P. richardsiae* cultured on different kinds of agar. (C) Comparison of different plate extractions (PE) on analytical HPLC. (D) UV spectrum of the active compound from this fungus. (E) Mass spectrum of the active compound. (F) Chemical structure of BAB, the antimicrobial activity from *P. richardsiae*.

Fungi produced a variety of structurally different compounds with antimicrobial activity

Using our antimicrobial identification strategy, 17 antimicrobial agents were successfully identified from 26 fungi (Table 1, Fig. 4F, Fig. S3) and the chemical data that were used to identify compounds are listed in the Supplementary Material. Previously, we found that two of these compounds, fusaric acid and anthracobic acid also induced developmental defects in a zebrafish screen and we have described these compounds before [20]. Some of the antimicrobial compounds that we identified

were reported to have other kinds of activities, including immunosuppressive activity of gliotoxin [35], anti-osteoporosis activity of norlichexanthone [36] and plant promoting activity of harzianic acid [37]. Structurally, these fungal secondary metabolites belong to a variety of chemical groups including polyketides (e.g. TMC-154, citrinin and BAB), lactones (e.g. dehydrocurvularin), lipopeptides (e.g. leucinostatins), terpenoids (e.g. helvolic acid) and piperazines (e.g. gliotoxin), suggesting our strategy was effective for purification and identification of diverse chemical groups.

A noteworthy compound we found in our screen is BAB, which was initially identified and described as a cytotoxin towards human cancer cells in 2015 [21]. No data were available about its antimicrobial activity. Therefore, we investigated its antimicrobial properties.

BAB has antimicrobial activity against Gram-positive bacteria

First, to determine the antimicrobial spectrum of BAB, we tested its minimum inhibitory concentration (MIC) on 13 bacterial strains (Table S4). Most Gram-positive bacteria were inhibited at MICs between 50 and 200 µg/mL, including a vancomycin-resistant *Enterococcus faecium* (VRE) strain. However, BAB had no effect on any of the Gram-negative bacteria we tested. This suggested that BAB is a selective antimicrobial against Gram-positive bacteria. Therefore, we chose a model organism of Gram-positive bacteria, *B. subtilis* strain 168, to further describe its antimicrobial property. The growth curves of *B. subtilis* in response to a concentration range of BAB showed that bacterial growth was affected from 30 µg/mL onwards, and that growth was completely arrested from 50 µg/mL onwards (Fig. 5A). The OD_{600} decreased at 30 µg/mL and higher, suggesting that BAB might induce cell lysis.

Some microorganisms, including *B. subtilis*, respond to harsh environments by entering a robust resting state, the endospore, which is self-protective. During that process, cells may also lyse [38]. To determine whether BAB destroyed the cells and/or induced the cells to form endospores, a sporulation assay was performed (Fig. 5B). In the control-treated samples, spores were clearly observed in the overnight culture with high cell density. Following BAB treatment, only cell debris was evident in the micrographs. This suggests that BAB destroyed the cells without inducing spore formation.

To determine if the cell lysis was due to a direct target of BAB in the cell membrane, a cell depolarization assay was performed using $DiSC_3(5)$. Treatment with carbonyl

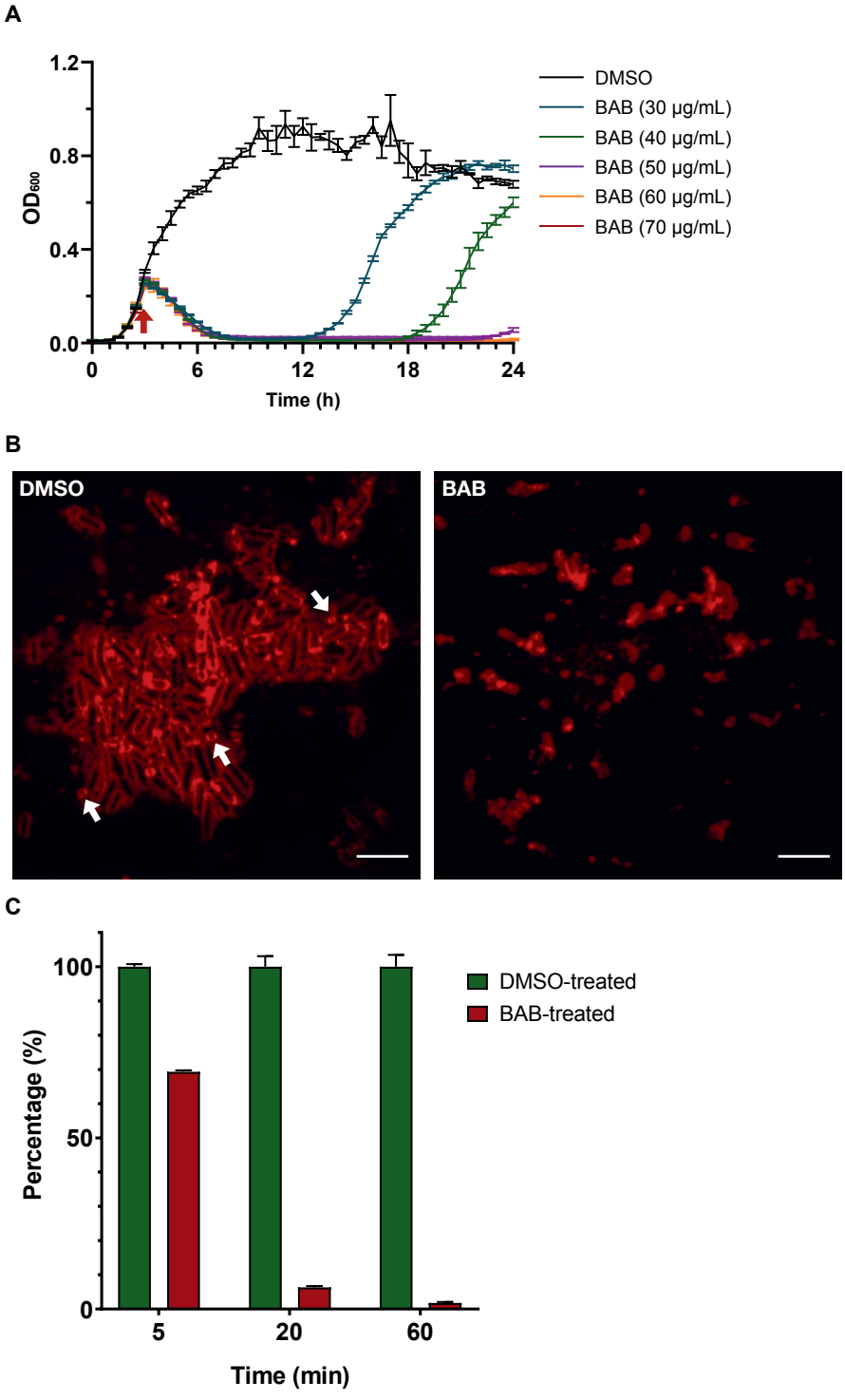
A
1.2
0.8
0.4
0.0
OD600
0
6
12
18
24
Time (h)
DMSO
BAB (30 µg/mL)
BAB (40 µg/mL)
BAB (50 µg/mL)
BAB (60 µg/mL)
BAB (70 µg/mL)
B
DMSO
BAB
C
100
50
0
Percentage (%)
5
20
60
Time (min)
DMSO-treated
BAB-treated

Fig. 5. Antimicrobial properties of BAB. (A) Growth curves of *B. subtilis* in the presence of a range of BAB concentrations. OD_{600} was measured every 30 min. BAB was added at 2 h 45 min (arrow indicated). The graph depicts the average and the SEM of biological triplicates. (B) No sporulation in response to BAB. *B. subtilis* cells from high intensity overnight culture were treated with DMSO (control) or BAB (250 µg/mL, 5 × MIC), stained with FM4-64 and imaged by confocal fluorescence microscopy. Representative images are shown. Example spores in the DMSO control are indicated with arrows. Scale bar is 5 µm. (C) Effect on respiratory chain activity measured by the reduction from blue resazurin to red resorufin at 540 nm. The average intensity of DMSO control in each group was set as 100% intensity and the percentage of each treated sample was calculated. The mean from biological triplicates was plotted with error bars representing the SEM.

cyanide m-chlorophenyl hydrazone (CCCP), a control compound that induces cell depolarization, led to an increase in fluorescence. Rifampin and DMSO treated samples were used as negative controls. Surprisingly, BAB treatment led to a sudden decrease (to an average of 33% of control) in fluorescence (Fig. S4A). However, the decrease in signal was due to a direct effect of BAB on $DiSC_3(5)$, because BAB also caused a decrease (to 33% of control) in fluorescence in cell-free medium (Fig. S4B). Therefore, interpretation of these data is hampered and we cannot conclude whether or not BAB affected cell depolarization.

Colorimetric analysis of respiratory chain activity using resazurin indicated that more than 90% of the cells had lost their viability at 20 min treatment (Fig. 5C). Taken together, BAB treatment inhibited bacterial growth in a dose-dependent manner and induced lysis of bacteria, but not sporulation. BAB treatment led to rapid respiratory chain activity arrest.

BAB affects energy metabolism

To further determine the targets of BAB, we applied a sensitivity screen on Nebraska Transposon Mutant Library (NTML). This library contains approximately 2,000 *S. aureus* transposon mutants, each with a distinct disruption of a non-essential gene in the genome [39]. We screened for mutants that were more sensitive to BAB, because the corresponding genes might be essential to compensate for the defects caused by BAB. First, five random strains were selected to determine the MIC. Next, 0.5 x MIC was applied to each of the 1,920 strains and affected strains were selected. As listed in Table 2, the growth of 23 strains was inhibited in the first run. A MIC assay was performed to verify these hits, confirming that 16 strains indeed were hypersensitive to BAB and thus were regarded as potential hits.

Notably among these hits, half were involved in energy metabolism (Table 2, Fig. S5), including two hits in glycolysis, two in the citric acid cycle, one in purine

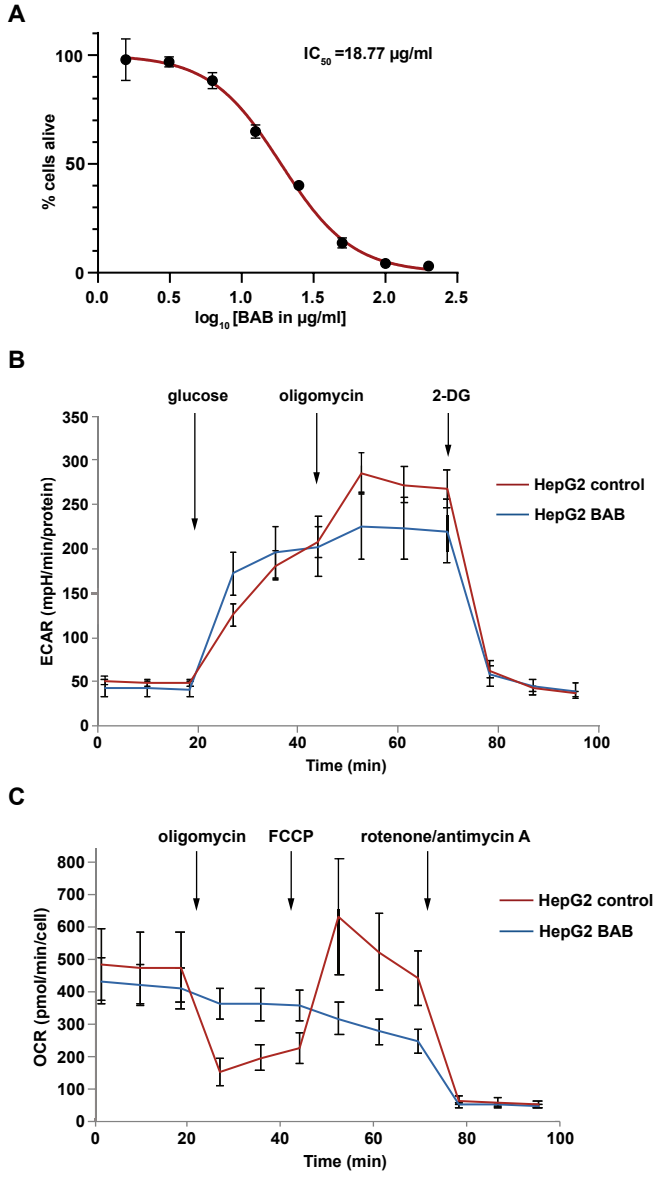

Fig. 6. Cytotoxicity of BAB on HepG2 cells may be caused by effects on energy metabolism. (A) HepG2 cells with BAB in different concentrations were incubated for 20 h and afterwards resazurin was added. The ability to reduce blue resazurin to red resorufin was measured at 540 nm. The average intensity of DMSO control was set as 100% alive and the percentage of intensity from each treated sample was calculated. The mean from biological triplicates was plotted with error bars representing the SEM in black. Nonlinear regression was analyzed and plotted in red, on which IC_{50} was based. (B, C) HepG2 cells either untreated or pre-treated with BAB were compared in a glycolysis and mitochondrial test using Seahorse technology to measure extracellular acidification rates (ECAR) in mpH/minute and oxygen

consumption rates (OCR) in pmol O_2/minute. (B) For the glycolysis stress test, 10 mM glucose, 5 μM oligomycin and 100 mM 2-deoxyglucose (2-DG) were injected into each well after 18, 36 and 65 minutes respectively. (C) For the mitochondrial stress test, 5 μM oligomycin, 2 μM FCCP and 1 μM of Rotenone and Antimycin A were injected to each well after 18, 45 and 63 minutes respectively. Both ECAR and OCR were normalized to individual protein amount, and data from biological triplicates were presented by mean with error bars representing the SEM.

Table 2. NTML screening suggests energy metabolism as target of BAB. 0.5 x MIC of BAB was tested on each of the 1,920 strains and 23 inhibited strains were selected. These hits were verified with MIC assay and 16 strains indeed were hypersensitive to BAB. The mutated gene with its gene function and involved pathway for each of the 16 hits is presented.

Number in NTML	Verification	Gene	Gene function	Pathway
NE91	Yes	kdpA	K+-transporting ATPase, A subunit	ATPase
NE353	Yes	/	bifunctional purine biosynthesis protein	purine biosynthesis
NE427	Yes	fumC	fumarate hydratase, class II	citric acid cycle
NE522	Yes	purB	adenylosuccinate lyase	purine biosynthesis
NE592	Yes	atpA	ATP synthase F1, alpha subunit	ATP synthesis
NE635	Yes	ribE	riboflavin synthase, alpha subunit	riboflavin synthesis
NE716	Yes	/	putative membrane protein	/
NE744	/	/	/	/
NE950	/	/	/	/
NE1004	/	/	/	/
NE1016	Yes	/	acetyltransferase	citric acid cycle
NE1040	Yes	mutY	A/G-specific adenine glycosylase	DNA repair
NE1260	Yes	pckA	phosphoenolpyruvate carboxykinase	Glycolysis
NE1263	Yes	mtlD	mannitol-1-phosphate 5-dehydrogenase	Glycolysis
NE1318	Yes	ribH	6,7-dimethyl-8-ribityllumazine synthase	riboflavin synthesis
NE1343	/	/	/	/
NE1345	/	/	/	/
NE1381	/	/	/	/
NE1494	Yes	rnc	ribonuclease III	RNA synthesis
NE1569	Yes	/	superantigen-like protein	immune system
NE1757	Yes	lspA	lipoprotein signal peptidase	/
NE1794	Yes	/	Holliday junction resolvase-like protein	DNA segregation
NE1833	/	/	/	/

biosynthesis, one in purine nucleotide cycle, one in ATP synthesis and one in the group of ATPases. The two riboflavin synthesis hits are also involved in energy metabolism. The remaining hits appeared not to have correlations with any of the other hits, or with each other. Based on these data, we hypothesized that BAB might affect energy metabolism.

From our experiments, it is evident that BAB has bactericidal activity on Gram-positive bacteria. We assessed cytotoxicity of BAB on eukaryotic cells as well and found that BAB is cytotoxic for HepG2 cells with an IC_{50} of 18.77 μg/mL (Fig. 6A). Given the apparent involvement of BAB in energy metabolism of bacteria, we wondered whether BAB also targets energy metabolism in eukaryotic cells. To investigate this, we assayed the effect of BAB on bioenergetics of eukaryotic cells. We compared HepG2 cells either untreated or pre-treated with BAB in a glycolysis and mitochondrial test using Seahorse technology. BAB pre-treatment consistently resulted in a more rapid increase in glycolysis, yet reduced glycolytic capacity (Fig. 6B). This is likely linked to the clear impairment of mitochondrial function due to BAB pre-treatment. Pre-treatment with BAB resulted in a strong reduction in ATP forming capacity by mitochondria and an almost complete block of the carbonyl cyanide 4-(trifluoromethoxy)phenylhydrazone (FCCP)-induced increase in mitochondrial respiration, suggesting that BAB blocks either complex I or II or both (Fig. 6C). This inhibition of mitochondrial respiration and ATP formation likely explains increased glycolysis to uphold sufficient cellular ATP in BAB treated cells. Irrespective, these data clearly show that BAB has an effect on cellular bioenergetics, most profoundly on mitochondrial respiration, and this may underlie the mechanism of BAB.

DISCUSSION

Here, we screened for antimicrobial compounds from a fungal secondary metabolite library. In the end, the antimicrobial agents from almost half of the selected fungi were successfully identified. This suggests that our approach using ethyl acetate extraction (liquid-liquid extraction or plate extraction), reversed phase preparative-HPLC, analytical-HPLC, MS/MS and NMR can reliably be used for identification of a wide range of structurally different antimicrobial compounds. Ethyl acetate facilitates extraction of both polar and non-polar biological compounds [40]. However, in practice, highly polar compounds were not extracted efficiently, indicating that other approaches might be needed to extract these compounds.

All but one of the antimicrobial agents that we identified (Table 1) have been described before. Rediscovery of compounds is a widely acknowledged problem with activity-guided discovery approaches. BAB had not been reported to have antimicrobial activity. Previously, this compound was reported to have anti-cancer properties [21]. Our study showed that it had strong anti-bacterial activity against Gram-positive bacteria. By a series of bioactivity assays, we found that BAB rapidly blocked oxidation-reduction in bacteria, concomitant with cell lysis. Whether the cell envelope was targeted directly could not be concluded from the data, because BAB directly affected the indicator dye, even in the absence of cells. The NTML screening suggested that BAB influenced energy metabolism in bacteria. This was in line with cell metabolism assays, which suggested that BAB inhibited mitochondrial metabolism completely in HepG2 cells. Although the cytotoxicity of BAB precludes its potential to be a clinical antibiotic, it is still interesting to study its targets in more detail, because this might result in identification of new targets for antibiotic discovery and this might help to better understand BAB's mechanism of inhibiting cancer cell growth.

We believe that there are more interesting fungi producing antimicrobial agents in our fungal library. In the analysis of positive hits, we made a selection and did not cover all of the hits from the initial screening. Among the remaining hits were many strains that are known producers of antimicrobials. Whereas these strains were not selected for further analysis, these are still interesting for further studies and have a chance to produce novel antimicrobials. Actually, much work is still being done with the genera of *Aspergillus* or *Penicillium*, and recently new antimicrobial compounds were identified from them [41–44]. In addition, many potential antimicrobial producing fungi may not have scored positive in our initial screen. These may have gone unnoticed due to low production of active compound, i.e. at levels below MIC. There are options to further screen these fungi, such as to enhance the yield of secondary metabolites by plate extractions instead of liquid-liquid extractions (cf. Fig. 2, 4, S1), to optimize the growth conditions for secondary metabolite production, or to activate silent gene clusters that often encompass the genes encoding the enzymes that produce secondary metabolites by co-culturing with histone deacetylase inhibitors, such as suberoylanilide hydroxamic acid or anacardic acid [45,46].

To conclude, we found 280 fungal strains with antimicrobial activity among a library of 10,207 fungi and subsequently identified 17 structurally distinct compounds from 26 strains out of the 56 fungi that were selected for further analysis. This indicates that our screening strategy worked for antimicrobial discovery and

our fungal collection is a promising source for bioactive compounds. Among the identified compounds, one antimicrobial agent, BAB, was an interesting compound with unknown MoA. We found that BAB treatment affected energy metabolism in both prokaryotic and eukaryotic cells.

ACKNOWLEDGEMENTS

We like to thank Albert Heck, Cees Versluis and Arjan Barendregt for their help with HRMS measurements, Geert-Jan Boons, Rob Liskamp, John Kruijtzer, Johan Kemmink and Justyna Dobruchowska for their help with NMR measurements, Ronnie Lubbers for critical reading of the manuscript and Yara Mangindaan, Helen Buttstedt and Harm van Es, students of the den Hertog Lab at the Hubrecht Institute for technical support. This project was supported by the Chinese Scholarship Council (CSC).

REFERENCES

[1] WA A. The Treasure Called Antibiotics. Ann Ibadan Postgrad Med 2016;14:56–7.

[2] Stone MRL, Butler MS, Phetsang W, Cooper MA, Blaskovich MAT. Fluorescent Antibiotics: New Research Tools to Fight Antibiotic Resistance. Trends Biotechnol 2018;36:523–36. https://doi.org/10.1016/j.tibtech.2018.01.004.

[3] Dcosta VM, King CE, Kalan L, Morar M, Sung WWL, Schwarz C, et al. Antibiotic resistance is ancient. Nature 2011;477:457–61. https://doi.org/10.1038/nature10388.

[4] Ling LL, Schneider T, Peoples AJ, Spoering AL, Engels I, Conlon BP, et al. A new antibiotic kills pathogens without detectable resistance. Nature 2015;517:455–9. https://doi.org/10.1038/nature14098.

[5] Park AJ, Krieger JR, Khursigara CM. Survival proteomes: The emerging proteotype of antimicrobial resistance. FEMS Microbiol Rev 2016;40:323–42. https://doi.org/10.1093/femsre/fuv051.

[6] Davies J. Origins and evolution of antibiotic resistance. Microbiologia 1996;12:9–16. https://doi.org/10.1128/mmbr.00016-10.

[7] Hancock REW. Mechanisms of action of newer antibiotics for Gram-positive pathogens. Lancet Infect Dis 2005;5:209–18. https://doi.org/10.1016/S1473-3099(05)70051-7.

[8] Gelband H, Miller-Petrie M, Pant S, Gandra S, Levinson J, Barter D, et al. The state of the world's antibiotics 2015. Wound Heal South Africa 2015;8:30–4.

[9] Butler MS, Buss AD. Natural products - The future scaffolds for novel antibiotics? Biochem Pharmacol 2006;71:919–29. https://doi.org/10.1016/j.bcp.2005.10.012.

[10] Aly AH, Debbab A, Proksch P. Fifty years of drug discovery from fungi. Fungal Divers 2011;50:3–19. https://doi.org/10.1007/s13225-011-0116-y.

[11] Keller NP, Turner G, Bennett JW. Fungal secondary metabolism - From biochemistry to genomics. Nat Rev Microbiol 2005;3:937–47. https://doi.org/10.1038/nrmicro1286.

[12] Bennett JW, Bentley R. What's in a Name?-Microbial Secondary Metabolism. Adv Appl Microbiol 1989;34:1–28. https://doi.org/10.1016/S0065-2164(08)70316-2.

[13] Brakhage AA. Regulation of fungal secondary metabolism. Nat Rev Microbiol 2013;11:21–32. https://doi.org/10.1038/nrmicro2916.

[14] Keller NP. Fungal secondary metabolism: regulation, function and drug discovery. Nat Rev Microbiol 2019;17:167–80. https://doi.org/10.1038/s41579-018-0121-1.

[15] Eisenman HC, Casadevall A. Synthesis and assembly of fungal melanin. Appl Microbiol Biotechnol 2012;93:931–40. https://doi.org/10.1007/s00253-011-3777-2.

[16] Tauber JP, Gallegos-Monterrosa R, Kovács ÁT, Shelest E, Hoffmeister D. Dissimilar pigment regulation in Serpula lacrymans and Paxillus involutus during inter-kingdom interactions. Microbiol (United Kingdom) 2018;164:65–77. https://doi.org/10.1099/mic.0.000582.

[17] RAISTRICK H. A region of biosynthesis. Proc R Soc Lond B Biol Sci 1950;136. https://doi.org/10.1142/9789812795984_0035.

[18] Blackwell M. The fungi: 1, 2, 3 ... 5.1 million species? Am J Bot 2011;98:426–38. https://doi.org/10.3732/ajb.1000298.

[19] Kück U, Bloemendal S, Teichert I. Putting Fungi to Work: Harvesting a Cornucopia of

Drugs, Toxins, and Antibiotics. PLoS Pathog 2014;10:3–6. https://doi.org/10.1371/journal.ppat.1003950.

[20] Hoeksma J, Misset T, Wever C, Kemmink J, Kruijtzer J, Versluis K, et al. A new perspective on fungal metabolites: identification of bioactive compounds from fungi using zebrafish embryogenesis as read-out. Sci Rep 2019;9:1–16. https://doi.org/10.1038/s41598-019-54127-9.

[21] Stierle AA, Stierle DB, Girtsman T, Mou TC, Antczak C, Djaballah H. Azaphilones from an Acid Mine Extremophile Strain of a Pleurostomophora sp. J Nat Prod 2015;78:2917–23. https://doi.org/10.1021/acs.jnatprod.5b00519.

[22] Kunst F, Ogasawara N, Moszer I, Albertini AM, Alloni G, Azevedo V, et al. The complete genome sequence of the gram-positive bacterium Bacillus subtilis. Nature 1997;390:249–56. https://doi.org/10.1038/36786.

[23] Zgoda JR, Porter JR. A convenient microdilution method for screening natural products against bacteria and fungi. Pharm Biol 2001;39:221–5. https://doi.org/10.1076/phbi.39.3.221.5934.

[24] Müller A, Wenzel M, Strahl H, Grein F, Saaki TNV, Kohl B, et al. Daptomycin inhibits cell envelope synthesis by interfering with fluid membrane microdomains. Proc Natl Acad Sci U S A 2016;113:E7077–86. https://doi.org/10.1073/pnas.1611173113.

[25] Schindelin J, Arganda-Carreras I, Frise E, Kaynig V, Longair M, Pietzsch T, et al. Fiji: An open-source platform for biological-image analysis. Nat Methods 2012;9:676–82. https://doi.org/10.1038/nmeth.2019.

[26] Lamsa A, Liu WT, Dorrestein PC, Pogliano K. The Bacillus subtilis cannibalism toxin SDP collapses the proton motive force and induces autolysis. Mol Microbiol 2012;84:486–500. https://doi.org/10.1111/j.1365-2958.2012.08038.x.

[27] Chen JL, Steele TWJ, Stuckey DC. Modeling and Application of a Rapid Fluorescence-Based Assay for Biotoxicity in Anaerobic Digestion. Environ Sci Technol 2015;49:13463–71. https://doi.org/10.1021/acs.est.5b03050.

[28] Ludikhuize MC, Meerlo M, Gallego MP, Xanthakis D, Burgaya Julià M, Nguyen NTB, et al. Mitochondria Define Intestinal Stem Cell Differentiation Downstream of a FOXO/Notch Axis. Cell Metab 2020;32:889-900.e7. https://doi.org/10.1016/j.cmet.2020.10.005.

[29] Breijyeh Z, Jubeh B, Karaman R. Resistance of gram-negative bacteria to current antibacterial agents and approaches to resolve it. Molecules 2020;25. https://doi.org/10.3390/molecules25061340.

[30] Cole RJ, Jarvis BB, Schweikert MA. Handbook of Secondary Fungal Metabolites. vol. 1–3. Elsevier; 2003.

[31] Nielsen KF, Smedsgaard J. Fungal metabolite screening: Database of 474 mycotoxins and fungal metabolites for dereplication by standardised liquid chromatography-UV-mass spectrometry methodology. J Chromatogr A 2003;1002:111–36. https://doi.org/10.1016/S0021-9673(03)00490-4.

[32] Yogabaanu U, Weber JFF, Convey P, Rizman-Idid M, Alias SA. Antimicrobial properties and the influence of temperature on secondary metabolite production in cold environment soil fungi. Polar Sci 2017;14:60–7. https://doi.org/10.1016/j.polar.2017.09.005.

[33] Shang Z, Li XM, Li CS, Wang BG. Diverse secondary metabolites produced by marine-derived fungus nigrospora sp. MA75 on various culture media. Chem Biodivers 2012;9:1338–48. https://

doi.org/10.1002/cbdv.201100216.

[34] Félix C, Salvatore MM, DellaGreca M, Ferreira V, Duarte AS, Salvatore F, et al. Secondary metabolites produced by grapevine strains of Lasiodiplodia theobromae grown at two different temperatures. Mycologia 2019;111:466–76. https://doi.org/10.1080/00275514.2019.1600342.

[35] Kataoka T, Nagai K. Molecular dissection of cytotoxic functions mediated by T cells. Prog. Biotechnol., vol. 22, Elsevier; 2002, p. 13–23. https://doi.org/10.1016/S0921-0423(02)80039-9.

[36] Wang K, Chen Y, Gao S, Wang M, Ge M, Yang Q, et al. Norlichexanthone purified from plant endophyte prevents postmenopausal osteoporosis by targeting ERα to inhibit RANKL signaling. Acta Pharm Sin B 2021;11:442–55. https://doi.org/10.1016/j.apsb.2020.09.012.

[37] Vinale F, Flematti G, Sivasithamparam K, Lorito M, Marra R, Skelton BW, et al. Harzianic acid, an antifungal and plant growth promoting metabolite from Trichoderma harzianum. J Nat Prod 2009;72:2032–5. https://doi.org/10.1021/np900548p.

[38] Smith TJ, Foster SJ. Characterization of the involvement of two compensatory autolysins in mother cell lysis during sporulation of Bacillus subtilis 168. vol. 177. 1995. https://doi.org/10.1128/jb.177.13.3855-3862.1995.

[39] Fey PD, Endres JL, Yajjala VK, Widhelm TJ, Boissy RJ, Bose JL, et al. A genetic resource for rapid and comprehensive phenotype screening of nonessential Staphylococcus aureus genes. MBio 2013;4:537–49. https://doi.org/10.1128/mBio.00537-12.

[40] Pihlström T, Blomkvist G, Friman P, Pagard U, Österdahl BG. Analysis of pesticide residues in fruit and vegetables with ethyl acetate extraction using gas and liquid chromatography with tandem mass spectrometric detection. Anal Bioanal Chem 2007;389:1773–89. https://doi.org/10.1007/s00216-007-1425-6.

[41] Zheng YY, Liang ZY, Shen NX, Liu WL, Zhou XJ, Fu XM, et al. New naphtho-pyrones isolated from marine-derived fungus penicillium sp. hk1-22 and their antimicrobial activities. Mar Drugs 2019;17. https://doi.org/10.3390/md17060322.

[42] Liu YJ, Zhang JL, Li C, Mu XG, Liu XL, Wang L, et al. Antimicrobial Secondary Metabolites from the Seawater-Derived Fungus Aspergillus sydowii SW9. Molecules 2019;24:4596. https://doi.org/10.3390/molecules24244596.

[43] Padhi S, Masi M, Panda SK, Luyten W, Cimmino A, Tayung K, et al. Antimicrobial secondary metabolites of an endolichenic Aspergillus niger isolated from lichen thallus of Parmotrema ravum. Nat Prod Res 2020;34:2573–80. https://doi.org/10.1080/14786419.2018.1544982.

[44] Jiang B, Wang Z, Xu C, Liu W, Jiang D. Screening and identification of Aspergillus activity against Xanthomonas oryzae pv. oryzae and analysis of antimicrobial components. J Microbiol 2019;57:597–605. https://doi.org/10.1007/s12275-019-8330-5.

[45] Chung YM, El-Shazly M, Chuang DW, Hwang TL, Asai T, Oshima Y, et al. Suberoylanilide hydroxamic acid, a histone deacetylase inhibitor, induces the production of anti-inflammatory cyclodepsipeptides from Beauveria felina. J Nat Prod 2013;76:1260–6. https://doi.org/10.1021/np400143j.

[46] Mafezoli J, Xu Y ming, Hilário F, Freidhof B, Espinosa-Artiles P, dos Santos LC, et al. Modulation of polyketide biosynthetic pathway of the endophytic fungus, Anteaglonium sp. FL0768, by copper (II) and anacardic acid. Phytochem Lett 2018;28:157–63. https://doi.org/10.1016/j.phytol.2018.10.011.

SUPPORTING INFORMATION

Table S1. Pathogenic bacteria used in this study. a= Gift from University Medical Center Utrecht; b= ATCC strains.

Strain	For initial screening	For BAB assay
Acinetobacter baumannii 1179 [a]		✓
Acinetobacter calcoaceticus [a]	✓	
Acinetobacter nosocomialis 14-8211 [a]		✓
Enterobacter cloacae complex MC04842 [a]		✓
Enterococcus faecium GV15A623 [a]		✓
Enterococcus faecium VRE GV16D030 [a]	✓	✓
Escherichia coli TEM-3 GVJS004 [a]	✓	✓
Klebsiella pneumoniae SHV-18 GVJS006 [a]	✓	✓
Listeria monocytogenes GV21-4a [a]		✓
Pseudomonas aeruginosa ATCC57853 [b]	✓	✓
Staphylococcus aureus MRSA [a]	✓	
Staphylococcus aureus MSSA 476 GVS0101 [a]		✓
Staphylococcus aureus MRSA USA300 [a]	✓	
Staphylococcus epidermidis GV08A1071 [a]		✓
Stenotrophomonas maltophilia GV20A226 [a]		✓
Streptococcus pneumoniae 05A396 [a]		✓

Table S2. MID of fungal extracts under different growth conditions of liquid culture. Numbers indicate the Maximum Inhibitory Dilution (MID) of fungal extracts that inhibit the growth of *B. subtilis*. Numbers were repetitive. a= Standard, b= Temperature, c= Oxygen content, d= Growth medium, e= Inoculating plate; f. MEA= Malt Extract Agar, OA= Oat Agar, CMA= Cornmeal Agar, PDA= Potato Dextrose Agar; g. CDB= Czapek Dox Broth, YE= Yeast Extract, MEB= Malt Extract Broth.

Variable	SD[a]	TEMP[b]	OC[c]	GM[d]	GM	IP[e]	IP	IP
Temperature	25 °C	15 °C	25 °C	25 °C	25 °C	25 °C	25 °C	25 °C
Shaking	No	No	Yes	No	No	No	No	No
Inoculating plate[f]	MEA	MEA	MEA	MEA	MEA	OA	CMA	PDA
Growth medium[g]	CDB+YE	CDB+YE	CDB+YE	MEB	CDB	CDB+YE	CDB+YE	CDB+YE
Pleurostomophora richardsiae	10	0	0	10	10	10	10	10
Clonostachys compactiuscula	10	10	10	160	20	20	20	20
Monochaetia lutea	40	10	10	40	20	80	80	80
Cristaspora arxii	20	0	0	20	0	20	20	20

Table S3. Assignments NMR-shifts + HMBC and COSY couplings for BAB. a= measured at 100 MHz, b= measured at 400 MHz, d= measured at 150 MHz, d= measured at 600 MHz, e= overlapping signals

berkchaetoazaphilone B (DMSO-d_6)						
	DMSO-d_6		$CDCl_3$			
#	δC[a]	δH[b]	δC[c]	δH[d]	HMBC[b]	COSY[b]
1	148.4	7,69 (s)	147.8	7.48 (s)	3, 4a, 8, 8a	-
3	161.9	-	161.1	-	-	-
4	108.4	6.41 (s)	108.3	6.14 (s)	3, 5, 8a, 10	-
4a	145.6	-	145.3	-	-	-
5	104.7	5.37 (s)	105.2	5.41 (s)	7, 8a	-
6	188.5	-	189.4	-	-	-
7	84.1	-	84.1	-	-	-
8	72.4	-	72.1	-	-	-
8a	107.4	-	107.7	-	-	-
9	19.0	1.46 (s)	18.7	1.61 (s)	6, 7, 8	-
10	42.9	2.48 (m)	42.7	2.56 (m)	3, 4, 11, 12	11
11	64.5	3.91 (m)	65.5	4.18 (m)	3	10,12
12	23.9	1.11 (d)	23.7	1.32 (d)	10, 11	11
13	166.5	-	165.5	-	-	
14	66.8	-	66.8	-	-	
15	197.0	-	195.7	-	-	
16	41.6	2.90 (m) 2.75 (m)	42.0	2.84 (m) 2.62 (m)	15, 17, 18-21[e]	17
17	23.0	1.41 (t)	23.2	1.50 (m)	15, 16, 18-21[e]	16
18	28.7	1.17[e]	28.9	1.20[e]	[e]	[e]
19	29.1	1.17[e]	29.2	1.28[e]	[e]	[e]
20	29.2	1.17[e]	29.2	1.28[e]	[e]	[e]
21	29.2	1.17[e]	29.3	1.28[e]	[e]	[e]
22	31.7	1.21[e]	31.8	1.23[e]	[e]	[e]
23	22.6	1.23[e]	22.6	1.28[e]	22	24
24	14.4	0.85 (t)	14.1	0.87 (t)	22, 23	23

Table S4. MICs of BAB on pathogenic bacteria. MICs of BAB on different bacteria were tested starting at a 400 mg/L which was then serially diluted with a factor 2.

Strain	Gram	MIC (mg/L)
Acinetobacter baumannii 1179	-	> 400
Acinetobacter nosocomialis 14-8211	-	> 400
Enterobacter cloacae complex MC04842	-	> 400
Escherichia coli TEM-3 GVJS004	-	> 400
Klebsiella pneumoniae SHV-18 GVJS006	-	> 400
Pseudomonas aeruginosa ATCC57853	-	> 400
Stenotrophomonas maltophilia GV20A226	-	> 400
Enterococcus faecium VRE GV16D030	+	200
*Enterococcus faecium*GV15A623	+	100
Listeria monocytogenes GV21-4a	+	100
Staphylococcus aureus MSSA 476 GVS0101	+	50
Staphylococcus epidermidis GV08A1071	+	200
Streptococcus pneumoniae 05A396	+	50

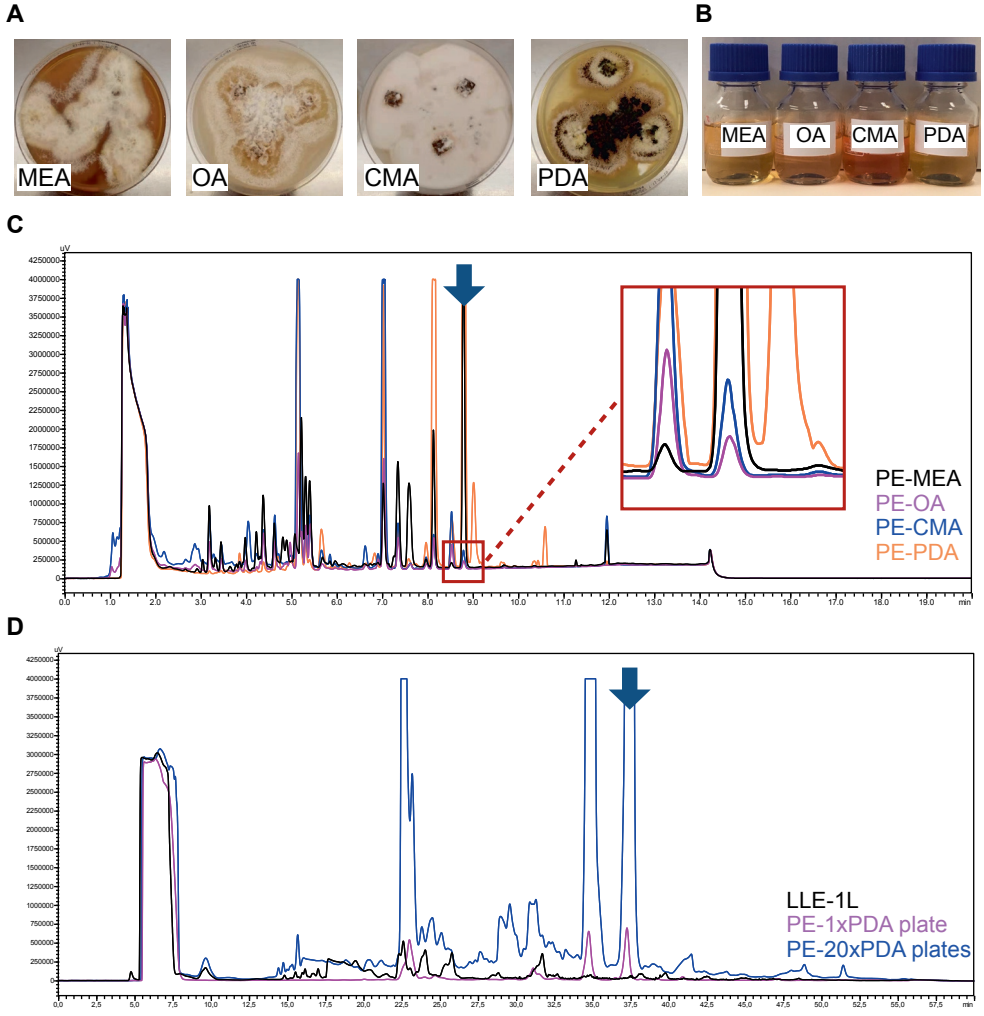

Fig. S1. Plate extraction profiles of fungus *Monochaetia lutea*. Fungus *M. lutea* was cultured on different kinds of agar (A) and extracted by plate extraction (PE) using ethyl acetate (B). The ethyl acetate extracts were then concentrated 1,000 times and analyzed on analytical HPLC (C). The comparison of liquid-liquid extraction (LLE) from 1L culture and PE from both 1 plate and from 20 plates is shown in (D). Arrow indicates active fraction, which was identified to be rugulosin A.

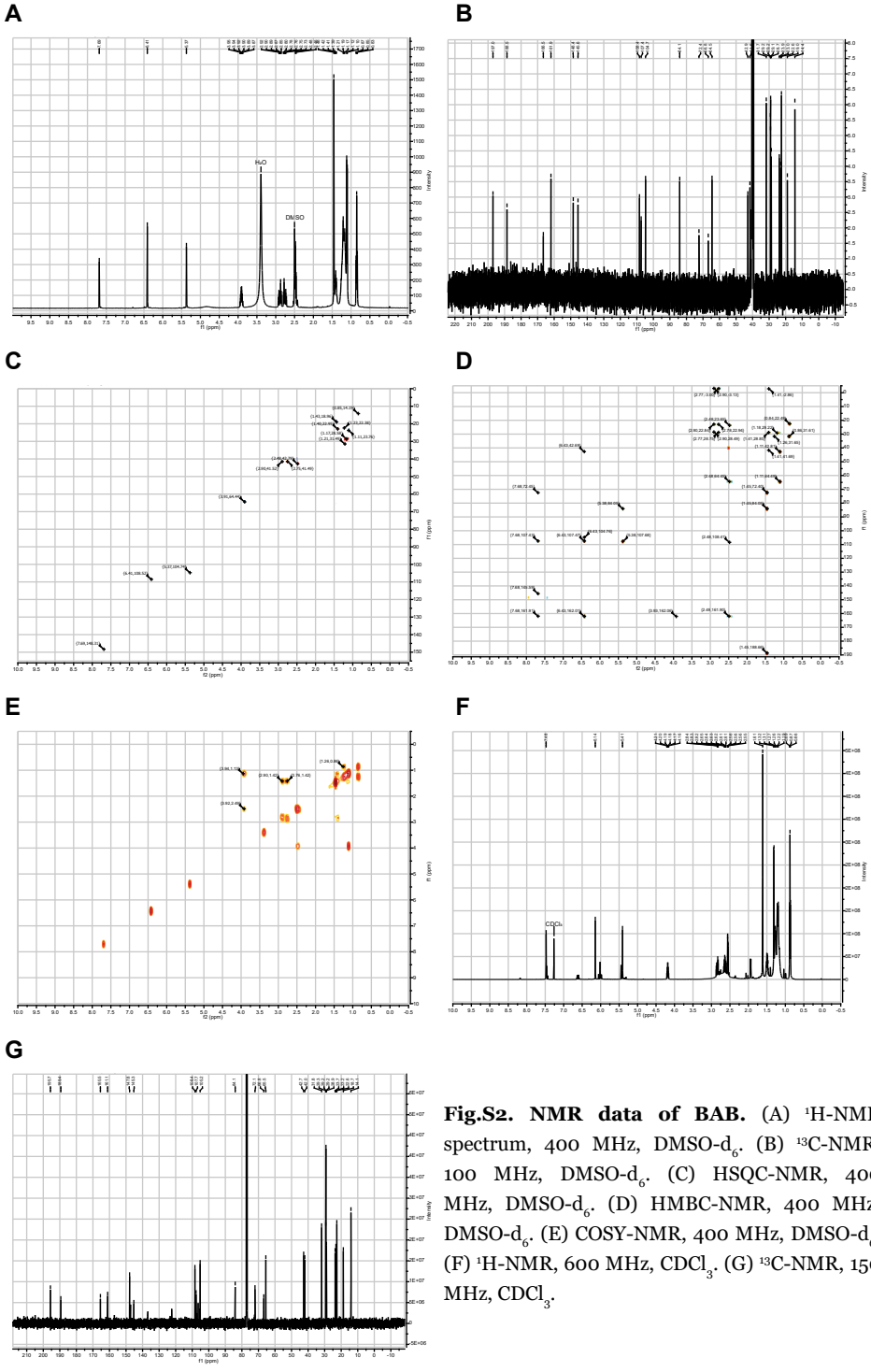

Fig.S2. NMR data of BAB. (A) ^{1}H-NMR spectrum, 400 MHz, DMSO-d_6. (B) ^{13}C-NMR, 100 MHz, DMSO-d_6. (C) HSQC-NMR, 400 MHz, DMSO-d_6. (D) HMBC-NMR, 400 MHz, DMSO-d_6. (E) COSY-NMR, 400 MHz, DMSO-d_6. (F) ^{1}H-NMR, 600 MHz, $CDCl_3$. (G) ^{13}C-NMR, 150 MHz, $CDCl_3$.

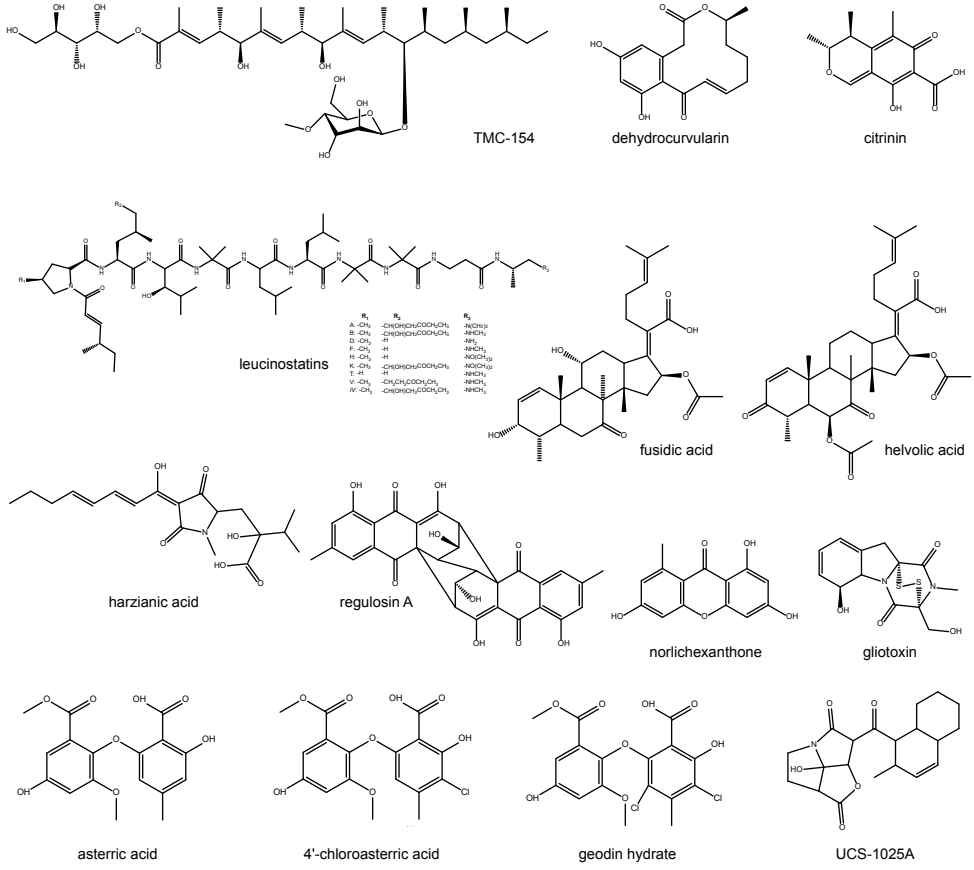

Fig. S3. Chemical structures of the antimicrobial compounds identified from this screen.

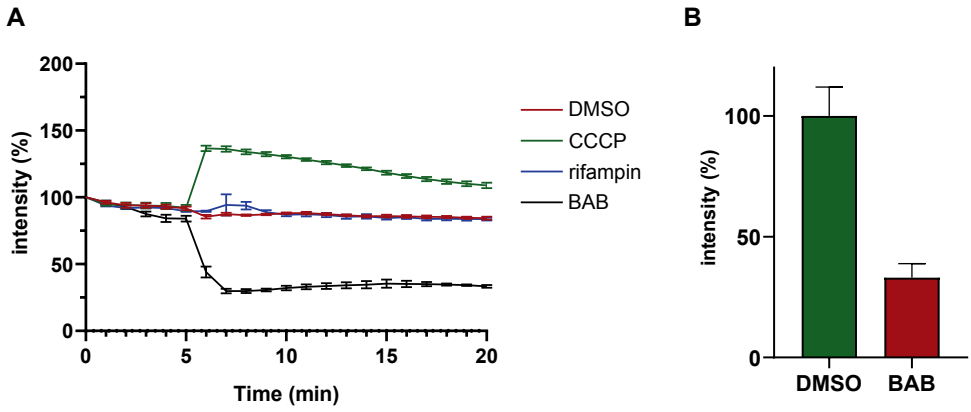

Fig. S4. Effect of BAB on membrane potential. Cell depolarization assay using $DiSC_3(5)$ dye. (A) *B. subtilis* membrane potential levels were quantified using the fluorescent dye $DiSC_3(5)$. Antimicrobials (as indicated) or DMSO were added after 5 min. The fluorescence is depicted as percentage of the value at the start (t = 0 min) over time (min). The mean from biological triplicates is plotted with error bars representing the SEM. Treatment with CCCP (positive control) resulted in an increase in signal due to release of the dye in the medium. Rifampin and DMSO (solvent control) did not affect fluorescence. Surprisingly, BAB treatment resulted in a decrease in signal. (B) Measurements of fluorescence intensity of $DiSC_3(5)$ in cell-free LB media showed direct, effect of BAB on $DiSC_3(5)$ fluorescence in the absence of cells to the same extent as in (A). The mean from technical triplicates is plotted with error bars representing the SEM.

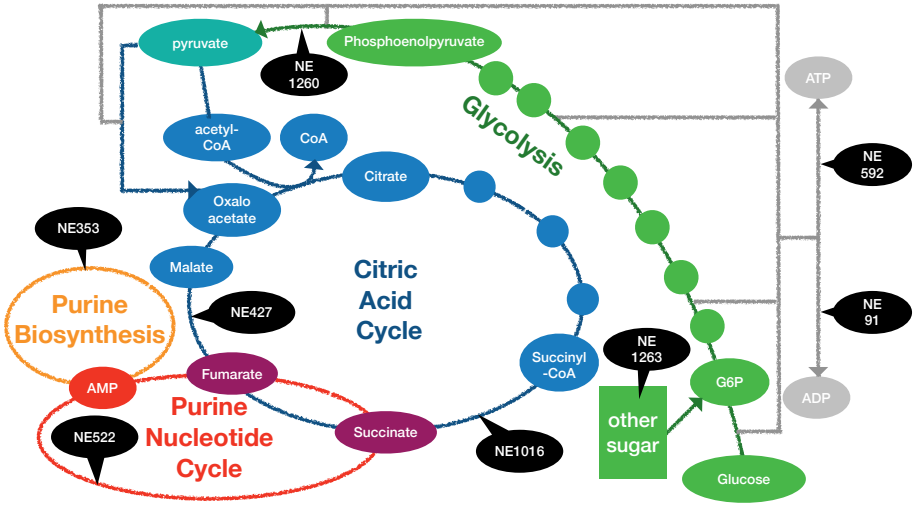

Fig. S5. Schematics on metabolism of energy. The correlation of glycolysis (green), citric acid cycle (blue), purine nucleotide cycle (red) and purine biosynthesis (orange) was listed in the scheme. The processes that involved ATP and ADP transformation were pointed in grey. The processes that NTML hits were involved were pointed in black.

Supplementary Notes

Anthracobic acid A: See the paper from Hoeksma et al. [1] for details.

Citrinin: $C_{13}H_{14}O_5$. HRMS: found 273.0706 (M+Na), calculated 273.0739 for $C_{13}H_{14}O_5Na$. ^{1}H-NMR (600MHz, DMSO-d_6): δ= 15.41 (s, OH); 8.63 (s, 1H); 5.00 (dd, *J*= 6.6 Hz, 1H); 3.60 (s, 1H); 3.22 (dd, *J*= 7.2 Hz, 1H); 1.98 (s, 3H); 1.27 (d, *J*= 6.7 Hz, 3H); 1.14 (d, *J*= 7.2 Hz, 3H). ^{13}C-NMR (150MHz, DMSO-d_6): δ= 183.0; 176.9; 174.6; 167.4; 141.5; 121.9; 106.9; 99.8; 82.6; 34.0; 18.5; 18.0; 9.5. UV-Vis λ_{max}: 236 nm, 332 nm. Data consistent with data published by Nielsen and Smedsgaard [2], Barber et al. [3] and Poupko et al. [4].

Asterric acid: $C_{17}H_{16}O_8$. HRMS: found 371.0734 (M+Na), calculated 371.0743 for $C_{17}H_{16}O_8Na$. ^{1}H-NMR (600MHz, DMSO-d_6): δ= 12.98 (bs, 1H); 11.21 (bs, 1H); 9.89 (s, 1H); 6.79 (s, 1H); 6.78 (s, 1H); 6.34 (s, 1H); 6.67 (s, 1H); 3.70 (s, 3H); 3.62 (s, 3H); 2.07 (s, 3H). ^{13}C-NMR (150 MHz, DMSO-d_6): δ= 170.3; 165.6; 160.4; 159.0; 155.6; 153.8; 143.7; 134.4; 125.8; 110.3; 108.0; 105.4; 105.2; 104.5; 56.5; 52.5; 21.9. UV-Vis λ_{max}: 209 nm, 248 nm (sh), 315 nm. Data consistent with data published by Nielsen and Smedsgaard [2] and Liu et al. [5]. Confirmed by commercially available compound.

Dehydrocurvularin: $C_{16}H_{18}O_5$. LCMS (ESI): 291.1 (M+H). ^{1}H-NMR (600MHz, DMSO-d_6): δ= 6.37 (m, 1H); 6.32 (s,1H); 6.24 (s, 2H); 4.74 (m, 1H); 3.38 (dd, *J*= 32.9, 15.6 Hz, 2H); 2.29, 2.18 (m, 2H); 1.82, 1.42 (m, 2H); 1.75, 1.46 (m, 2H); 1.11 (d, *J*= 6.4 Hz. 3H). ^{13}C-NMR (150MHz, DMSO-d_6): δ= 198.1; 170.8; 159.5; 157.9; 154.3; 134.2; 133.0; 118.5; 110.0; 101.9; 72.6; 40.0; 33.8; 33.2; 24.3; 20.4. UV-Vis λ_{max}: 201 nm, 225 nm, 294 nm, 330 nm (sh). Data consistent with data published by Nielsen and Smedsgaard [2] and Kumar et al. [6].

Geodin hydrate: $C_{17}H_{14}Cl_2O_8$. HRMS: found 438.9919 (M+Na), calculated 438.9963 for $C_{17}H_{14}Cl_2O_8Na$. ^{1}H-NMR (600MHz, DMSO-d_6): δ= 9.66 (s, OH); 6.70 (d, *J*= 2.8 Hz, 1H); 6.61 (d, *J*= 2.8 Hz, 1H); 3.63 (s, 3H); 3.54 (s, 3H); 2.43 (s, 3H). ^{13}C-NMR (150 MHz, DMSO-d_6): δ= 165.4; 163.6; 154.3; 152.6; 151.2; 150.6; 136.8; 136.7; 124.3; 116.3; 116.2; 113.5; 107.5; 105.2; 56.7; 52.3; 18.6. UV-Vis λ_{max}: 215 nm, 323 nm. Data consistent with data published by Nielsen and Smedsgaard [2] and Liu et al. [5]. Confirmed by commercially available compound.

4'-Chloroasterric acid: $C_{16}H_{13}ClO_8$. HRMS: found 405.0327 (M+Na), calculated 405.0353 for $C_{17}H_{15}ClO_8Na$. ^{1}H-NMR (600MHz, DMSO-d_6): δ= 9.93 (s, 1H); 6.80 (d, *J*= 2.8 Hz, 1H); 6.79 (d, *J*= 2.8 Hz, 1H); 5.90 (s, 1H); 3.71 (s, 3H); 3.63 (s, 3H); 2.17 (s, 3H). ^{13}C-NMR (150MHz, DMSO-d_6): 171.1; 165.2; 157.6; 156.9; 155.7; 153.6; 142.0; 134.2; 125.4; 113.7; 108.2; 106.7; 105.3; 104.5; 56.5; 52.4; 20.9. UV-Vis λ_{max}: 208 nm, 249 nm (sh), 321 nm. Data consistent with data published by Liu et al. [5].

Fusaric acid: See the paper from Hoeksma et al. [1] for details.

Fusidic acid: $C_{31}H_{48}O_6$. HRMS: found 539.3337 (M+Na), calculated 539.3349 for $C_{31}H_{48}O_6$. UV-Vis λ_{max}: 200 nm, 220 (sh) nm. Data consistent with data published by Nielsen and Smedsgaard [2]. Confirmed by commercially available compound.

Gliotoxin: $C_{13}H_{14}N_2O_4S_2$. HRMS: found 327.0490 (M+H), calculated 327.0490 for $C_{13}H_{15}N_2O_4S_2$. ^{1}H-NMR (600MHz, DMSO-d_6): δ= 6.03 (m, 1H); 5.97 (m, 1H); 5.65 (d, 1H, *J*= 9.7 Hz); 4.86 (m, 1H); 4.55 (d, *J*= 13.1 Hz, 1H); 4.34 (d, *J*= 12.7 Hz, 1H); 4.23 (d, *J*= 12.7 Hz, 1H); 4.07 (d, *J*= 11.4 Hz), 3.74 (d, *J*= 11.4 Hz) (1H); 3.64 (m, 1H); 3.11 (s, 3H); 3.00 (s, 1H). ^{13}C-NMR (150MHz, DMSO-d_6): δ= 166.0; 164.6, 133.3, 130.1; 124.1; 119.3; 78.8; 76.3; 73.2; 69.8; 59.2; 36.3; 28.1. UV-Vis λ_{max}: 200 nm, 268 nm. Data consistent with data published by Kaouadji et al. [7] and Sun et al. [8].

Harzianic acid: $C_{19}H_{27}NO_6$. HRMS: found 388.1750 (M+Na), calculated 388.1736 for $C_{19}H_{27}NO_6Na$. Elemental composition analyses: C 61,4%; O 21,8%; H 7,0%; N 3,8%. ^{1}H-NMR (600 MHz, $CDCl_3$): δ= 7.55 (m, 1H); 7.00 (d, *J*= 15.1 Hz, 1H); 6.38 (m, 1H), 6.37 (m, 1H); 3.63 (dd, *J*= 10.6, 1,0 Hz, 2H); 2.97 (s, 3H); 2.48-1.89 (d, 2H); 2.24 (dd, 2H); 2.02 (m, 1H); 1.50 (m, 2H); 0.99 (m, 3H); 0.99 (m, 3H); 0.95 (t, 3H). ^{13}C-NMR (150 MHz, $CDCl_3$): δ= 197.3; 176.7; 176.3; 173.2; 149.9; 147.6; 129.6; 119.1; 99.7; 79.9; 64.1; 36.0; 35.5; 33.8; 26.6; 21.8; 17.5; 16.2; 13.7. UV-Vis λ_{max}: 244 nm, 363 nm. Data consistent with data published by Sawa et al. [9].

Helvolic acid: $C_{33}H_{44}O_8$. HRMS: found 595.3248 (M+Na), calculated 595.3248 for $C_{33}H_{44}O_8Na$. ^{1}H-NMR (400 MHz, $CDCl_3$): δ= 7.33; 5.87; 5.25; 5.10; 2.78; 2.63; 2.45; 2.26; 2.11; 1.96; 1.69; 1.59; 1.44; 1.27; 1.18; 0.96. UV-Vis λ_{max}: 202 nm, 232 nm. Data consistent with data published by Nielsen and Smedsgaard [2] and Tschen et al. [10].

Leucinostatins: Leucinostatin A: $C_{62}H_{111}N_{11}O_{13}$. LCMS (ESI+): 1218.9 (M+H). MS-MS fragmentation: 1218.9 (base), 960.9, 875.8, 762.7, 649.6, 631.6, 564.5, 546.5, 435.2, 222.2. UV-Vis λ_{max}: 222 nm. Leucinostatin B: $C_{61}H_{109}N_{11}O_{13}$. LCMS (ESI+): 1205.4 (M+H). MS-MS fragmentation: 1205 (base), 960.9, 875.8, 762.7, 649.6, 631.6, 564.5, 546.5, 435.4, 222.2.

Leucinostatin D: $C_{57}H_{103}N_{11}O_{11}$. LCMS (ESI+): 1119.1 (M+H). MS-MS fragmentation: 1119 (base), 860.9, 775.8, 662.7, 549.5, 531.5, 464.5, 446.5, 335.3, 222.2.

Leucinostatin F: $C_{56}H_{101}N_{11}O_{11}$. LCMS (ESI+): 1105.7 (M+H). MS-MS fragmentation: 1105 (base), 860.9, 775.8, 662.7, 549.5, 531.5, 464.5, 446.5, 335.3, 222.2. Leucinostatin H: $C_{57}H_{103}N_{11}O_{12}$. LCMS (ESI+): 1135.5 (M+H). MS-MS fragmentation: 1135 (base), 860.9, 775.8, 662.7, 549.5, 531.5, 464.5, 446.5, 335.3, 222.2. Leucinostatin K: $C_{62}H_{111}N_{11}O_{14}$. LCMS (ESI+): 1235.2 (M+H). MS-MS fragmentation: 1234.8 (base), 960.9, 875.8, 762.7, 649.6, 631.6, 564.5, 546.5, 435.4, 222.2.

Leucinostatin T: $C_{55}H_{99}N_{11}O_{11}$. LCMS (ESI+): 1091.7 (M+H). MS-MS fragmentation: 1091 (base), 846.8, 761.7, 648.6, 535.5, 517.5, 450.4, 432.4, 321.3. 208.2. Leucinostatin V: $C_{61}H_{109}N_{11}O_{12}$. LCMS (ESI+): 1189.1 (M+H). MS-MS fragmentation: 1189 (base), 944.9, 859.9; 746.8, 633.6, 615.6, 548.6, 530.6, 419.4, 222.2.

Leucinostatin *IV*: $C_{61}H_{111}N_{11}O_{12}$. LCMS (ESI+): 1190.4 (M+H). MS-MS fragmentation: 1191 (base), 946.8, 875.8, 762.7, 649.6, 631.6, 617.5, 564.5, 546.5, 435.4, 222.2. Data consistent with data published by Isogai et al. [11] and Martinez and Morales [12].

Norlichexanthone: $C_{14}H_{10}O_5$. HRMS: found 259.0619 (M+H), calculated 259.0606 for $C_{14}H_{11}O_5$. ^{1}H-NMR (300 MHz, DMSO-d_6): δ= 6.66 (1H); 6.52 (1H); 6.28 (1H); 6.13 (1H); 2.73 (3H). Data consistent with data published by Nielsen and Smedsgaard [2] and Kawakami et al. [13].

Rugulosin A: $C_{30}H_{22}O_{10}$. HRMS: found 543.1292 (M+H), calculated 543.1291 for $C_{30}H_{23}O_{10}$. LCMS (ESI): 543.2 (M+H). ^{1}H-NMR (600 MHz, DMSO-d_6): δ= 14.73 (bs, OH); 11.41 (s, OH); 7.48 (d, *J*= 0.9 Hz, 1H); 7.22 (s, 1H); 4.41 (m, 1H); 3.39 (s, 1H); 2.81 (d, *J*= 6.0 Hz, 1H); 2.45 (s, 3H). ^{13}C-NMR (150 MHz, DMSO-d_6): δ= 194.4; 186.5; 181.1; 160.6; 148.1; 132.5; 124.5; 121.0; 114.6; 106.6; 69.0; 58.8; 56.1; 48.2; 21.9. UV-Vis λ_{max}: 250 nm, 392 nm. Data consistent with data published by Yamazaki et al. [14].

TMC-154: $C_{41}H_{72}O_{14}$. HRMS: found 811.4790 (M+Na), calculated 811.4820 for $C_{41}H_{72}O_{14}Na$. ^{1}H-NMR (600 MHz, DMSO-d_6): δ= 6.69 (dd, *J*= 14.8, 7.2Hz, 1H); 5.26 (d, *J*= 8.6 Hz, 1H); 5.21 (d, *J*= 8.6 Hz, 1H); 5.12 (d, *J*= 9.6 Hz, 1H); 4.86 (m, 1H); 4.55 (m, 1H); 4.16 (s, 1H); 3.88 (d, *J*= 8.2 Hz, 1H); 3.85[a*]; 3.67[a*]; 3.61[a*]; 3.59[a*]; 3.53[a*]; 3.44 (s, 1H); 3.43(s, 1H); 3.41 (s, 1H); 3.33 (d, *J*= 3.1 Hz, 1H); 3.31 (d, *J*= 2.8 Hz, 1H); 3.12 (m, 1H) ; 2.89 (m, 1H); 2.57 [a*]; 2.56 [a*]; 2.50 [a*]; 2.43 [a*]; 1.81 (s, 3H); 1.58 (s, 3H); 1,57 (s, 3H); 1.53 (s, 3H); 1.28[a]; 1.21-1.11 (2H) [a*]; 1.20 [a*]; 0.92 (d, *J*= 6.5 Hz, 3H); 0.82 [a*]; 0.79 [a*]; 0.78 [a*]; 0.72 (d, *J*= 6.3

Hz, 3H). ^{13}C-NMR (150 MHz, DMSO-d_6)*: δ= 167.4, 146.5, 138.2, 136.7, 136.1, 131.8, 131.1, 130.3, 127.3, 96.5, 86.2, 81.6, 81.2, 77.5, 76.9, 74.4, 73.4, 71.6, 70.2, 68.0, 64.0, 63.2, 61.3,60.0, 44.3, 37.4, 36.4, 34.4, 32.5, 30.2, 29.7, 21.9, 19.1, 17.8, 16.9, 12.9, 11.6, 11.6, 11.5. [a]= no multiple assignment due to overlapping peaks, *=tentative assignments based on HSQC and HMBC-NMR. UV-Vis λ_{max}: 195 nm, 227 nm (sh). Data consistent with data published by Kohno et al. [15].

UCS-1025A $C_{20}H_{25}NO_5$ HRMS: found 382.1623 (M+Na), calculated 382.1630 for $C_{20}H_{25}NO_5Na$. ^{1}H-NMR (500 MHz, $CDCl_3$): δ= 5.57 (m, 1H); 5.40 (d, *J*= 9.9 Hz, 1H); 4.73 (s, 1H); 4.06 (s, 1H); 3.88, 3.36 (m, 2H); 3.25 (d, *J*= 8.9 Hz 1H); 3.18 (dd, *J*= 11.2, 5,3 Hz, 1H); 2.90 (d, 1H), 2.77 (m, 1H); 2.56 (m, 1H); 1.76 (m, 5H); 1.51 (m, 1H); 1.32 (m, 2H); 1.07 (m, 1H); 0.88 (m, 1H); 0.78 (d, *J*= 7.0 Hz, 3H). ^{1}H-NMR (100 MHz, $CDCl_3$): δ= 209.2; 173.8; 166.2; 130.6; 130.3; 100,5; 80.2; 66.3; 58.8; 47.6; 42.1; 41.8; 36.7; 32.8; 30.1; 29.9; 29.8; 26.5; 26.4; 17.6. UV-Vis λ_{max}: 202 nm, 262 nm. Data consistent with data published by Mizukami et al. [16], Nikai et al. [17] and Agatsuma et al. [18].

References

[1] Hoeksma J, Misset T, Wever C, Kemmink J, Kruijtzer J, Versluis K, et al. A new perspective on fungal metabolites: identification of bioactive compounds from fungi using zebrafish embryogenesis as read-out. Sci Rep 2019;9:1–16. https://doi.org/10.1038/s41598-019-54127-9.

[2] Nielsen KF, Smedsgaard J. Fungal metabolite screening: Database of 474 mycotoxins and fungal metabolites for dereplication by standardised liquid chromatography-UV-mass spectrometry methodology. J Chromatogr A 2003;1002:111–36. https://doi.org/10.1016/S0021-9673(03)00490-4.

[3] Barber J, Cornford JL, Howard TD, Sharples D. The structure of citrinin in vivo. J Chem Soc Perkin Trans 1 1987;2:2743–4. https://doi.org/10.1039/p19870002743.

[4] Poupko R, Luz Z, Destro R. Carbon-13 NMR of citrinin in the solid state and in solutions. J Phys Chem A 1997;101:5097–102. https://doi.org/10.1021/jp970681t.

[5] Liu D, Yan L, Ma L, Huang Y, Pan X, Liu W, et al. Diphenyl derivatives from coastal saline soil fungus Aspergillus iizukae. Arch Pharm Res 2015;38:1038–43. https://doi.org/10.1007/s12272-014-0371-z.

[6] Ganesh Kumar C, Mongolla P, Sujitha P, Joseph J, Suresh Babu K, Suresh G, et al. Metabolite profiling and biological activities of bioactive compounds produced by Chrysosporium lobatum strain BK-3 isolated from Kaziranga National Park, Assam, India. Springerplus 2013;2:1–9. https://doi.org/10.1186/2193-1801-2-122.

[7] Kaouadji M, Steiman R, Murandi FS, Krivobok S, Sage L. Gliotoxin: Uncommon1h couplings and revised1h- and13c-nmr assignments. J Nat Prod 1990;53:717–9. https://doi.org/10.1021/np50069a032.

[8] Sun Y, Takada K, Takemoto Y, Yoshida M, Nogi Y, Okada S, et al. Gliotoxin analogues from a marine-derived fungus, penicillium sp., and their cytotoxic and histone methyltransferase inhibitory activities. J Nat Prod 2012;75:111–4. https://doi.org/10.1021/np200740e.

[9] Sawa R, Mori Y, Iinuma H, Naganawa H, Hamada M, Yoshida S, et al. Harzianic acid, a new antimicrobial antibiotic from a fungus. J Antibiot (Tokyo) 1994;47:731–2. https://doi.org/10.7164/antibiotics.47.731.

[10] Tschen JSM, Chen LL, Hsieh ST, Wu TS. Isolation and phytotoxic effects of helvolic acid from

plant pathogenic fungus Sarocladium oryzae. Bot Bull Acad Sin 1997;38:251–6.

[11] Isogai A, Nakayama J, Takayama S, Suzuki A, Kusai A. Structural Elucidation of Minor Components of Peptidyl Antibiotic P168s (Leucinostatins) by Tandem Mass Spectrometry. Biosci Biotechnol Biochem 1992;56:1079–85. https://doi.org/10.1271/bbb.56.1079.

[12] Martinez AFC, Moraes LAB. Liquid chromatography-tandem mass spectrometry characterization of five new leucinostatins produced by Paecilomyces lilacinus CG - 189. J Antibiot (Tokyo) 2015;68:178–84. https://doi.org/10.1038/ja.2014.120.

[13] Kawakami H, Suzuki C, Yamaguchi H, Hara K, Komine M, Yamamoto Y. Norlichexanthone produced by cultured endolichenic fungus induced from Pertusaria laeviganda and its antioxidant activity. Biosci Biotechnol Biochem 2019;83:996–9. https://doi.org/10.1080/09168451.2019.1585746.

[14] Yamazaki H, Koyama N, Oura S, Tomoda H. New rugulosins, Anti-MRSA antibiotics, produced by Penicillium radicum FKI-3765-2. Org Lett 2010;12:1572–5. https://doi.org/10.1021/ol100298h.

[15] Kohno J, Asai Y, Nishio M, Sakurai M, Kawano K, Hiramatsu H, et al. TMC-171A, B, C and TMC-154, novel polyketide antibiotics produced by Gliocladium sp. TC 1304 and TC 1282. J Antibiot (Tokyo) 1999;52:1114–23. https://doi.org/10.7164/antibiotics.52.1114.

[16] Mizukami T, Ogawa H, Nakai R, Asai A, Yamashita Y, Ando K, et al. Furoindolizines, EP0849267B, European Patent Office, 2001.

[17] Nakai R, Ogawa H, Asai A, Ando K, Agatsuma T, Matsumiya S, et al. UCS1025A, a novel antibiotic produced by Acremonium sp. J Antibiot (Tokyo) 2000;53:294–6. https://doi.org/10.7164/antibiotics.53.294.

[18] Agatsuma T, Akama T, Nara S, Matsumiya S, Nakai R, Ogawa H, et al. UCS1025A and B, New Antitumor Antibiotics from the Fungus Acremonium Species. Org Lett 2002;4:4387–90. https://doi.org/10.1021/ol026923b.

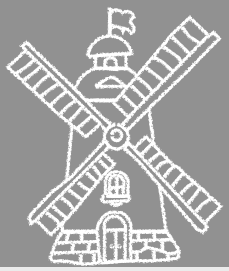

Classification of Antimicrobial Mechanism of Action using Dynamic Bacterial Cytological Profiling

CHAPTER 4

Xudong Ouyang[1,2], Jelmer Hoeksma[1], Tjalling K. Siersma[3], Leendert W. Hamoen[3] and Jeroen den Hertog[1,2]

1. Hubrecht Institute-KNAW and University Medical Center Utrecht, Utrecht, the Netherlands
2. Institute Biology Leiden, Leiden University, Leiden, the Netherlands
3. Swammerdam Institute for Life Sciences, University of Amsterdam, Amsterdam, the Netherlands

Adapted from doi: 10.1101/2021.09.08.459470

ABSTRACT

Antimicrobial resistance is a major threat to human health. Basic knowledge of antimicrobial mechanism of action (MoA) is imperative for patient care and for identification of novel antimicrobials. Recently, imaging-based Bacterial Cytological Profiling (BCP) was developed to predict MoAs of antibacterial compounds against Gram-negative bacteria. Here, we developed a simple, quantitative time-lapse fluorescence imaging method using a membrane dye and a nucleoid dye to track the morphological changes of *Bacillus subtilis* cells in response to antimicrobials for up to 60 min. Dynamic Bacterial Cytological Profiling (DBCP) facilitated assignment of the MoAs of 14 distinct, known antimicrobial compounds to the five main classes. Using this method, we found that the poorly studied antimicrobial, harzianic acid, a secondary metabolite purified from the fungal culture of *Oidiodendron flavum*, targets the cell envelope. We conclude that DBCP is a simple method, which facilitates rapid classification of the MoA of antimicrobials in functionally distinct classes.

INTRODUCTION

As the number of untreatable infections caused by multidrug-resistant "superbugs" is increasing globally, antimicrobial resistance is becoming a major threat to human health [1,2]. New antimicrobials with distinct working mechanisms are required to combat bacteria that have become resistant to all known antimicrobials. Although thousands of small molecules have now been screened for antibacterial activity in countless screening programs, the yield of useful compounds from these is relatively low [3]. One of the reasons is the lack of insight into antimicrobial mechanism of action (MoA), which makes it difficult to determine the value of a new compound. Therefore, understanding the MoA is fundamental for identification of novel antimicrobials.

Recently, imaging-based Bacterial Cytological Profiling (BCP) was developed, a method similar to cytological profiling of eukaryotic cells [4–6]. BCP utilizes high resolution fluorescent microscopy to observe changes of fluorescent bacterial cells (due to fluorescent dye staining or fluorescent reporter gene expression) in response to antibacterial compounds and compares cytological profiles with cells treated with control antimicrobials. For Gram-negative bacteria, this method was applied on *Escherichia coli* by generating BCP profiles using a single strain with nucleoid and cell membrane staining at the single-cell level [4]. Several parameters, including cell size, cell shape, DNA and membrane dye intensity were quantified in individual cells and antimicrobials were rapidly and successfully classified into five main classes. For Gram-positive bacteria, a panel of GFP-reporters was generated covering many pathways and this panel was successfully used for in-depth analysis of antimicrobial targets [7–9]. However, no single reporter was generated covering more than two main antimicrobial classes. This suggests that for classification of unknown antimicrobial candidates against Gram-positive bacteria, multiple reporters will be needed each time to assign to one of the five MoA classes, cell membrane, cell wall, protein, DNA or RNA, which is laborious.

Here, we developed a method to rapidly distinguish the effect of anti-bacterial compounds from all of the five main classes. To achieve this, we used time-lapse imaging of fluorescent dye-stained *B. subtilis* to record dynamic changes. We improved the imaging protocol to make it simple and functional for bacterial long-term imaging. Using this method, dubbed Dynamic Bacterial Cytological Profiling (DBCP), we observed bacteria over time and established fluorescence intensities qualitatively and quantitatively. It allowed to rapidly distinguish between antimicrobials from all of the five different classes. Finally, we purified an

antimicrobial activity from the fungal culture of *Oidiodendron flavum* and identified it to be harzianic acid, an understudied fungal secondary metabolite. Using DBCP, we established that harzianic acid targets the cell membrane and cell wall.

MATERIALS AND METHODS

Strains and reagents

B. subtilis 168 was used for imaging in this study [10]. *O. flavum* (CBS 366.71) was obtained from Westerdijk Fungal Biodiversity Institute (the Netherlands) and used for biologically active compound production. Commercial antimicrobials were purchased from Sigma Aldrich (Table 1). FM4-64, 4′,6-diamidino-2-phenylindole (DAPI), SYTO-9 and SYTOX-Green were purchased from Thermo Fisher Scientific.

Microdilution assay

MIC was determined by broth microdilution assay. Early exponential-phase cultures of *B. subtilis* were diluted 1:100 into Luria-Bertani (LB) medium, and distributed in 96-wells plates. Antimicrobials were tested 1:10 of the stock, then serially diluted with a factor 2. Bacterial growth was visually inspected after overnight incubation at 37 °C.

Confocal microscopy

Microscopy was performed as described before with minor modification [7]. Briefly, bacterial cultures in early exponential-phase were treated with antimicrobials (2.5 × MIC) or 1% dimethyl sulfoxide (DMSO) as control for up to 60 min. Afterwards, 1.5 μM FM4-64 was used for membrane staining. 5 μM DAPI, 50 nM SYTO-9 or 0.5 μM SYTOX-Green was applied to stain nucleoids. Samples were then immobilized on microscope slides covered with an agarose pad containing 1% agarose and LB medium, and imaged. Confocal microscopy was carried out using a Perkin Elmer UltraView VoX spinning disk microscope system and Volocity v6.3 software. Z-stack images were collected over a length of 3 μm with 0.2 μm intervals to acquire signals from the whole cells. Three independent experiments were done using each antimicrobial (biological triplicates). Images were analyzed using Fiji [11].

Time-lapse microscopy

A single well agarose pad (2 mL in size) containing 0.75% agarose, 1.5 μM FM4-64, 50 nM SYTO-9 and LB medium was made by a trimmed syringe to immobilize bacterial cells on its surface. Bacterial culture in early exponential-phase was treated with 1.5 μM FM4-64 and 25 nM SYTO-9 for 10 min, and then 5 μL of it was transferred onto the agarose pad for imaging. Time-lapse images were collected using the spinning disk microscope system described above for 30 to 60 min with 3 min intervals. 400 μL LB medium with antimicrobials (2.5 × MIC) or 1% DMSO (control) was added into the well on the agarose pad after the second image was taken to make sure the cells were growing normally. Images were analyzed using Fiji.

Dynamic cytological patterns

Stack images were merged by Z projection using max intensity and cell morphological patterns were measured by Fiji. A wide line (width: 20-pixel, i.e. 1.3 μm) was drawn to cover a whole cell and the intensity of both membrane signal and nucleoid signal over the line was acquired with the tool Plot Profile. The graphs of Plot Profile from each series of time-lapse imaging were then re-plotted into one heatmap with GraphPad Prism v8.4.1 to generate the dynamic cytological patterns.

Dynamic cytological profiling

Stack images were merged by Z projection using max intensity. One cell unit was defined as a cell without any septa shown in the image of the initial time point. Cell status analysis was done by counting cells by eye in each of the three cell type categories (intact cell, no-nucleoid cell and disintegrated cell). Cell morphology analysis was done by measuring the length and intensity of both membrane and nucleoid using Fiji. Bar graphs and line chart were plotted using GraphPad Prism v8.4.1.

Identification of biologically active compound

O. flavum was cultured on Malt Extract Agar (MEA) for 14 days. Secondary metabolites were extracted using ethyl acetate and separated using a Shimadzu preparative high performance liquid chromatography (HPLC) system with a C18 reversed phase Reprosil column (10 μm, 120 Å, 250 × 22 mm). The mobile phase was 0.1% trifluoroacetic acid in water (buffer A) and 0.1% trifluoroacetic acid in acetonitrile (buffer B). A linear gradient was applied of buffer B (5–95%) for 40

minutes. Fractions were collected and tested on *B. subtilis*. The active fraction was assessed for its purity through Shimadzu LC-2030 analytical HPLC using a Shimadzu Shim-pack GISTC18-HP reversed phase column (3 μm, 4.6 × 100 mm). LC-MS was performed on a Shimadzu LC-system connected to a Bruker Daltonics μTOF-Q mass spectrometer. High resolution mass spectrometry (HRMS) was measured on an LCT instrument (Micromass Ltd, Manchester UK). Elemental composition analyses were performed by Mikroanalytisch Labor Kolbe (Oberhausen, Germany). Finally, the compound was dissolved in 400 μL $CDCl_3$ + 0,03% TMS and analyzed by Nuclear Magnetic Resonance (NMR) spectroscopy. More specifically, ^{1}H-NMR, Hetronuclear Single Quantum Coherence (HSQC), Hetronuclear Multile-Bond Correlation (HMBC) and Correlation spectroscopy (COSY) spectra were measured at 600 MHz using a Bruker instrument. ^{13}C-NMR was measured on the same instrument at 150 MHz.

RESULTS AND DISCUSSION

BCP did not fully distinguish antimicrobials from five main classes

Most antimicrobials for Gram-positives fall into one of five main classes based on their MoA: cell membrane, cell wall, protein, DNA or RNA [12]. We set out to use BCP to distinguish MoAs between different classes of antimicrobials against Gram-positive bacteria. To this end, we selected one antimicrobial from each class. *B. subtilis* was treated for 60 min with the antimicrobials using 2.5 × MIC (Table 1) to ensure the inhibitory effects. The cells were stained with FM4-64 (red, cell membrane) and DAPI (blue, nucleoid), immobilized and imaged. Ampicillin (cell wall class) treatment for 60 min did not alter the appearance of cells compared to control treatment (Fig. 1). The other four antimicrobials induced variations both with respect to membrane and nucleoid staining. On the membrane, bright fluorescent foci appeared in response to all four antimicrobials, suggesting that the cytoskeleton was affected [13]. However, similar foci were also sometimes observed in the control, precluding the presence of foci as a criterion to distinguish between antimicrobial classes. Nucleoid staining was divided into two groups: decondensed nucleoids in response to CCCP (cell membrane class) and rifampin (RNA class), and shorter, more condensed nucleoids in response to moxifloxacin (DNA class) and chloramphenicol (protein class). Taken together, analysis of membrane and nucleoid staining of immobilized cells after treatment with antimicrobials for 60 min was not sufficient to definitively distinguish between

the five classes of antimicrobials. Nevertheless, some differences were observed and we hypothesized that the response over time might be distinct. To investigate the dynamics of the cells' responses to antimicrobials, we set up time-lapse imaging of bacteria stained with fluorescent dyes.

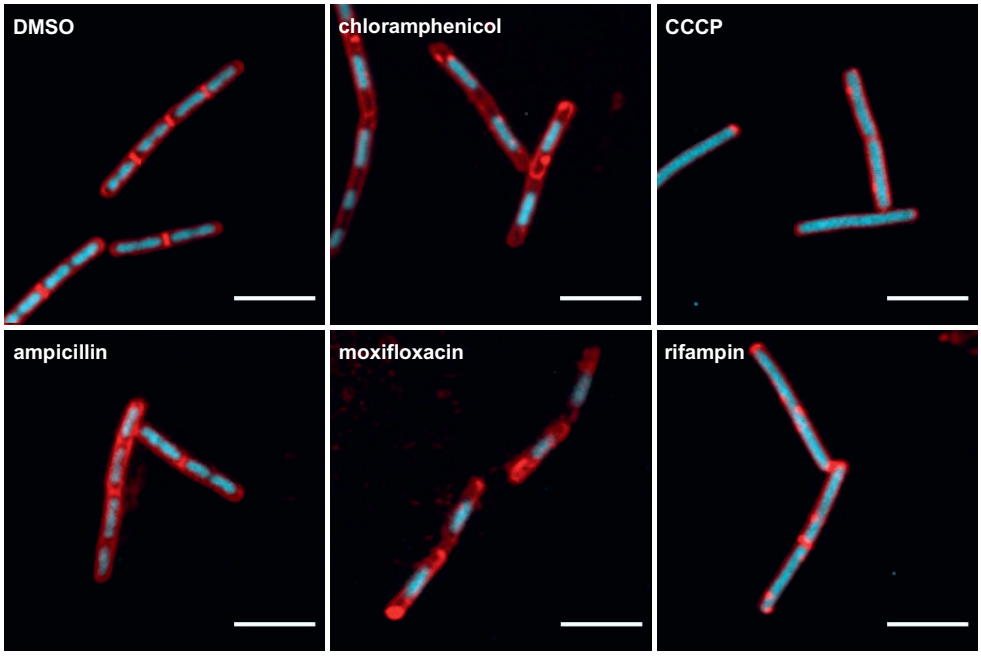

Fig. 1. Cytological profiling of antimicrobial activities. *B. subtilis* cells were treated with an antimicrobial from one of the five main MOA classes or 1% DMSO (control) for 60 min. The antimicrobials we selected were: ampicillin for cell wall, CCCP for cell membrane, chloramphenicol for protein, moxifloxacin for DNA and rifampin for RNA. The concentrations of antimicrobials were 2.5 × MIC. Cells were stained with FM4-64 (red, cell membrane) and DAPI (blue, nucleoid), immobilized and imaged by confocal fluorescence microscopy. Representative images are shown. Scale bar is 5 μm.

DBCP distinguished antimicrobials from distinct MoA classes

To acquire dynamic cytological profiles, SYTO-9 was used as nucleoid dye, because DAPI is toxic to bacterial cells. SYTO-9 shows low bacterial toxicity, fast staining, high fluorescence intensity in the green spectrum and therefore good compatibility with FM4-64 fluorescence.

To enable time-lapse imaging of bacteria, we designed the following workflow (Fig. 2). A thick agarose pad providing enough nutrition to sustain cell growth and the well on top of the agarose was convenient for adding antimicrobial solutions to bacteria at any stage of the imaging process. Images were taken every three minutes, which was sufficient to obtain information about the dynamics of antimicrobial treatment, but not too frequent thus preventing cells from laser damage. To confirm that the bacteria were growing healthily, two images were acquired before antimicrobials were added. To facilitate quantitative dynamic imaging of individual cells, the fluorescence intensity was integrated and quantified along the length of the cell and plotted. Control cells treated with DMSO showed steady growth over the course of 60 min (Fig. 3). DBCP was initially performed with the same antimicrobials as in the static BCP experiment. Images were collected for 60 min and resulting movies are shown in Movie S1-S6.

Cells treated with different classes of antimicrobials had notably distinct profiles. The ampicillin and CCCP profiles stood out, because the nucleoid fluorescence signals suddenly became almost undetectable (Fig. 3). Ampicillin treatment inhibited cell growth and subsequently, the nucleoid fluorescence was lost. Strikingly, the membrane fluorescence at the septum started to decrease a few minutes after cell growth was inhibited. Part of the membrane fluorescence was lost at the end of the imaging series, showing that cells treated with ampicillin disintegrated, which was

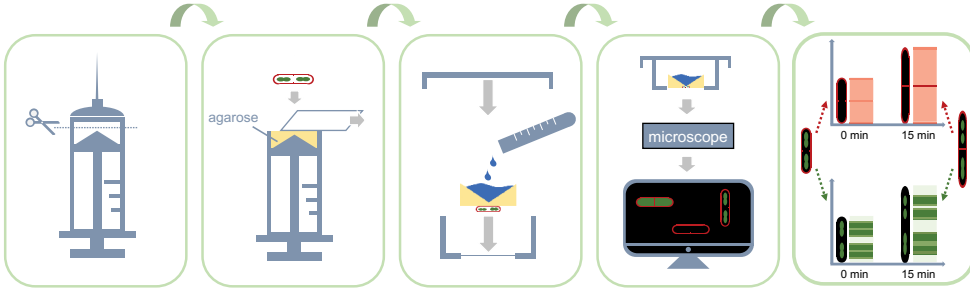

Fig. 2. Workflow for time-lapse imaging of bacteria. A single well LB agarose pad was made using a trimmed syringe to immobilize bacterial cells on its surface. A glass slide was used to keep the agarose surface flat and smooth. Upon solidification of the agarose, the glass slide was removed and drops with bacterial cultures were added onto the surface. Once the drops were dry, the agarose pad with bacteria was transferred into a confocal dish for imaging. The thick agarose pad provided enough nutrition to sustain growing cells, allowing time-lapse imaging for hours, even overnight. The well on top of the agarose pad was used for easy addition of antimicrobial solutions to bacteria at any stage of the imaging process. After imaging, raw micrographs were converted into dynamic patterns by quantifying the fluorescence intensities of the membrane and nucleoid staining separately along the length of the bacteria.

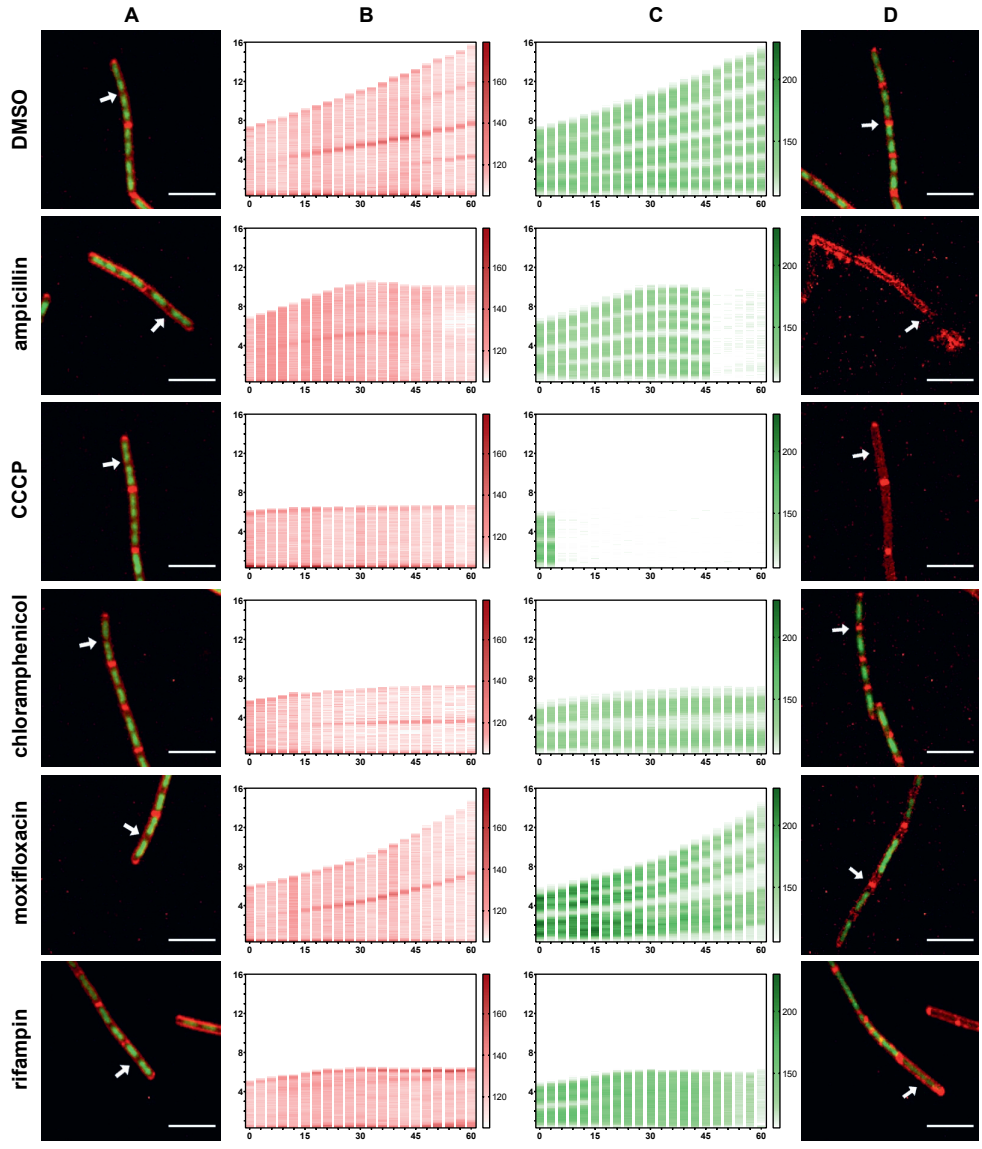

Fig. 3. Distinct dynamic profiling patterns of cells upon antimicrobial treatments. *B. subtilis* cells were treated with antimicrobials (2.5 × MIC) as indicated or 1% DMSO (control). The antimicrobials we selected were: ampicillin for cell wall, CCCP for cell membrane, chloramphenicol for protein, moxifloxacin for DNA and rifampin for RNA. Cells were stained with FM4-64 (red, cell membrane) and SYTO-9 (green, nucleoid) and imaged by time lapse confocal fluorescence microscopy for 60 min with 3 min intervals. Column A and D show the actual micrographs of the first and the last picture of the series (contrast was adjusted for individual graph to show details). The FM4-64 (column B) and SYTO-9 (column C) signals in a single cell (arrow in micrographs) were quantified over the length of the cell and plotted (y-axis, numbers in μm) over time (x-axis, numbers in min). Representative cells are shown. Scale bar is 5 μm.

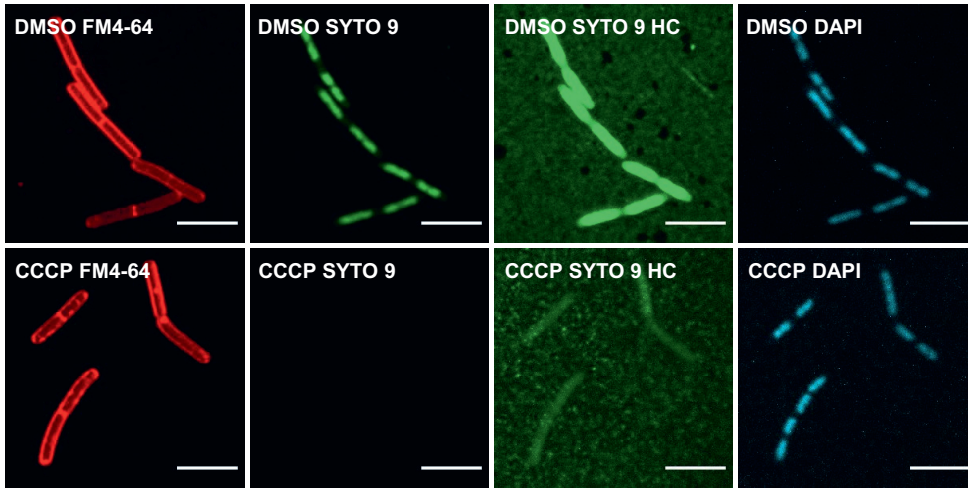

Fig. 4. Dual nucleoid staining of cells following CCCP treatment for 3 min. *B. subtilis* cells were treated with CCCP (2.5 × MIC) or 1% DMSO (control) for 3 min. Cells were stained with FM4-64 (red, cell membrane), SYTO-9 (green, nucleoid) and DAPI (blue, nucleoid), immobilized and imaged by confocal fluorescence microscopy. Representative images are shown. Scale bar is 5 µm. SYTO-9 graphs were shown both in normal contrast and high contrast (HC).

also evident from the actual micrograph (Fig. 3D). Interestingly, this pattern was not observed with ampicillin treated cells in Fig. 1. This discrepancy is likely caused by the different imaging methods that were used. Time lapse imaging of the same cell showed disintegration of the cell (Fig. 3D), whereas treatment in liquid medium for 60 min and subsequent transfer for imaging may cause disintegrated cells to go unnoticed and only intact cells are imaged (Fig. 1). In response to CCCP, the membrane pattern remained normal. However, the nucleoid fluorescence intensity decreased sharply already after 6 min of treatment and cells stopped growing at the same time. The apparent loss of SYTO-9 staining was unexpected, because CCCP-treatment did not significantly affect DAPI-stained nucleoids (Fig. 1). Double labeling of nucleoids with SYTO-9 and DAPI showed that CCCP-treatment for 3 min already greatly reduced the SYTO-9 signal. In high contrast, SYTO-9 was still detectable. Yet, DAPI labeling appeared not to be affected in the same CCCP-treated cells (Fig. 4). Similar results were obtained after CCCP-treatment for 60 min (Fig. S1B). These results indicate that rapid reduction in SYTO-9 labeling of nucleoids was not due to loss of nucleoids from the cells, but rather to loss of SYTO-9 fluorescence by rapid changes in local conditions, e.g. membrane potential, pH and/or ion concentration.

Table 1. List of antimicrobials used in this study. The MIC was determined by our stain of *Bacillus subtilis* strain 168 in this study.

Class	Sub-class	Antimicrobials	MIC (mg/L)	Mode of Action
Cell wall	Penicillin	Ampicillin	5	Binding to Penicillin-binding protein [23]
	Penicillin	Penicillin G	5	Binding to Penicillin-binding protein [23]
	Glycopeptide	Vancomycin	0.25	Binding to D-Ala-D-Ala moiety of peptidoglycan [24]
Cell	Proton ionophore	CCCP	0.4	Transporting protons across membranes [21]
membrane	Polychloro phenoxy	Triclosan	2.5	Disrupting cellular ionic homeostasis at bactericidal
	phenols			concentration [22]
	Lantibiotics	Nisin	2.5	Generating pores on cell membrane [20]
Protein	Amphenicols	Chloramphenicol	2.5	Inhibiting the peptidyl transferase activity [27]
	Fusidanes	Fusidic acid	0.13	Binding to the elongation factor G (EF-G) [29]
	Aminoglycoside	Gentamicin	2.5	Binding to the A-site on the 16S ribosomal RNA [28]
DNA	Quinolone	Moxifloxacin	0.05	Inhibiting DNA gyrase A and topoisomerase IV [17]
	Quinolone	Nalidixic acid	1.5	Inhibiting DNA gyrase A and topoisomerase IV [18]
	Mitomycin	Mitomycin C	0.06	Cross-linking and alkylating of DNA [19]
RNA	Rifamycin	Rifampin	0.13	Inhibiting bacterial RNA polymerase [25]
	Actinomycines	Actinomycin D	0.03	Inhibiting bacterial RNA synthesis by binding to DNA
				at the transcription initiation complex [26]
Unknown	Harzianic acid	Harzianic acid	50	Unknown

Chloramphenicol and moxifloxacin induced shorter nucleoids relative to the cell size (Fig. 3), but the dynamics were different. In chloramphenicol treated cells, the extension of nucleoids was totally arrested, and the nucleoids compacted, resulting in an apparent increase in space between the nucleoids. In moxifloxacin-treated cells, the nucleoids still extended, but slower than the cells themselves, resulting in an increase in the space between nucleoids. Rifampin induced the nucleoid signal to gradually spread over the cells, suggesting that the nucleoids decondensed, which is in line with previous studies [14,15]. Taken together, these results suggest that DBCP distinguished the MoA of antimicrobials from five major classes.

Rapid loss of nucleoid staining was distinct in cells treated with antimicrobials from cell membrane and cell wall classes

In order to determine whether the DBCP profiles were conserved in each class, we tested 14 distinct antimicrobials from the five main antimicrobial classes (Table 1) using DBCP. All the profiles were first analyzed by eye for nucleoid visibility and membrane integrity to derive cell status, which was featured into three types: intact cells, having both visible membrane and nucleoid fluorescence; no-nucleoid

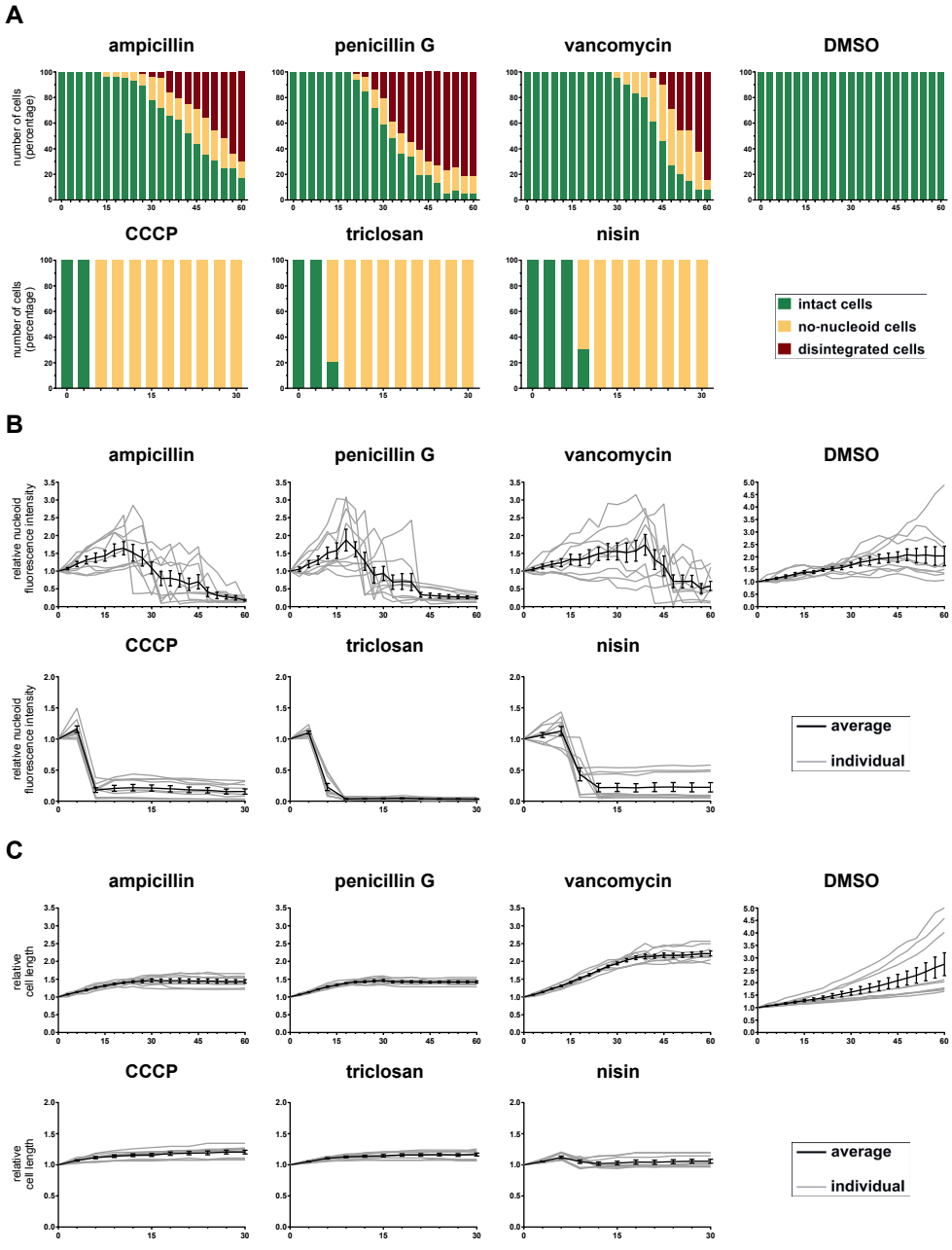

Fig. 5. DBCP of cells treated with antimicrobials from the cell membrane and cell wall classes. *B. subtilis* cells were treated with antimicrobials (2.5 × MIC) as indicated or 1% DMSO (control). Cells were stained with FM4-64 (red, cell membrane) and SYTO-9 (green, nucleoid), and imaged by time lapse confocal fluorescence microscopy with 3 min intervals. Three distinct cell types were identified: intact cells (cells with visible membrane and nucleoid fluorescence), no-nucleoid cells (cells with

apparently intact membrane, but without visible nucleoid fluorescence), and disintegrated cells (cells with disintegrated membrane and no detectable nucleoid). The number of cells of the three types were counted from biological triplicate imaging series (n > 40). In-depth cell morphology analysis was done on 9 cells in total per condition, i.e. 3 cells per biological triplicate. The cell length and nucleoid intensity data were quantified in these cells at each timepoint. (A) The number of cells in each cell type, intact cells (green), no-nucleoid cells (yellow) and disintegrated cells (red), was determined and plotted as percentage (y-axis, numbers in %) over time (x-axis, min). (B) Overall nucleoid intensity, i.e. the SYTO-9 fluorescence intensity inside a whole cell, corrected for background, was determined for individual cells over time and was depicted as percentage of the value at the start (t = 0 min) (y-axis) over time (x-axis, min). The mean of antimicrobial-treated cells was plotted in black with error bars representing the SEM. Gray lines represent individual antimicrobial-treated cells on which the mean was based. (C) Cell length was determined using the membrane signal (FM4-64) and was represented as percentage, relative to the initial length (y-axis, numbers in %) over time (x-axis, min). The mean of antimicrobial-treated cells was plotted in black with error bars representing the SEM. Gray lines represent individual antimicrobial-treated cells on which the mean was based.

cells, intact cells without visible nucleoid fluorescence; and disintegrated cells, no detectable nucleoid fluorescence and a disintegrated membrane. Cell status was evaluated over time to determine the changes in the ratios of each cell type during treatment.

As expected, antimicrobials within the cell membrane class (triclosan, nisin and CCCP) and the cell wall class (ampicillin, penicillin G and vancomycin) showed distinct profiles by cell status analysis and were readily distinguished from the other three classes (Fig. 5A, S1C). The percentage of intact cells decreased strongly after treatment with antimicrobials from the cell membrane and cell wall classes, compared to the other three classes. However, some antimicrobials from RNA and protein classes, including rifampin, gentamicin and chloramphenicol, also induced loss of nucleoid fluorescence in a small proportion of the cells (Fig. S1C). Quantification of nucleoid intensity of individual cells over time indicated that rifampin, gentamicin and chloramphenicol treatment resulted in gradual loss of nucleoid intensity (Fig. S1D). In contrast, treatment with cell membrane-active and cell wall-active antimicrobials resulted in a sharp decrease of nucleoid fluorescence intensity in each individual cell (Fig. 5B). Next, to distinguish the classes further, quantitative analysis of the changes in the membrane fluorescence intensity, cell length and the nucleoid length was done over time. Differences in membrane appearance and nucleoid shape were also recorded.

To distinguish the cell membrane class from the cell wall class, we evaluated the percentage of intact cells (Fig. 5A) and the inhibition of cell growth (Fig. 5C). Cell wall-active antimicrobial treatment induced loss of nucleoid fluorescence and inhibition of

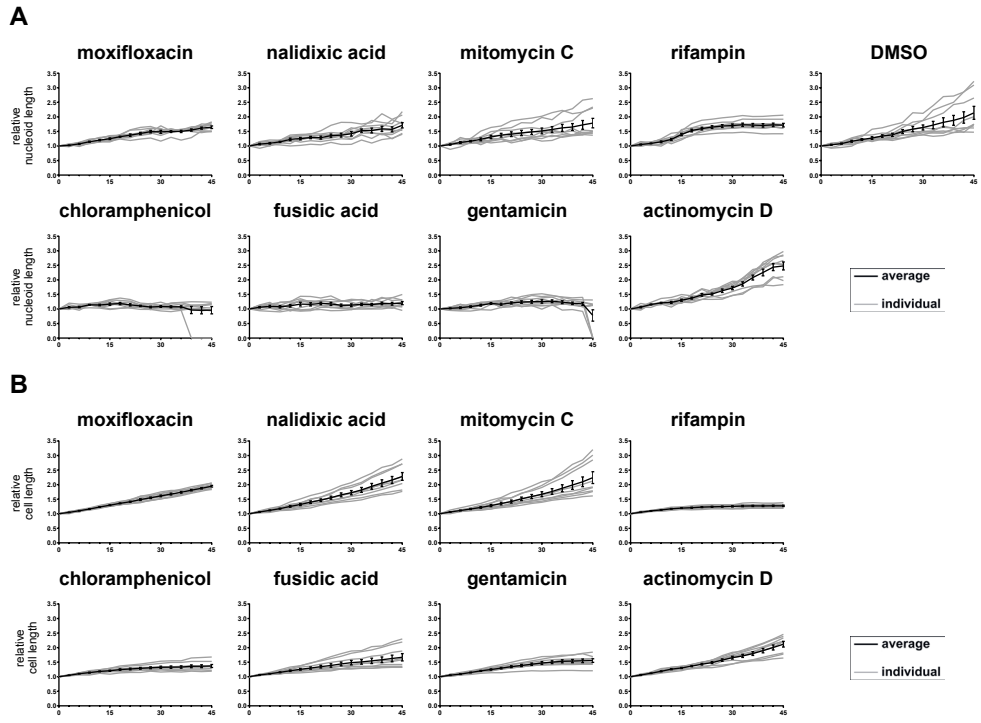

Fig. 6. DBCP of cells treated with antimicrobials from the DNA, RNA and protein classes. *B. subtilis* cells were treated with antimicrobials (2.5 × MIC) as indicated or 1% DMSO (control). Cells were stained with FM4-64 (red, cell membrane) and SYTO-9 (green, nucleoid), and imaged by time lapse confocal fluorescence microscopy with 3 min intervals. Cell morphology data were analyzed from biological triplicate imaging series in triplicate, hence from 9 cells in total per antimicrobial and processed as described in the legend to Fig. 5. Nucleoid length, i.e. the length of all the nucleoids inside one cell added together, is shown in (A) and cell length in (B). In case nucleoid fluorescence was not detectable, the nucleoid length was recorded as 0 μm. The mean of antimicrobial-treated cells was plotted in black with error bars representing the SEM. Gray lines represent individual antimicrobial-treated cells on which the mean was based. DMSO control is depicted in Fig. 5C.

cell growth after 15 - 30 min of treatment. Cell wall-active antimicrobials also induced disintegration of cells within 12 min after losing nucleoid fluorescence. Disintegrated cells were only observed upon treatment with cell wall-active antimicrobials, making this both a unique and a conserved trait for this class. In contrast, cell membrane-active antimicrobials induced simultaneous arrest of cell growth and loss of nucleoid fluorescence at an early stage of the antimicrobial treatment. These results indicate that the loss of nucleoid fluorescence is the first effect of cell membrane-active antimicrobials and distinguishes the class of cell membrane-active antimicrobials

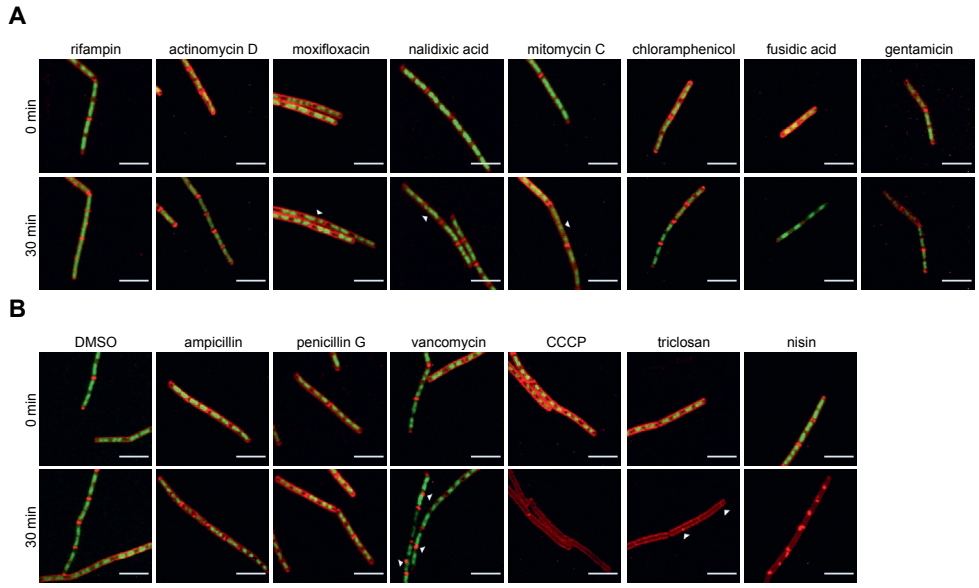

Fig. 7. Cell membrane and nucleoid staining of cells after 0 min and 30 min treatment with different antimicrobials. Cells treated with antimicrobials from DNA, RNA and protein class are in (A) and from cell membrane, cell wall classes and DMSO control are in (B). Special patterns induced by moxifloxacin, nalidixic acid, mitomycin C, triclosan and vancomycin are indicated by arrow heads. Representative images are shown. Scale bar is 5 μm.

from the other classes. Like for CCCP, co-staining of nucleoids using SYTO-9 and DAPI indicated that loss of SYTO-9 fluorescence was not caused by loss of nucleoids themselves (Fig. S1E). Taken together, DBCP facilitates the distinction between cell wall and cell membrane active antimicrobials.

Next, we assessed differences between the cells treated with the three non-envelope-associated classes of antimicrobials. Since most of the cells remained intact during treatment (Fig. S1C), we investigated the potential differences in cell morphology, first focusing on changes in nucleoid length (Fig. 6A, S1F) in comparison with changes in cell length (Fig. 5C, 6B). To visualize this comparison, the ratio between nucleoid length and cell length was calculated (Fig. S1G). If not detectable, the nucleoid length was recorded as 0 μm. In response to cell wall and cell membrane active antimicrobials, nucleoid fluorescence was lost abruptly. In contrast, the two antimicrobials from the RNA class (rifampin and actinomycin D) induced an increase in nucleoid length compared to cell length, albeit with different dynamics. This indicated that an increased ratio of nucleoid length to cell length was conserved

following treatment with antimicrobials from the RNA class, which is consistent with a previous report about nucleoid compaction [16]. In comparison, treatment with antimicrobials from both the DNA class (moxifloxacin, mitomycin C and nalidixic acid) and the protein class (chloramphenicol, fusidic acid and gentamicin) reduced nucleoid length compared to cell length (Fig. S1G). For cells treated with antimicrobials from the protein class, nucleoid elongation stopped immediately, suggesting DNA elongation was blocked shortly after the antimicrobial was added. Since cell growth was not totally inhibited (fusidic acid) or was inhibited more slowly than the inhibition of nucleoid growth (chloramphenicol and gentamicin), the ratio of nucleoid length to cell length was reduced. The antimicrobials from the DNA class did not inhibit nucleoid elongation completely, but reduced it to some extent. Additionally, during treatment, the separation of nucleoids seemed to be poorly controlled and unusual shapes of nucleoids were often observed (e.g. Fig. 7A at 30 min), in line with known effects of these antimicrobials on DNA replication [17–19]. Hence, each class of antimicrobials we tested generated a unique and reproducible DBCP profile.

DBCP distinguished sub-classes within the cell membrane, cell wall and RNA classes

Subsequently, we investigated whether DBCP was also able to distinguish sub-classes within the five main classes. In the cell membrane class, the growth curve of nisin-treated cells was notable, showing stabilized and even decreased cell size when the drug was added (Fig. 5C), which might due to loss of turgor pressure. In addition, big membrane blobs were observed after loss of nucleoid intensity at 30 min (Fig. 7B). Triclosan and CCCP generated highly similar profiles, but there was still a detectable morphological difference between the treated cells at 30 min (Fig. 7B). CCCP did not induce effects on the membrane, whereas triclosan induced small fluorescent membrane foci. These results are in line with their MoAs: nisin generates pores in the membrane, whereas triclosan and CCCP destroy membrane polarization, albeit at different levels [20–22]. This indicates that DBCP may be used to distinguish between cell membrane-active antimicrobials.

When comparing the profiles within the cell wall class, vancomycin was found to generate a different profile than ampicillin and penicillin G. The cell growth inhibition in response to vancomycin was delayed by 20 min compared to the other two (Fig. 5C). Before cell growth inhibition at 30 min, some fluorescent blobs were detected on the membrane, indicating membrane aggregates during vancomycin treatment,

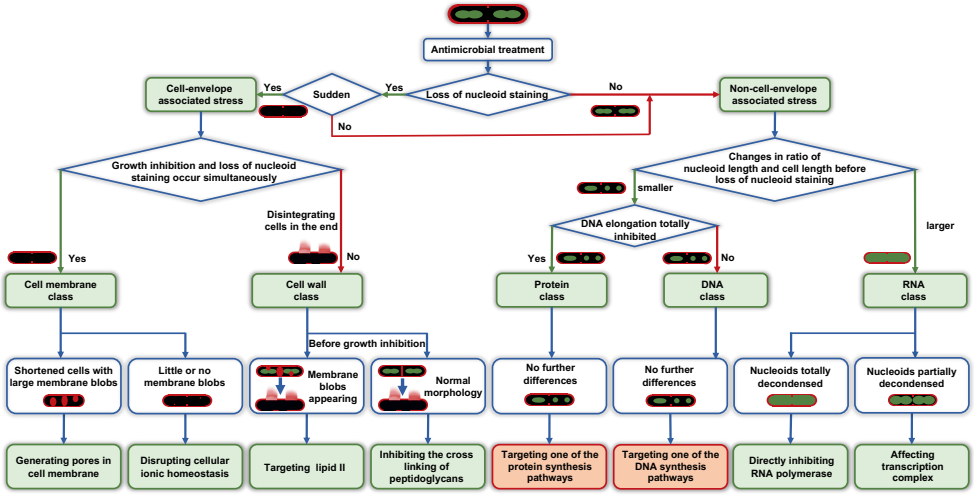

Fig. 8. Schematic representation of the DBCP-guided antimicrobial MOA identification. Green boxes indicate well-identified categories or mechanisms, whereas red ones indicate not well-identified. DBCP distinguishes antimicrobial MOAs at three levels. Briefly, *B. subtilis* cells were treated with antimicrobials and imaged. At the first level, based on the loss of nucleoid staining, every antimicrobial was grouped into cell-envelope associated stress or non-cell-envelope associated stress. If the nucleoid staining was suddenly lost, they would fall into cell-envelope stress group. At the second level, five main MOA classes were identified. For the group of cell-envelope stress, if growth inhibition and loss of nucleoid staining occurred simultaneously, cell membrane was supposed to be affected. If growth inhibition occurred before loss of nucleoid staining, cell wall was determined to be affected if disintegrated cells were observed. For the group of non-cell-envelope associated stress, the changing of nucleoid length / cell length ratio before loss of nucleoid staining were measured. If the ratio was becoming larger during imaging, RNA synthesis was supposed to be affected. If the ratio was becoming smaller, the nucleoid growth had to be checked. If DNA elongation was inhibited, the antimicrobial would fall into protein class; if not, into DNA class. At the third level, sub-classes would be identified within cell membrane, cell wall and RNA classes. Protein and DNA classes could not be further distinguished because the differences within these classes were not evident. For the cell membrane class, if cells became shorter and large membrane aggregates were observed, probably pores were generated in the cell membrane. If there were little or no membrane blobs, the cellular ionic homeostasis was supposed to be disrupted. To further distinguish within cell wall class, we looked back to the time before growth inhibition. If cells were normal, the cross linking of peptidoglycans, which was the last step of cell wall synthesis, might be affected. If thicker membrane septa or big membrane blobs were observed, lipid II synthesis might be affected. For the RNA class, the extent of nucleoid decondensing was different between different targets. If RNA polymerase was targeted, nucleoids would be totally decondensed. If transcription complex was affected, the decondensing of nucleoids would be gentler.

which is distinct from cells treated with ampicillin or penicillin G (Fig. 7B). Ampicillin and penicillin G generated similar DBCP profiles and they both inhibit cross linking of peptidoglycans [23], whereas vancomycin affects lipid II synthesis [24]. Thus, we conclude that DBCP is able to distinguish antimicrobials of the cell wall class.

Rifampin of the RNA class induced rapid elongation of the nucleoid whereas cell length was almost constant, resulting in an increase in nucleoid length: cell length ratio (Fig. 6A, B and S1G), indicating that the nucleoids in these cells were decondensed [16] and almost fully filled the cells (Fig. 7A). Although the increase in the ratio of nucleoid length to cell length was also observed in actinomycin D treated cells, it was much slower than in rifampin treated cells, suggesting that actinomycin D has a different target to block RNA synthesis, which is consistent with previous reports [25,26].

Next, we explored differences of the profiles of antimicrobial treatments within the protein class and the DNA class. Whereas most of the dynamic changes were similar among the three selected antimicrobials of the protein class, changes in nucleoid intensity were distinct for each antimicrobial (Fig. S1D). None of the fusidic acid treated cells showed a reduction in nucleoid intensity, whereas half of the chloramphenicol treated cells and all of the gentamicin treated cells showed a decrease in nucleoid intensity. This might be related to their different MoAs [27–29], but the large variability in nucleoid intensities in chloramphenicol treated cells precluded nucleoid intensity as a good parameter to distinguish between antimicrobials within the protein category. For the DNA class of antimicrobials, the responses were too similar to distinguish between them.

Taken together, DBCP facilitated distinction between antimicrobials from the five main classes, and allowed to distinguish sub-classes within the cell membrane, cell wall and RNA classes, using the scheme, depicted in Fig. 8.

Identification of harzianic acid

Previously, we screened fungal metabolites from more than 10,000 fungi for bioactive compounds [30]. Here, we screened this library for antimicrobial activity against Gram-positive bacteria (*S. aureus*). One of the fungi, *O. flavum* (CBS 366.71), produced high antimicrobial activity. The active compound was purified and the chemical characteristics (Table 2, Fig. S2) were consistent with data previously reported for harzianic acid [31,32] (Fig. 9A).

Harzianic acid: $C_{19}H_{27}NO_6$, dark yellow powder. HRMS: found 388.1750 (M+Na), calculated 388.1736 for $C_{19}H_{27}NO_6Na$. Elemental composition analyses: C 61,4%; O

21,8%; H 7,0%; N 3,8%. NMR (600 MHz, $CDCl_3$): See Table 2. UV-Vis λ_{max}: 244 nm, 363 nm.

Table 2: Assignments NMR-shifts, HMBC and COSY couplings for harzianic acid (in $CDCl_3$).
a= measured at 150 MHz, b= measured at 600 MHz, c= overlapping signals

		Harzianic acid ($CDCl_3$)		
#	δC[a]	δH[b]	HMBC[b]	COSY[b]
1	13.7	0.95 (t), 3H	2, 3	2
2	21.8	1.50 (m), 2H	1, 3, 4	1, 3
3	35.5	2.24 (dd), 2H	1, 2, 4, 5	3, 4 or 5[c]
4	149.9	6.37[c] (m), 1H	2, 3, 5, 6, 7[c]	3, 6[c]
5	129.6	6.38[c] (m), 1H	2, 3, 6, 7[c]	3, 6[c]
6	147.6	7.55 (m), 1H	4, 5, 7, 8	4 or 5[c], 7
7	119.1	7.00 (d, *J*=15.1 Hz), 1H	5, 6, 8, 10	6
8	176.7	-	-	-
9	173.2	-	-	-
10	99.7	-	-	-
11	197.3	-	-	-
12	64.1	3.63 (dd, *J*= 10.6, 1,0 Hz), 2H	9, 11, 13, 14, 18,	13
13	33.8	1.89 (dd), 1H 2.48 (d), 1H	11, 12, 14, 15, 19	12
14	79.9	-	-	-
15	36.0	2.02 (m), 1H	13, 14, 16, 17, 19	16 or 17[c]
16	17.5	0.99[c] (m), 3H	14, 15[c]	15
17	16.2	0.99[c] (m), 3H	14, 15[c]	15
18	26.6	2.97 (s), 3H	9, 12	-
19	176.3	-	-	-

MoA identification of harzianic acid

Little is known about harzianic acid, a compound with antimicrobial activity that was isolated from fungi decades ago [31]. Harzianic acid also has antifungal activity and plant growth promoting activity [32–35]. The antimicrobial MoA of harzianic acid is unknown. DBCP was used to get insight into the MoA of harzianic acid. Imaging data were analyzed to assess cell status and cell morphology (Fig. 9B, S1). Harzianic acid induced loss of nucleoid fluorescence at an early stage of treatment. Cell growth was totally inhibited at an early stage as well. This was reminiscent of the initial action of

cell membrane-active antimicrobials. Cell length actually appeared to decrease when the drug was added, suggesting loss of turgor pressure. Big membrane aggregates were observed when intact cells lost their nucleoid fluorescence, i.e. from 9 min onwards (Movie S7). These effects were similar to the effects of nisin, suggesting that harzianic acid generated pores in the membrane. Cell status data also indicated that part of the cells disintegrated. Note the gaps along the membrane at 30 min (Fig. 9C) or from 18 min onwards (Movie S7). Whereas disintegrated membranes were evident in nisin-treated cells as previously shown by BCP [36], we did not observe disintegrated cells in response to nisin by DBCP up to 30 min treatment.

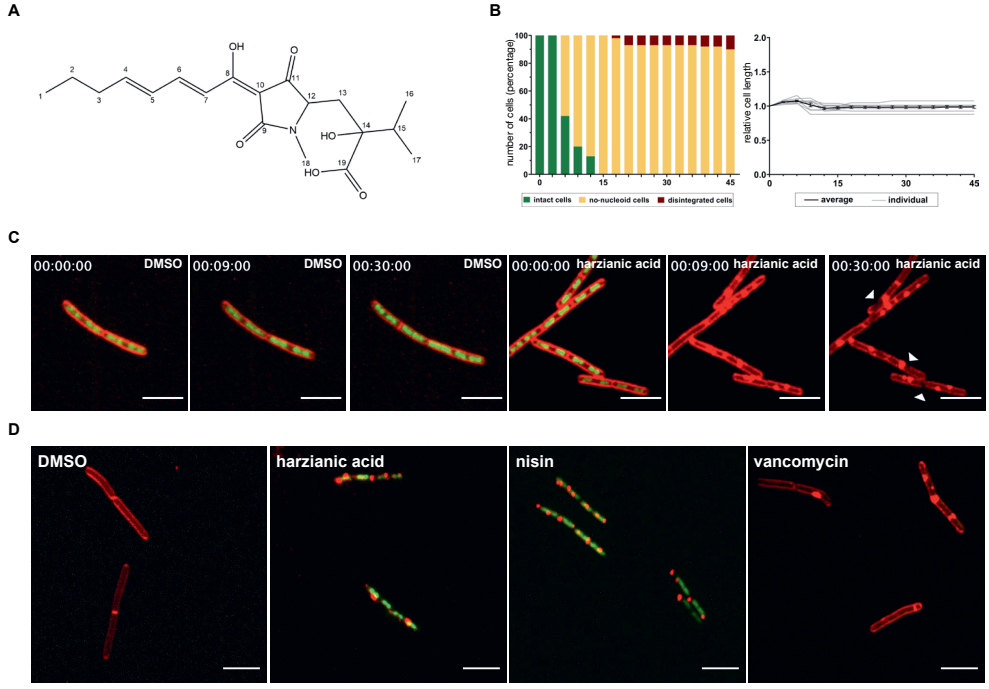

Fig. 9. MOA identification of harzianic acid. (A) Chemical structure of harzianic acid. (B) DBCP profiles of harzianic acid. *B. subtilis* cells were treated with harzianic acid (2.5 × MIC). Cells were stained, imaged, analyzed and plotted as in Fig. 5. (C) Examples of micrographs of cells at 0 min, 9 min and 30 min that were used for the quantifications in (D). Disintegrated cells at 30 min are indicated by arrow heads. DMSO treated cells are shown as control. Representative images are shown. Scale bar is 5 µm. (D) Cell permeability assay. *B. subtilis* cells were treated with antimicrobials (2.5 × MIC) or 1% DMSO (control) for 60 min. Cells were stained with FM4-64 (red, cell membrane) and SYTOX-Green (green, nucleoid), and imaged by confocal fluorescence microscopy. Representative images are shown. Scale bar is 5 µm.

Disintegration of part of the cells in response to harzianic acid may therefore suggest that harzianic acid also partially affects the cell wall.

The final disintegrated cell membrane showed similarities to the cell membrane of vancomycin treated cells, but the dynamics suggested that pore formation in the membrane was the initial effect of harzianic acid. To investigate this, non-cell permeable SYTOX Green was used to stain nucleoids. Evidently, treatment with harzianic acid or nisin, but not vancomycin or vehicle control (DMSO) induced SYTOX Green staining of the nucleoid (Fig. 9D). In conclusion, harzianic acid generated pores in the membrane and eventually appeared to affect the cell wall.

CONCLUSION

DBCP facilitates profiling of changes over time in cell morphology and viability. With the obtained parameters, antimicrobials may be classified at three levels. DBCP does not require prior knowledge of the antimicrobial MoAs. Hence, DBCP may be used to rapidly distinguish the MoA class and subclass of known and unknown antimicrobials.

ACKNOWLEDGEMENTS

The authors would like to thank Anko de Graaff of the Hubrecht Imaging Centre for help with imaging, and Samantha van der Beek and Maja Solman for help with developing the imaging protocol. This project was supported by the Chinese Scholarship Council (CSC).

REFERENCES

[1] Blair JMA, Webber MA, Baylay AJ, Ogbolu DO, Piddock LJV. Molecular mechanisms of antibiotic resistance. Nat Rev Microbiol 2015;13:42–51. https://doi.org/10.1038/nrmicro3380.

[2] Hancock REW. Mechanisms of action of newer antibiotics for Gram-positive pathogens. Lancet Infect Dis 2005;5:209–18. https://doi.org/10.1016/S1473-3099(05)70051-7.

[3] Payne DJ, Gwynn MN, Holmes DJ, Pompliano DL. Drugs for bad bugs: Confronting the challenges of antibacterial discovery. Nat Rev Drug Discov 2007;6:29–40. https://doi.org/10.1038/nrd2201.

[4] Nonejuie P, Burkart M, Pogliano K, Pogliano J. Bacterial cytological profiling rapidly identifies the cellular pathways targeted by antibacterial molecules. Proc Natl Acad Sci U S A 2013;110:16169–74. https://doi.org/10.1073/pnas.1311066110.

[5] Lamsa A, Lopez-Garrido J, Quach D, Riley EP, Pogliano J, Pogliano K. Rapid Inhibition Profiling in Bacillus subtilis to Identify the Mechanism of Action of New Antimicrobials. ACS Chem Biol 2016;11:2222–31. https://doi.org/10.1021/acschembio.5b01050.

[6] Sun Y, Heidary DK, Zhang Z, Richards CI, Glazer EC. Bacterial Cytological Profiling Reveals the Mechanism of Action of Anticancer Metal Complexes. Mol Pharm 2018;15:3404–16. https://doi.org/10.1021/acs.molpharmaceut.8b00407.

[7] Müller A, Wenzel M, Strahl H, Grein F, Saaki TNV, Kohl B, et al. Daptomycin inhibits cell envelope synthesis by interfering with fluid membrane microdomains. Proc Natl Acad Sci U S A 2016;113:E7077–86. https://doi.org/10.1073/pnas.1611173113.

[8] Zhu JH, Wang BW, Pan M, Zeng YN, Rego H, Javid B. Rifampicin can induce antibiotic tolerance in mycobacteria via paradoxical changes in rpoB transcription. Nat Commun 2018;9. https://doi.org/10.1038/s41467-018-06667-3.

[9] Wenzel M, Rautenbach M, Vosloo JA, Siersma T, Aisenbrey CHM, Zaitseva E, et al. The multifaceted antibacterial mechanisms of the pioneering peptide antibiotics tyrocidine and gramicidin S. MBio 2018;9:1–20. https://doi.org/10.1128/mBio.00802-18.

[10] Kunst F, Ogasawara N, Moszer I, Albertini AM, Alloni G, Azevedo V, et al. The complete genome sequence of the gram-positive bacterium Bacillus subtilis. Nature 1997;390:249–56. https://doi.org/10.1038/36786.

[11] Schindelin J, Arganda-Carreras I, Frise E, Kaynig V, Longair M, Pietzsch T, et al. Fiji: An open-source platform for biological-image analysis. Nat Methods 2012;9:676–82. https://doi.org/10.1038/nmeth.2019.

[12] Peach KC, Bray WM, Winslow D, Linington PF, Linington RG. Mechanism of action-based classification of antibiotics using high-content bacterial image analysis. Mol Biosyst 2013;9:1837–48. https://doi.org/10.1039/c3mb70027e.

[13] Strahl H, Bürmann F, Hamoen LW. The actin homologue MreB organizes the bacterial cell membrane. Nat Commun 2014;5:1–11. https://doi.org/10.1038/ncomms4442.

[14] Bakshi S, Choi H, Weisshaar JC. The spatial biology of transcription and translation in rapidly growing Escherichia coli. Front Microbiol 2015;6:1–15. https://doi.org/10.3389/fmicb.2015.00636.

[15] Chen CR, Malik M, Snyder M, Drlica K. DNA gyrase and topoisomerase IV on the bacterial chromosome: Quinolone-induced DNA cleavage. J Mol Biol 1996;258:627–37. https://doi.org/10.1006/jmbi.1996.0274.

[16] Cabrera JE, Cagliero C, Quan S, Squires CL, Ding JJ. Active transcription of rRNA operons condenses the nucleoid in Escherichia coli: Examining the effect of transcription on nucleoid structure in the absence of transertion. J Bacteriol 2009;191:4180–5. https://doi.org/10.1128/JB.01707-08.

[17] Drlica K, Zhao X. DNA gyrase, topoisomerase IV, and the 4-quinolones. Microbiol Mol Biol Rev 1997;61:377–92.

[18] Sugino A, Peebles CL, Kreuzer KN, Cozzarelli NR. Mechanism of action of nalidixic acid: Purification of Escherichia coli nalA gene product and its relationship to DNA gyrase and a novel nicking-closing enzyme. Proc Natl Acad Sci U S A 1977;74:4767–71. https://doi.org/10.1073/pnas.74.11.4767.

[19] Paz MM, Zhang X, Lu J, Holmgren A. A new mechanism of action for the anticancer drug Mitomycin C: Mechanism-based inhibition of thioredoxin reductase. Chem Res Toxicol 2012;25:1502–11. https://doi.org/10.1021/tx3002065.

[20] Prince A, Sandhu P, Kumar P, Dash E, Sharma S, Arakha M, et al. Lipid-II Independent Antimicrobial Mechanism of Nisin Depends on Its Crowding and Degree of Oligomerization. Sci Rep 2016;6:1–15. https://doi.org/10.1038/srep37908.

[21] Kasianowicz J, Benz R, McLaughlin S. The kinetic mechanism by which CCCP (carbonyl cyanide m-Chlorophenylhydrazone) transports protons across membranes. J Membr Biol 1984;82:179–90. https://doi.org/10.1007/BF01868942.

[22] Russell AD. Whither triclosan? J Antimicrob Chemother 2004;53:693–5. https://doi.org/10.1093/jac/dkh171.

[23] Williamson R, Hakenbeck R, Tomasz A. In vivo interaction of β-lactam antibiotics with the penicillin-binding proteins of Streptococcus pneumoniae. Antimicrob Agents Chemother 1980;18:629–37. https://doi.org/10.1128/AAC.18.4.629.

[24] Boger DL. Vancomycin, teicoplanin, and ramoplanin: Synthetic and mechanistic studies. Med Res Rev 2001;21:356–81. https://doi.org/10.1002/med.1014.

[25] Wehrli W. Rifampin: Mechanisms of action and resistance. Rev Infect Dis 1983;5:S407–11. https://doi.org/10.1093/clinids/5.Supplement_3.S407.

[26] Sobell HM. Actinomycin and DNA transcription. Proc Natl Acad Sci U S A 1985;82:5328–31. https://doi.org/10.1073/pnas.82.16.5328.

[27] Siibak T, Peil L, Xiong L, Mankin A, Remme J, Tenson T. Erythromycin- and chloramphenicol-induced ribosomal assembly defects are secondary effects of protein synthesis inhibition. Antimicrob Agents Chemother 2009;53:563–71. https://doi.org/10.1128/AAC.00870-08.

[28] Borovinskaya MA, Pai RD, Zhang W, Schuwirth BS, Holton JM, Hirokawa G, et al. Structural basis for aminoglycoside inhibition of bacterial ribosome recycling. Nat Struct Mol Biol 2007;14:727–32. https://doi.org/10.1038/nsmb1271.

[29] Dobie D, Gray J. Fusidic acid resistance in Staphylococcus aureus. Arch Dis Child 2004;89:74–7. https://doi.org/10.1136/adc.2003.019695.

[30] Hoeksma J, Misset T, Wever C, Kemmink J, Kruijtzer J, Versluis K, et al. A new perspective on fungal metabolites: identification of bioactive compounds from fungi using zebrafish embryogenesis as read-out. Sci Rep 2019;9:1–16. https://doi.org/10.1038/s41598-019-54127-9.

[31] Sawa R, Mori Y, Iinuma H, Naganawa H, Hamada M, Yoshida S, et al. Harzianic acid, a new antimicrobial antibiotic from a fungus. J Antibiot (Tokyo) 1994;47:731–2. https://doi.

org/10.7164/antibiotics.47.731.

[32] Vinale F, Manganiello G, Nigro M, Mazzei P, Piccolo A, Pascale A, et al. A novel fungal metabolite with beneficial properties for agricultural applications. Molecules 2014;19:9760–72. https://doi.org/10.3390/molecules19079760.

[33] De Tommaso G, Salvatore MM, Nicoletti R, DellaGreca M, Vinale F, Bottiglieri A, et al. Bivalent metal-chelating properties of harzianic acid produced by Trichoderma pleuroticola associated to the gastropod Melarhaphe neritoides. Molecules 2020;25. https://doi.org/10.3390/molecules25092147.

[34] Vinale F, Flematti G, Sivasithamparam K, Lorito M, Marra R, Skelton BW, et al. Harzianic acid, an antifungal and plant growth promoting metabolite from Trichoderma harzianum. J Nat Prod 2009;72:2032–5. https://doi.org/10.1021/np900548p.

[35] De Filippis A, Nocera FP, Tafuri S, Ciani F, Staropoli A, Comite E, et al. Antimicrobial activity of harzianic acid against Staphylococcus pseudintermedius. Nat Prod Res 2020;0:1–6. https://doi.org/10.1080/14786419.2020.1779714.

[36] Lamsa A, Liu WT, Dorrestein PC, Pogliano K. The Bacillus subtilis cannibalism toxin SDP collapses the proton motive force and induces autolysis. Mol Microbiol 2012;84:486–500. https://doi.org/10.1111/j.1365-2958.2012.08038.x.

SUPPORTING INFORMATION

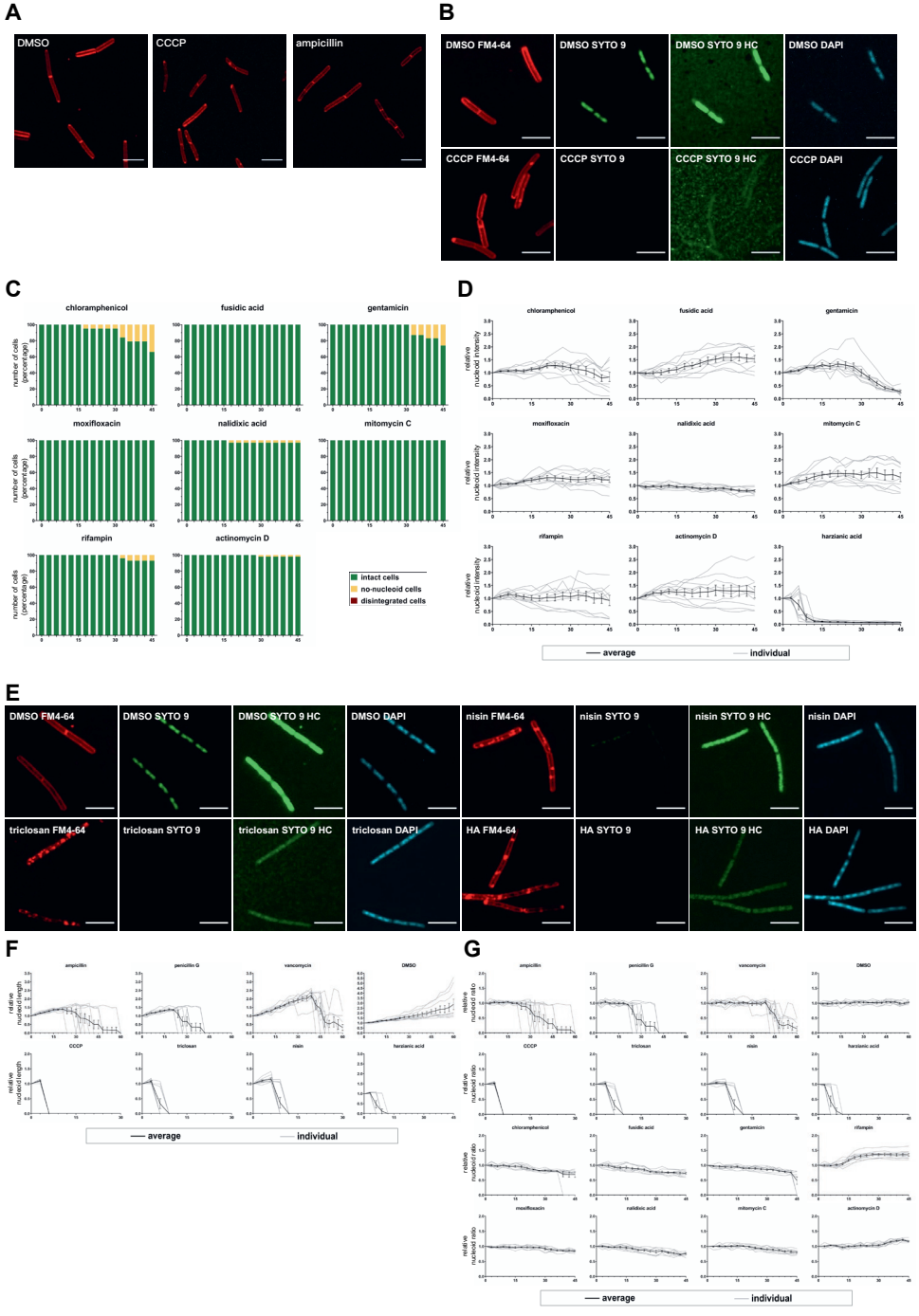

Fig. S1. Additional BCP and DBCP profiles.

(A) Cell permeability assay. *B. subtilis* cells were treated with antimicrobials (2.5 × MIC) or 1% DMSO (control) for 60 min. Cells were stained with FM4-64 (red, cell membrane) and SYTOX-Green (green, nucleoid), and imaged by confocal fluorescence microscopy. Representative images are shown. Scale bar is 5 μm.

(B) Dual nucleoid staining of cells following CCCP treatment for 60 min. *B. subtilis* cells were treated with CCCP (2.5 × MIC) or 1% DMSO (control) for 60 min. Cells were stained with FM4-64 (red, cell membrane), SYTO-9 (green, nucleoid) and DAPI (blue, nucleoid), and imaged by confocal fluorescence microscopy. Representative images are shown. Scale bar is 5 μm. SYTO-9 graphs were shown both in normal contrast and high contrast (HC).

(C) Changes in cell status upon antimicrobial treatment. *B. subtilis* cells were treated with antimicrobials (2.5 × MIC) as indicated. Cells were stained with FM4-64 (red, cell membrane) and SYTO-9 (green, nucleoid), and imaged by time lapse confocal fluorescence microscopy with 3 min intervals. Three distinct cell types were identified: intact cells (cells with visible membrane and nucleoid fluorescence), no-nucleoid cells (cells with apparently intact membrane, but without visible nucleoid florescence) and disintegrated cells (cells with disintegrated membrane and no detectable nucleoid). The number of cells of the three types were counted from biological triplicate imaging series (n > 20). The ratio of cell types, intact cells (green), no-nucleoid cells (yellow) and disintegrated cells (red), was determined and plotted as percentage (y-axis, numbers in %) over time (x-axis, min). See Fig. 5A for DMSO control as this figure is an extension.

(D) Changes in nucleoid intensity upon antimicrobial treatment. *B. subtilis* cells were treated with antimicrobials (2.5 × MIC) as indicated. Cells were stained and imaged as in (C). Cell morphology data were collected from 9 cells in total per treatment, i.e. technical triplicates from biological triplicate imaging series. Overall nucleoid intensity, i.e. the SYTO-9 fluorescence intensity inside a whole cell, corrected for background, was determined for individual cells over time and was depicted as percentage of the value at the start (t = 0min) (y-axis) over time (x-axis, min). The mean of antimicrobial-treated cells was plotted in black with error bars representing the SEM. Gray lines represent individual antimicrobial-treated cells on which the mean was based. See Fig. 5B for DMSO control as this figure is an extension.

(E) Dual nucleoid staining of cells following treatment with antimicrobials from cell membrane class or harzianic acid (HA) for 3 min. *B. subtilis* cells were treated with antimicrobials (2.5 × MIC) as indicated or 1% DMSO (control) for 3 min. Cells were stained with FM4-64 (red, cell membrane), SYTO-9 (green, nucleoid) and DAPI (blue, nucleoid), and imaged by confocal fluorescence microscopy. Representative images are shown. Scale bar is 5 μm. SYTO-9 graphs were shown both in normal contrast and high contrast (HC).

(F) Changes in nucleoid length upon antimicrobial treatment. *B. subtilis* cells were treated with antimicrobials (2.5 × MIC) as indicated or 1% DMSO (control). Cells were stained, imaged and analyzed as in (D). Nucleoid length, the addition of the length of all the nucleoids inside one cell, was determined for individual cells and depicted as percentage of the value at the start (t = 0min) (y-axis) over time (x-axis, min). The mean of antimicrobial-treated cells was plotted in black with error bars representing the SEM. Gray lines represent individual antimicrobial-treated cells on which the mean was based. This figure is an extension of Fig. 6A, where the first 45 min of DMSO control has already shown.

(G) Changes in the ratio of nucleoid length to the cell length upon antimicrobial treatment. *B. subtilis* cells were treated with antimicrobials (2.5 × MIC) as indicated or 1% DMSO (control). Cells were stained,

imaged and analyzed as in (D). The ratio of the nucleoid length to the cell length, was calculated for individual cells over time and was depicted as percentage of the value at the start (t = omin) (y-axis) over time (x-axis, min). The mean of antimicrobial-treated cells was plotted in black with error bars representing the SEM. Gray lines represent individual antimicrobial-treated cells on which the mean was based.

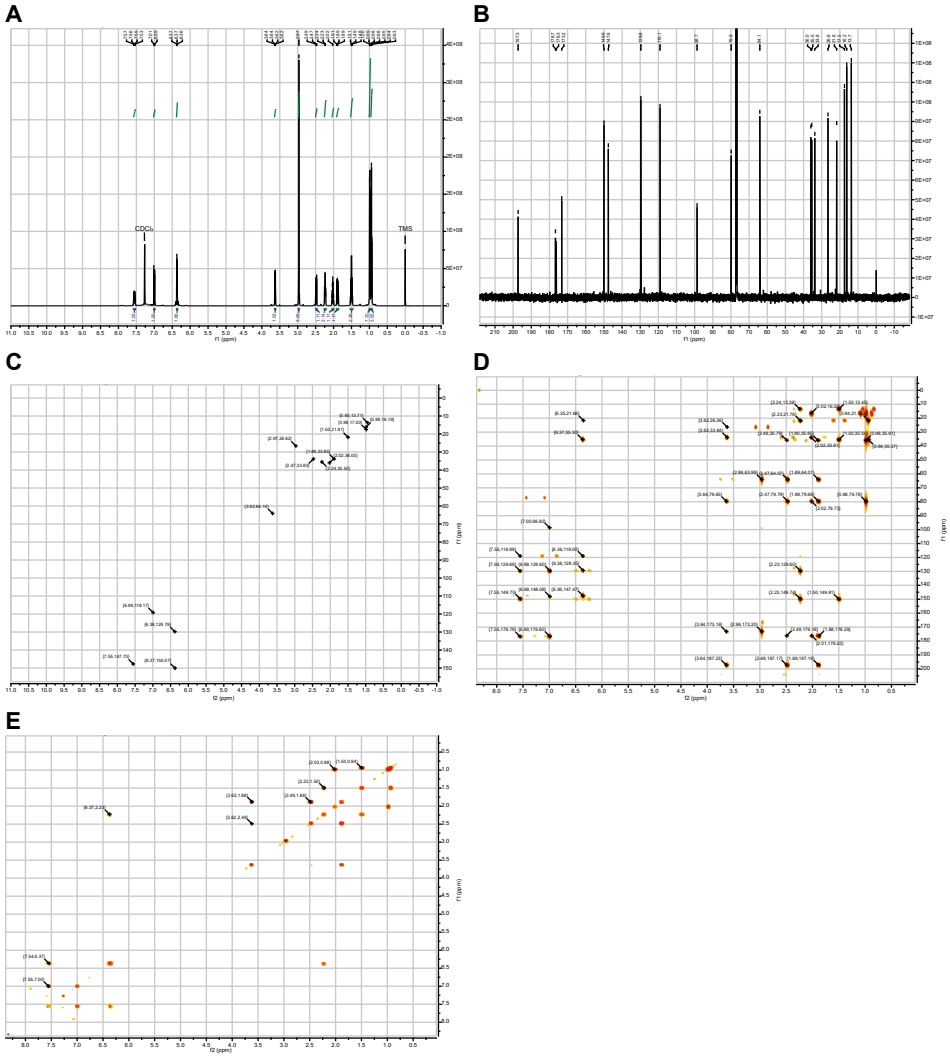

Fig. S2. NMR spectroscopy of harzianic acid. (A) ^{1}H-NMR spectrum, 600 MHz, $CDCl_3$. (B) ^{13}C-NMR spectrum, 150 MHz, $CDCl_3$. (C) HSQC spectrum, 600 MHz, $CDCl_3$. (D) HMBC spectrum, 600 MHz, $CDCl_3$. (E) COSY spectrum, 600 MHz, $CDCl_3$.

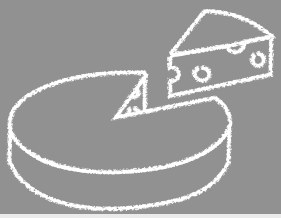

Harzianic Acid, a Multi-Target Antimicrobial Agent Against Gram-Positive Bacteria

CHAPTER 5

Xudong Ouyang[1,2], Wouter A.G. Beenker[1], Jelmer Hoeksma[1], Samantha van der Beek[1] and Jeroen den Hertog[1,2]

1. Hubrecht Institute-KNAW and University Medical Center Utrecht, Utrecht, the Netherlands
2. Institute Biology Leiden, Leiden University, Leiden, the Netherlands

ABSTRACT

The thermophilic fungus *Oidiodendron flavum* is a saprobe that is commonly isolated from soil. Previously, we identified a Gram-positive bacteria-selective antimicrobial secondary metabolite (SM) from this fungal species, harzianic acid (HA). With an imaging-based mechanism of action (MoA) identification strategy, we predicted that HA targets the cell envelope. Here, we investigated the MoA of HA in more detail, using *Bacillus subtilis*. HA targeted the cell membrane, but only at high concentrations. We isolated a HA-resistant strain, M9015, and discovered that the mutant harbors five mutations in the coding region of four distinct genes. Further analysis of these genes might provide more insight into the MoA of HA at low concentrations. We conclude that HA is a multi-target antimicrobial agent against Gram-positive bacteria.

INTRODUCTION

The genus of *Oidiodendron* was established under the *Myxotrichaceae* family by Robak in 1932 [1]. Species of *Oidiodendron* are known as saprobes and are commonly isolated from a wide range of habitats, including soil, decaying plant materials, marine sediments and decomposing human hair [2–5]. They primarily occur through the temperate regions, with a few exceptions from tropical and subtropical locales. The widespread distribution of this genus is in connection with their excellent adaptive capacity, by which they establish various interactions with other organisms [6–8].

An important fungal trait for interaction with their surroundings is the production of secondary metabolites (SMs), which are not essential for fungal growth [9]. These compounds are chemically distinct small molecule compounds (in most cases < 3 kDa) often with biological activities that are produced at specific stages of growth to perform important functions, including survival from harsh environments, communication with invaders or alteration of fungal development [10]. SMs are synthesized along different pathways than primary metabolites [11] and they are excellent sources of potential therapeutic drugs [12]. Whereas the genus of *Oidiodendron* has drawn much attention with respect to studies of morphology and taxology [6,13], there are not many investigations into their ability to produce SMs.

Oidiodendron flavum is a thermophilic fungus and a member of the genus *Oidiodendron* [6]. Previously, we identified an antimicrobial SM from this fungal species, harzianic acid (HA). HA was first isolated as a novel antimicrobial agent from a fungal strain *Trichoderma harzianum* in 1994 [14]. Surprisingly, subsequent research focused more on the activity of HA as a plant promotor rather than an antimicrobial [11,15]. Therefore, not much data is available regarding its antimicrobial activity yet. Since HA strongly inhibits bacterial growth, it is suggested to be a promising candidate to achieve clinical application. Thus, further research into identification of its mechanism of action (MoA) is required.

Recently, we developed an imaging-based strategy, dynamic bacterial cytological profiling (DBCP), to classify antimicrobials into different classes based on their MoAs and hypothesized that HA targets the cell envelope (**Chapter 4**). Here, we applied several assays to confirm this hypothesis and to unravel further details about its MoA. In addition, we isolated HA-resistant bacteria and identified four mutated genes, which provides further insight into its MoA.

MATERIALS AND METHODS

Strains and reagents

B. subtilis strain 168 was used for MoA identification in this study [16]. *O. flavum* (CBS 366.71) was obtained from the Westerdijk Fungal Biodiversity Institute (the Netherlands) and used for biologically active compound production. Pathogenic bacterial strains used for activity tests were either obtained from ATCC or they were clinical isolates (kind gift from University Medical Center Utrecht, the Netherlands) and they are listed in Table S1. Commercial antimicrobials and resazurin were purchased from Sigma Aldrich. FM4-64, $DiSC_3(5)$ and SYTOX-Green were purchased from Thermo Fisher Scientific.

Microdilution assay

Minimum Inhibitory Concentration (MIC) was determined by broth microdilution assay as previously described [17]. The freshly prepared early exponential-phase cell cultures of different strains were diluted 1 : 100 into Luria-Bertani (LB) medium, and then distributed in a 96-wells plate. Antimicrobials were tested starting at a 10 × dilution of the stock in DMSO, which was then serially diluted with a factor 2. MIC was defined as the lowest dilution at which bacteria did not grow, based on visual inspection after an overnight incubation at 37 °C.

Growth curves

Overnight bacterial cultures of *B. subtilis* were diluted 1 : 50 into fresh LB medium and incubated at 37 °C with shaking. For the accurate MIC of HA determination, OD_{600} of cultures were measured by a FLUOstar microplate reader (BMG Labtech) every 30 min for 24 h. At an early exponential-phase of cultures with an OD_{600} of 0.3, different concentrations of HA were added. For the comparison of *B. subtilis* strain 168 and M9015, OD_{600} of both cultures was measured using a Bioscreen C Microbiology Reader every 15 min for 24 h.

Confocal microscopy

Microscopy was performed following the protocol described before with minor modification [18]. Briefly, samples were immobilized on microscope slides covered with an agarose pad containing 1% agarose and LB medium, and imaged. Confocal microscopy was carried out using a Perkin Elmer UltraView VoX spinning disk

microscope system, consisting of a Leica DMI6000 microscope equipped with a 100 × NA1.47 oil objective, a Yokogawa X1 spinning disk unit, a Hamamatsu Orca Flash4.0 V3 camera, and Volocity v6.3 software. Z-stack images were collected over a length of 3 μm with 0.2 μm intervals to acquire signals from the whole cells. Experiments were done with biological triplicates. Images were analyzed using Fiji [19].

Sporulation inhibition assay

This assay was applied as previously described with modifications [20]. The freshly prepared early exponential-phase cell cultures of *B. subtilis* with an OD_{600} of 0.3 in LB media were centrifuged and resuspended in 1/10 of the original volume. Antimicrobials (5 × MIC) or DMSO (control) were added and 15 μL of the mixtures were transferred into 1.5 mL tubes to incubate with rolling at 37 °C for 5 h. Cells were then stained with FM 4–64, immobilized and imaged.

Cytotoxicity assay

For the cytotoxicity assay, HepG2 cells were seeded in 96-well plates and grown in DMEM low glucose medium (ThermoFisher, 10567014) supplemented with 10% FBS. Test compounds were added in different concentrations, with a final concentration of 1% DMSO and cells were incubated for 20 h at 37 °C with 5% CO_2. Next, resazurin was added to reach a final concentration of 0.1 mM. After 3 h incubation, the fluorescence was measured on a PHERAstar microplate reader (BMG Labtech) using an excitation wavelength of 540 nm and emission wavelength of 590 nm. The average intensity of DMSO control was set as 100% alive and the percentage of intensity from each treated sample was calculated. IC_{50} was calculated using nonlinear regression in GraphPad Prism. Experiments were conducted in biological triplicates.

Resazurin assay

This assay was applied as previously described with modifications [18]. Resazurin is an oxidation–reduction indicator (excitation at 530-570 nm, emission at 580-590 nm) [21]. Freshly prepared early exponential-phase *B. subtilis* cultures with an OD_{600} of 0.3 in LB medium were treated with antimicrobials (5 × MIC) or DMSO (control) for 5, 30 and 60 min. Untreated cells and boiled cells (95°C for 10 min) were used to calculate the standard respiration and no respiration, respectively. Next, cells were washed with medium by centrifugation and afterwards resuspended in medium to adjust the OD_{600} to 0.15. Cells were then incubated with 30 μg/mL resazurin for 45

min at 37 °C. Absorbance of different samples was measured using a 540 nm/590 nm filter.

Cell depolarization assay and cell permeability assay

$DiSC_3(5)$ is commonly applied for cell depolarization assay because it generally accumulates in well-energized cells. Disruption of membrane potential releases this probe from cells into the medium, resulting in an increase of overall fluorescence in the cell suspension [22]. SYTOX green was used in the cell permeability assay. This dye is cell impermeable and its fluorescence signal increases significantly when bound to DNA [23]. To perform these assays, the freshly prepared early exponential-phase cell cultures with an OD_{600} of 0.3 in LB medium were stained with $DiSC_3(5)$ or SYTOX green for 10 min. Then the fluorescence was measured on a PHERAstar microplate reader (BMG Labtech) using a 540 nm/590 nm filter for $DiSC_3(5)$, or a 485 nm/520 nm filter for SYTOX green. Experiments were conducted in biological triplicates.

Lipid assay

This assay was applied as previously described with modifications [24]. The appropriate amounts of antagonists lipid I, lipid II and C_{55}-P in $CHCI_3$: MeOH (1 : 1) were added to the 96-well plates and the solvent was evaporated. The antagonists were re-dissolved in LB containing antimicrobials (2 × and/or 1 × MIC) or 1% DMSO in solution. The freshly prepared early exponential-phase cell cultures of *B. subtilis* were diluted 1 : 100 into LB medium, and then distributed in the 96-wells plate with antagonists and antimicrobials. After incubation overnight at 37 °C, bacterial growth was inspected visually.

Screening for HA-resistant mutants

To obtain HA-resistant mutants, we grew *B. subtilis* in the presence of 1 x MIC of HA in LB medium at 37 °C with shaking. Once bacterial growth was observed, it was sequentially transferred to medium with 2-fold higher concentrations of HA. The whole process was set for a period of 28 days.

Scanning electron microscopy

Overnight cultures of *B. subtilis* strain 168 and M9015 were transferred to fresh LB medium and grown to mid-log phase. Bacterial cells were then washed, fixed,

dehydrated, mounted onto 12.5 mm specimen stubs and coated with gold to 1 nm as previously described [25]. Samples were imaged using a Phenom PRO desktop SEM (Phenom-World BV). Cell width was measured from 10 cells for each strain from triplicate images using Fiji.

Peptidoglycan analysis

This assay was performed following a previous protocol [26]. The overnight bacterial culture of *B. subtilis* was diluted 1 : 50 into 400 mL fresh LB medium and incubated at 37 °C with shaking until reaching expected cell density. The cell culture was then chilled on ice and centrifuged at 5,000 x g for 10 min at 4 °C. After washing twice with cold PBS, the cell pellet was resuspended in 10 mL PB (25 mM sodium phosphate, pH 6.0), disrupted using beads beater, mixed with 10 mL of 10% (w/v) SDS in a boiling water bath, boiled for 30 min and incubated at 37 °C overnight. Next, the sample was centrifuged at 45,000 x g for 30 min at 20 °C to pellet the insoluble peptidoglycan, which was then washed with 10 mL of PB 4-6 times, suspended in 2 mL PB and transferred to a microcentrifuge tube. After adding 200 µg/mL of pronase and incubating for 2 h at 37 °C with agitation, TCA hydrolysis was performed at 4 °C for 18 h with constant shaking. Afterwards, the hydrolyzed sample was centrifuged at 45,000 x g for 30 min at 20 °C to pellet the insoluble peptidoglycan, which was then washed three times, suspended in 5 mL PB. After digestion of peptidoglycan using 0.5 mg/mL lysozyme overnight and reduction of sugars using sodium borohydride for 20 min, sample was ready for HPLC analysis, which was performed using a Shimadzu LC-2030 system with PDA detection (190-800 nm) and a Shimadzu Shim-pack GISTC18-HP reversed phase column (3 µm, 4.6 × 100 mm). The mobile phase was 50 mM sodium phosphate pH = 4.33 (buffer A) and 50 mM sodium phosphate pH = 5.1 with 15% (v/v) methanol (buffer B). A flow rate of 0.5 mL/min was applied using the following protocol: buffer A for 10 minutes followed by a linear gradient of buffer B (0–100%) for 120 minutes, 100% buffer B for 10 minutes, another linear gradient of buffer B (100–0%) for 5 minutes and finally buffer A for 5 minutes.

Genomic DNA sequencing

The bacterial cell wall of *B. subtilis* was lysed using 0.5 mg/mL lysozyme for 1 h at 37 °C. Next, genomic DNA was isolated using the Wizard Genomic DNA purification Kit (Promega) and sequenced by Illumina Next Generation Sequencing in University Medical Center Utrecht.

Bioinformatic analysis

The raw sequencing reads were subjected to a panel of bioinformatic analyses including quality control using FastQC and Trimmomatic, alignment to reference genome using BWA-MEM algorithm and variant calling using Integrative Genomics Viewer (IGV). The published genome sequence of *Bacillus subtilis* subsp. *subtilis* str. 168 was used as the reference genome, which has a NCBI accession number of NC_000964.3.

RESULTS

HA is a selective antimicrobial against Gram-positive bacteria

HA was tested against a panel of 14 pathogenic bacteria, including seven Gram-positive and seven Gram-negative strains (Table S1). The growth of all Gram-positive bacteria was affected with Minimum Inhibitory Concentrations (MICs) ranging from 25 to 200 μg/mL. The panel included antibiotic-resistant pathogenic bacteria, which were sensitive to HA, e.g. methicillin resistant *Staphylococcus aureus* (MRSA) at 200 μg/mL and vancomycin resistant *Enterococcus faecium* (VRE) at 100 μg/mL. No inhibition was observed in response to HA of any of the Gram-negative bacteria tested up to 400 μg/mL This indicates that HA is a selective antimicrobial agent against Gram-positive bacteria. Next, to assess the toxicity of this compound on human cells, cytotoxicity assays were done using the HepG2 cell line, originating from human liver. The IC_{50} for HA was 226.6 μg/mL (Fig. 1A), indicating that human cells have a higher tolerance for HA than Gram-positive bacterial cells.

HA induced lysis of Bacillus subtilis cells

To further explore the antimicrobial properties of HA against Gram-positive bacteria, a model Gram-positive organism, *B. subtilis* strain 168, was used for the following assays. First, to obtain an accurate MIC, the growth curves of *B. subtilis* were measured in the presence of a range of HA concentrations (Fig. 1B). Although cells were also affected at concentrations of 30 and 40 μg/mL, total inhibition of cell growth after 18 h (overnight) was only seen at a concentration of 50 μg/mL and higher, suggesting that the correct MIC for *B. subtilis* was 50 μg/mL. In the following assays, we used 250 μg/mL (5 × MIC) HA to ensure the effects on cells, unless specified differently. Interestingly, a decrease in OD_{600} was observed 30 min after addition of the compound with all concentrations of HA, even with the lowest

concentration, 30 μg/mL. This decrease was not observed with vehicle control (DMSO), indicating that this decrease was not an artefact. These results suggest that HA induced cell lysis soon after addition to the cells. Some microorganisms, including *B. subtilis*, respond to harsh environments by entering a robust resting state, the endospore, which is self-protective. During that process, cells may also lyse [27]. To determine whether HA destroyed the cells and/or induced the cells to form endospores, a sporulation assay was performed. In the control-treated cultures (Fig. 1C), spores were generated by some of the cells during high-density culturing overnight. However, following overnight HA treatment, no intact cells were observed and no clear spores were observed either (Fig. 1D). These results suggest that HA destroyed the cells without inducing spore formation.

Pore formation is the initial effect of HA on bacterial cells

Using DBCP, we previously predicted that HA generated pores on the bacterial cell membrane and inhibited cell growth immediately after addition to cells (**Chapter 4**). To confirm this mechanism, we first investigated bacterial cell viability using a resazurin assay [21]. Our results (Fig. 1E) showed that after 5 min treatment, 99% of cells lost their viability. None of the cells seemed to be viable after HA treatment for 60 min. This confirms that HA has an immediate effect when added to bacteria.

Next, we used $DiSC_3(5)$ to detect changes in transmembrane potential [22]. Carbonyl cyanide *m*-chlorophenyl hydrazone (CCCP) and nisin were selected as positive controls, because they are known to destroy the membrane potential by disruption of cellular ionic homeostasis and generation of pores in the cell membrane, respectively [28,29]. Similar to treatment with CCCP or nisin, HA induced a sudden increase of fluorescence in cells (Fig. 1F), suggesting that disruption of the membrane potential was an immediate effect.

To determine whether the loss of membrane potential was due to a pore-forming activity or not, cell permeability was investigated with SYTOX green [23]. As shown in Fig. 1G, the fluorescence intensity of the cell suspension gradually increased upon HA and nisin treatment, but not CCCP treatment. This suggests that the disruption of membrane potential in response to HA was caused by pore formation.

Vancomycin- and nisin-induced cell lysis is caused by binding to lipid II [29,30]. To determine if HA-induced pore formation was also mediated by binding to lipid II in the membrane, lipids were added to the bacterial cultures prior to addition of HA. If HA binds directly to lipid II or precursors, the externally added lipids will quench HA and hence, addition of HA will not affect bacterial growth [24]. Several

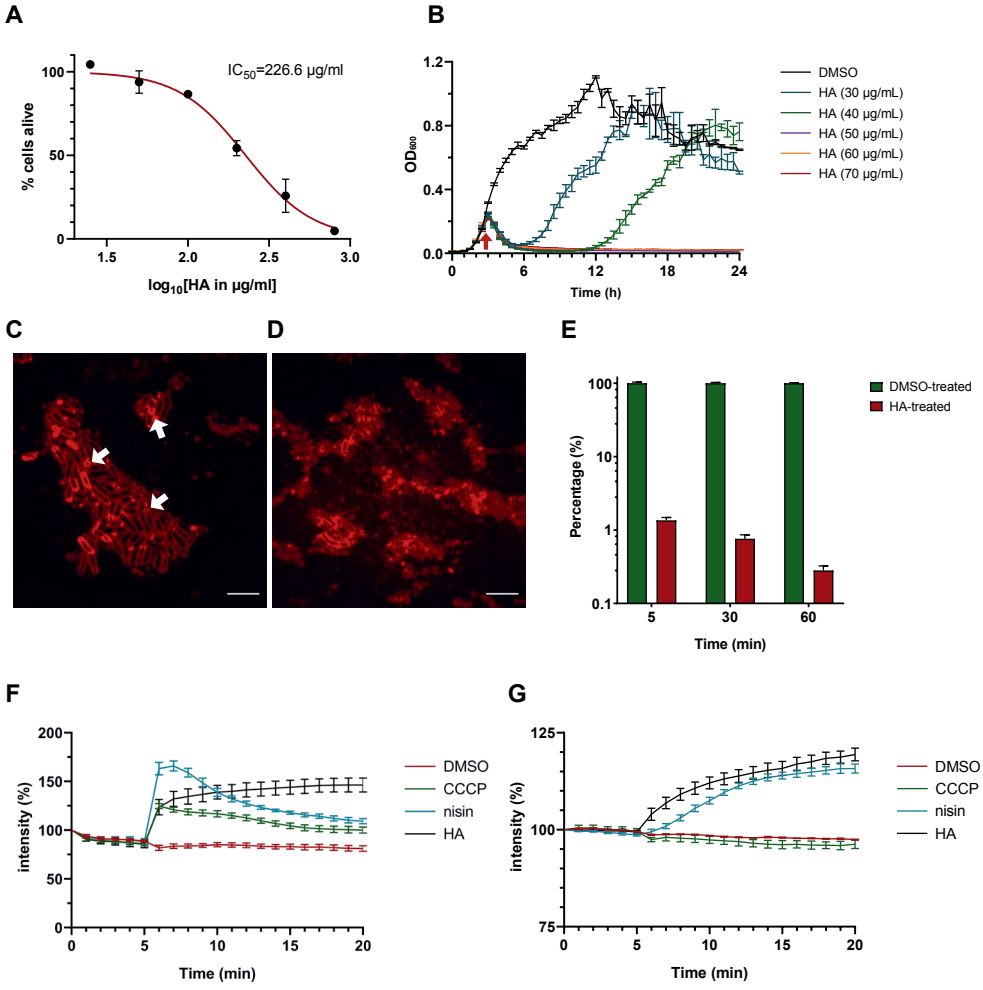

Fig. 1. Antimicrobial property of HA. (A, B) HA inhibits eukaryotic cell growth and bacterial growth. (A) Cytotoxicity assay. HepG2 cells were incubated with HA in different concentrations for 20 h before addition of resazurin. The ability to reduce blue resazurin to red resorufin was measured at 540 nm. The average intensity of DMSO control was set as 100% alive and the percentage of intensity from each treated sample was calculated. The mean from biological triplicates was plotted with error bars representing the SEM in black. Nonlinear regression was analyzed and plotted in red, on which IC_{50} was based. (B) Growth curves of *B. subtilis* strain 168/WT in the presence of a range of HA concentrations. OD_{600} was measured every 30 min. HA was added at 2.5 h (arrow). The graph depicts the average and the SEM of biological triplicates. (C, D) No sporulation in response to HA. *B. subtilis* cells from a high density overnight culture were treated with (C) DMSO (control) or (D) HA (250 µg ml^{-1}, 5 × MIC), stained with FM4-64 and imaged by confocal fluorescence microscopy. Representative images are shown. Example spores in the DMSO

control are indicated with arrows. Scale bar is 5 μm. (E) HA rapidly blocks respiratory chain activity in *B. subtilis*. Effect on respiratory chain activity measured by the reduction from blue resazurin to red resorufin at 540 nm. The average intensity of DMSO control in each group was set to 100% intensity. HA (250 μg ml^{-1}, 5 × MIC) was added and after 5, 30 and 60 min, the percentage of conversion was calculated relative to the control. The mean from biological triplicates was plotted with error bars representing the SEM. The log 10 format was used for the scale of the Y axis. (F, G) HA treatment induced membrane permeability. (F) Membrane potential measurement. *B. subtilis* membrane potential levels were quantified using the fluorescent dye $DiSC_3(5)$. CCCP (2 μg ml^{-1}, 5 × MIC), nisin (12.5 μg ml^{-1}, 5 × MIC) or HA (250 μg ml^{-1}, 5 × MIC) (as indicated) or DMSO was added after 5 min. The fluorescence was depicted as percentage of the value at the start (t = 0min) (y-axis) over time (x-axis, min). The mean from biological triplicates was plotted with error bars representing the SEM. (G) Membrane permeability measurement. Experiments were performed as in (F), except for using a different dye SYTOX-Green for quantifying membrane permeability.

lipid II precursors were selected: C55P, lipid I and lipid II. Vancomycin (0.5 μg/mL, 2 × MIC) and nisin (5 μg/mL, 2 × MIC) were used as positive controls for this assay. *B. subtilis* cells were treated with these control antimicrobials in the presence or absence of 10 μM of the different lipids and bacterial cell growth was determined (Table S2). The antimicrobial effects of nisin and vancomycin were quenched by exogenous lipid I and lipid II as expected. C55P also affected antimicrobial activity of nisin. For HA, both 2 × MIC (100 μg/mL) and 1 × MIC (50 μg/mL) were tested in the presence of 10 μM or even 150 μM of the different lipids. However, the activity of HA was not affected by addition of any of these lipids, suggesting the mechanism underlying pore formation by HA and nisin are distinct.

Screening for HA-resistant mutants

Knowledge about antimicrobial resistance may provide insight into the underlying MoA. Inducing resistance by prolonged exposure to increasing concentrations of antimicrobial agents is a proven method. To obtain insight into the MoA of HA, we grew *B. subtilis* in the presence of 1 x MIC of HA for three days. Under these conditions, three colonies grew and these were transferred sequentially to medium with 2-fold higher concentrations of HA. Over a period of 28 days, one colony was successfully grown in medium with 4 × MIC of HA. Resistance against an antimicrobial may be due to either gene mutation or gene expression adaptation. To

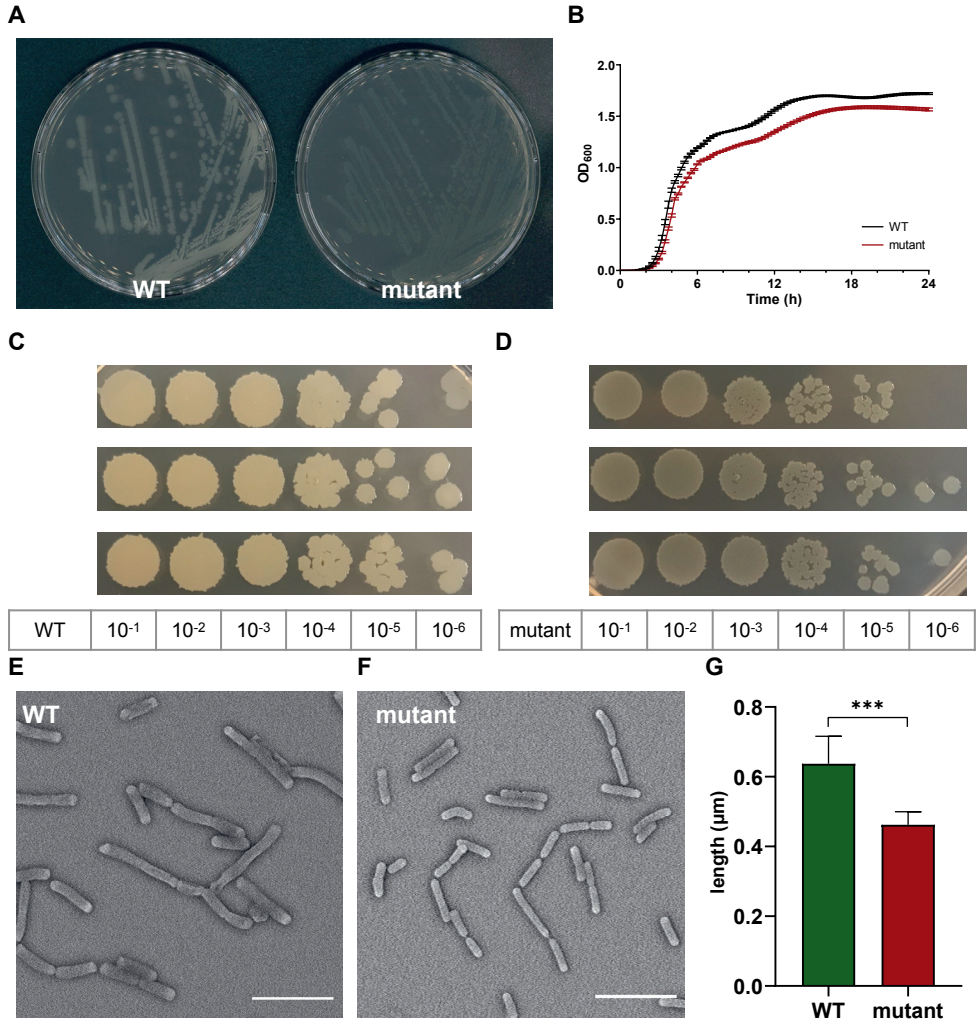

Fig. 2. HA-resistant M9015 colonies are translucent and mutant cells are smaller. (A) *B. subtilis* strain 168/WT and M9015 plated on LB agar. (B) Growth curves of WT and M9015. OD_{600} was measured and the mean from biological triplicates was plotted with error bars representing the SEM. (C and D) CFU counting. The overnight cultures (18 h) of WT and M9015 were serially diluted, and 5 µL of each diluted sample was dropped on LB agar. Experiments were performed with biological triplicates. (E and F) The cells from overnight cultures (18 h) of WT and M9015 were fixed and imaged by scanning electron microscopy. Representative images are shown. The width of cells was measured and plotted in (G); mean with error bars representing the SEM is depicted; *** indicates p≤0.001 by student t-text.

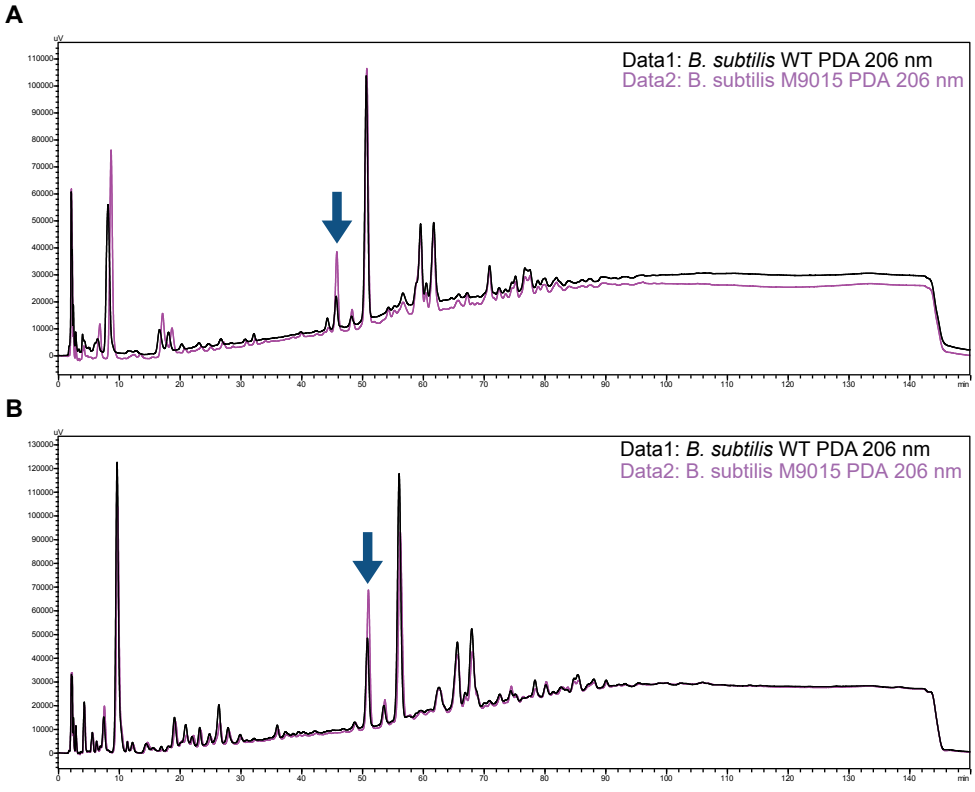

Fig. 3. Similar peptidoglycan pattern between *B. subtilis* strain 168 and M9015. Peptidoglycan of both strains from overnight culture (A) and exponential phase culture (B) were isolated, digested and analyzed by analytical HPLC. The arrow in each figure indicated the peak that differed most between the two strains.

distinguish between these possibilities, we cultured the resistant bacteria without HA for ten serial passages. Finally, an accurate microdilution assay showed that this strain, dubbed *B. subtilis* strain M9015, had a maximum tolerance of 250 μg/mL, which is 5 × higher than the MIC of wild type *B. subtilis* strain 168. HA resistance persisted in the M9015 strain, suggesting that resistance is caused by mutations in the genome.

The M9015 strain was not only resistant to HA, but the colonies also had a different appearance on agar plates than wild type. *B. subtilis* strain M9015 colonies had a more translucent appearance, but the colony size did not differ much between the wild type and M9015 strains (Fig. 2A). We assumed that this interesting phenotype

might be due to a slower growth rate (i.e. less cells), smaller cell size or a structural change in the cell wall (i.e. cells were more translucent). To investigate this, the growth curves of the strains were first compared. The growth pattern of both strains was similar, but the mutant had a 15 min longer period in the lag phase and a 0.2 lower final optical density at 600 nm in the stationary phase (Fig. 2B). Next, the number of cells in the overnight culture was determined (Fig. 2C, D). The cell density in the mutant strain was 2.2×10^8 CFU/mL, which was 57% higher than wild type (1.4×10^8 CFU/mL). Comparison of the cell size using a scanning electron microscope (Fig. 2E, F) showed that M9015 mutant cells were 27 ± 5 % smaller than wild type cells (Fig. 2G). These results suggest that the cell size affected the appearance of M9015 colonies.

To determine if there were changes in the structure of the cell wall that also contributed to the translucent phenotype, we analyzed the peptidoglycans. To this end, the cell wall was isolated from overnight cultures of both strains, followed by lysozyme digestion and HPLC analysis. Almost all peaks were matching between the M9015 mutant and wild type (Fig. 3A). However, one peak (arrow indicated) in the mutant sample was higher than in wild type. Peptidoglycan analysis of exponential phase cultures of these two strains showed similar results (Fig. 3B). It is unlikely that

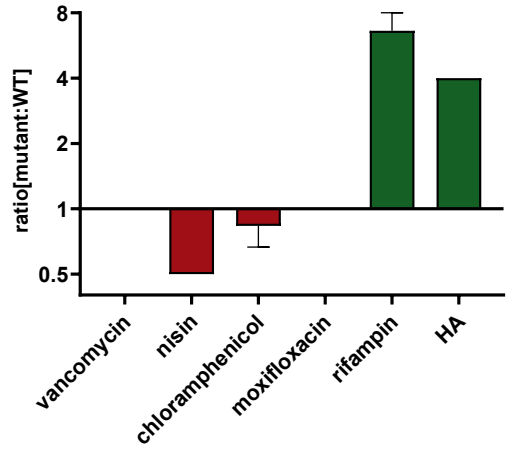

Fig. 4. HA-resistant M9015 strain is also resistant to rifampin. MICs of selected antimicrobials against WT or M9015 were measured. The ratio of the MIC of a certain antimicrobial against M9015 to that against WT was calculated. The mean of the ratio from biological triplicates was plotted with error bars representing the SEM. The red bars indicated that M9015 was more sensitive to certain antimicrobial whereas the green bars indicated the opposite. The log 2 format was used for the scale of Y axis.

the slight difference in peptidoglycan composition of the cell wall contributed to the different appearance of the M9015 strain. However, this remains to be determined definitively.

Cross resistance of the M9015 strain to other antimicrobials might provide valuable insight into the resistance class of this mutant strain. Therefore, we compared the MICs on M9015 mutant and wild type strains of antimicrobials from five major classes: nisin, vancomycin, chloramphenicol, moxifloxacin and rifampin. Interestingly, M9015 showed reduced sensitivity to rifampin, an RNA class antimicrobial, to a similar extent as HA (i.e. 4- to 8-fold; Fig. 4). No significant differences were observed for any of the other antimicrobials, which included antimicrobials targeting the cell envelope. It is surprising that the HA-resistant M9015 strain is also more resistant to the RNA class antimicrobial rifampin, because our earlier DBCP experiments suggested that HA targets the cell envelope.

Identification of mutations in M9015 by genomic sequencing

In order to determine which pathway(s) was/were affected in M9015, the genomes of M9015 mutant and wild type strains were sequenced by Next Generation Sequencing. The published genome sequence of *Bacillus subtilis* subsp. *subtilis* str. 168 was used as the reference genome. The mapping of the reads from our wild type strain against this referenced genome showed high coverage (only around 2,000 mutation sites), suggesting this reference is applicable, which facilitated the alignment of our sequencing data. Bioinformatic comparison of the wild type and mutant genomes resulted in the identification of ten potential variations (Table S3), five of which were suggested to be reliable by the Integrative Genomics Viewer (Fig. S1, S2). These five mutations were located in the coding region of four different genes, *ymaB*, *flgL*, *atpE* and *yusO* (twice).

The mutations in *ymaB* and *atpE* were single-base substitutions causing an amino acid substitution in their protein products. YmaB is a putative Nudix hydrolase with RNA pyrophosphohydrolase activity [31], and the mutation we found resulted in a p.L138P substitution (Fig. 5A). Although both these amino acids are non-polar and hydrophobic, their structures differ substantially, which might affect the activity of YmaB. The function of this gene is not clearly described in literature yet, and therefore the effect of the observed mutation remains unclear. The *atpE* gene encodes the subunit c of ATP synthase [32]. In M9015, we identified a p.A51V substitution (Fig. 5B). The property of these two amino acids is quite similar, but the larger size of Val in the mutant might affect the activity of AtpE severely.

Fig. 5. Mutated genes of M9015. The genes of *ymaB* (A), *atpE* (B), *yusO* (C) and *flgL* (D) are shown. Each gene was presented with DNA sequence (grey line with numbers indicating the length of DNA) and protein sequence (green line with green blocks indicating the sites of initiation codon). Red blocks in the mutated gene and protein sequences indicate the mutated sites.

The *yusO* gene expresses YusO, a transcription repressor, which binds to the *yusOP* promoter region and thus represses *yusOP* expression. YusP confers low-level resistance to fusidic acid, novobiocin, streptomycin, and actinomycin [33]. This gene was disrupted by two insertions in M9015 mutant cells: a single-base insertion (c.199_200insA), introducing a frame shift and stop-codon and an in-frame nine-base insertion (c.454_455insGAGGAAACG). Therefore, the gene product would be different from the wild type strain (Fig. 5C). Instead of expressing YusO, the M9015 mutant might produce two (non-functional) truncated proteins from this gene, dubbed YusO-m1 and YusO-m2. In YusO-m1, the frame shift would result in a premature stop p.A67D fsX10. There is an alternate initiation site just past the

single base pair insertion in *yusO*, which might initiate the expression of YusO-m2. The nine base pair insertion near the 3' end of *yusO* would lead to a three amino acids duplication near the C-terminus of YusO-m2 (p.G153_G155dup). However, whether YusO-m1 and/or YusO-m2 proteins are stably expressed in M9015 remains to be determined. Hence, it is not unlikely that mutation of *yusO* might contribute to HA resistance. However, it has been reported that mutation of YusO did not confer resistance to rifampin [33], which is not in line with our results that M9015 is resistant to rifampin. This suggests that the other mutations in M9015 might also contribute to its resistance.

The *flgL* gene expresses FlgL, a flagellar hook-filament junction protein, which has a function in motility and chemotaxis [34]. It had a one base pair deletion in M9015 cells, resulting in a truncated FlgL protein (p.K35SfsX9, FlgL-m1, Fig. 5D). Potentially, a second FlgL protein, FlgL-m2 starting from Met47 of FlgL was produced in M9015 cells as well (Fig. 5D). It has been suggested that disruption of this gene may lead to reduced motility, which might contribute to the translucent appearance of M9015 colonies as well.

HA may have multiple targets and only generate pores on the membrane at high concentration

Interestingly, none of the mutated genes we identified are involved in the pathways of cell membrane synthesis or cell wall synthesis. Instead, slow-growth (*atpE*),

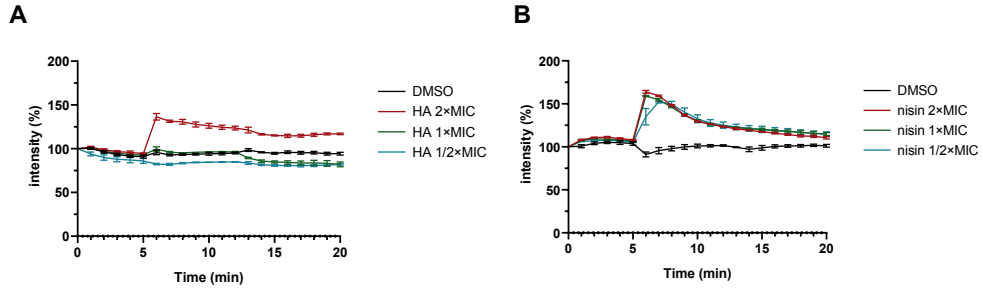

Fig. 6. HA affects cell depolarization only at high concentration. *B. subtilis* membrane potential levels were quantified as in Figure 1F and G. Different concentrations of HA (A) or nisin (B) were added after 5 min. DMSO was used as control. The fluorescence was depicted as percentage of the value at the start (t = 0min) (y-axis) over time (x-axis, min). The mean from biological triplicates was plotted with error bars representing the SEM.

slow-movement (*flgL*), pumping out antimicrobials (*yusO*) and RNA hydrolysis issues (*ymaB*) may individually or collectively lead to HA resistance. Nevertheless, we observed effects of HA on the cell envelope (Fig. 1F, G). We hypothesized that HA might have multiple targets including a target in the membrane. This effect is in a way reminiscent of triclosan, which is a multi-target antimicrobial that has specific targets in the membrane only at high concentrations [35]. To investigate this hypothesis, we performed depolarization assays with different concentrations of HA. The results showed that HA did not affect cell membrane at 0.5 × MIC or 1 x MIC (Fig. 6A). Only at 2 x MIC of HA, effects on the cell membrane were observed. Nisin treatment on the other hand showed effects on membrane polarization at all concentrations tested, even at 0.5 x MIC (Fig. 6B). These results suggest that HA is a multi-target antimicrobial and that the cell membrane was targeted at higher concentrations of HA.

DISCUSSION

Here, we describe the antimicrobial property of HA. The minimum concentration of HA to inhibit *B. subtilis* growth overnight was 50 μg/mL, which was around 4 to 5 times less than the IC_{50} of human cells (Fig. 1A, B). This suggested HA not to be very toxic. Treatment of bacteria with HA at concentrations below 50 μg/mL led to rapid arrest of bacterial growth and even lysis of the cells (a reduction in OD_{600}). Interestingly, following treatment with 30 or 40 μg/mL HA, bacterial growth recovered 3 to 9 hours after the start of treatment, respectively (Fig. 1B). The mechanism underlying recovery of the bacterial growth following treatment with HA below 50 μg/mL remains to be determined. The cells showed delayed but similar growth kinetics to control samples. HA may be degraded by the few live cells, or HA may be exhausted or quenched by the bacterial cells. The remaining live cells appear not to be affected by the previous presence of HA in the medium and are now able to grow freely again at the same growth rate as untreated cells.

HA was suggested to be a multi-target antimicrobial agent that generates pores in the cell membrane at high concentrations. Some antimicrobials affect membrane integrity without direct targeting of the membrane. For instance, gentamycin exclusively targets ribosomes, which results in misfolded membrane proteins. Eventually, this will lead to membrane defects [36,37]. However, the pore formation by HA is unlikely caused by such indirect mechanisms, because higher concentrations (i.e. 2 × MIC) of HA induced cell depolarization immediately after the addition of this compound (Fig. 1F, 6A). Since HA did not bind to any of the

provided lipids in our study (Table S2), the mechanism of the pore formation is still unclear. To further study the mechanism, other approaches, e.g. molecular dynamics simulations to model pore formation in lipid bilayers [38,39], might provide insight into the underlying mechanism.

To further study the MoA of HA, we selected a low-level HA-resistant strain, *B. subtilis* strain M9015, by continuous exposure to HA. The colonies of the M9015 mutant were more translucent than the wild type. We examined this phenotype in relation to HA-resistance. In the comparison of the growth patterns and cell size between mutant and wild type, we found that the size of M9015 cells was smaller. Smaller cell size might contribute to the translucent appearance of colonies, because the colonies will be thinner when the cells are smaller. The observed apparent reduction in growth might also be caused by reduced cell size, because the same number of bacterial cells will have a lower OD_{600} when the cells are smaller. Comparison of the components of cell wall by peptidoglycan analysis indicated that there was only one peak with a subtle difference between WT and mutant (arrow in Fig. 3). However, the connection between the difference in cell wall, the smaller cell size and HA-resistance remains to be determined.

Finally, we sequenced the genomes of the M9015 mutant and wild type cells, resulting in the discovery of four mutated genes. None of these genes has a direct effect on the cell envelope. However, this may give an indication of the targets of HA at lower concentrations. The mutations of *flgL* and *atpE* seem to contribute to reduced cell mobility and cell size, respectively, which may contribute to a reduced growth rate. It is noteworthy that it was reported previously that slow growth actually conferred non-heritable antibiotic resistance in *Salmonella enterica* [40]. The mutation of *yusO* may confer resistance to some extent, because *yusO* has been implicated in antimicrobial resistance before [33]. Yet, it has been reported that *yusO* is not involved in rifampin resistance [33], whereas we found that the HA-resistant strain M9015 had cross resistance to rifampin. Therefore, it is more likely that other mutation(s) contribute(s) to HA resistance. The fourth gene that was found to be mutated in M9015 cells was *ymaB*, which might also be involved in the resistance. The *ymaB* gene is involved in RNA metabolism [31], and mutation of this gene might contribute to the observed rifampin-resistance of M9015 cells. Further study of these four genes for instance by targeted inactivation of each gene separately and/or in combinations may provide more insight into the role of these genes in antimicrobial resistance. Alternatively, it would be interesting to rescue these genes in the mutant individually and exclude the genes that do not contribute to antimicrobial resistance. We have attempted to rescue the mutated genes in the M9015 strain several times

but the cloning failed. This might due to the gene *flgL*, which was reported to be a component of ComK regulon [41]. ComK is the competence master regulator of *B. subtilis* [42], and defective ComK function might affect the ability to make these bacteria competent. Hence, the alternate approach to inactivate each of the four genes individually and/ or in combination might help to further unravel the mechanism of action of HA.

To conclude, our results suggest HA to be a multi-target antimicrobial agent against Gram-positive bacteria. It targeted the cell membrane, but only at high concentrations. We have developed a HA-resistant strain, M9015, and discovered that mutant colonies had a more translucent appearance than wild type, which may be due to reduced cell size. The M9015 strain showed cross resistance to rifampin. However, it remains to be determined whether HA also belongs to the RNA class of antimicrobials. M9015 harbors five mutations in the coding region of four distinct genes. Further analysis of these genes might provide more insight into the MoA of HA at low concentrations.

ACKNOWLEDGEMENTS

The authors would like to thank Anko de Graaff of the Hubrecht Imaging Centre for help with imaging, Ad Fluit of the Medical Microbiology department of UMC Utrecht for clinical bacterial isolates, Eefjan Breukink (Utrecht University) for Lipid II and derivatives, Ronnie Lubbers for critical reading of the manuscript and Marieke Kuijk for help with antimicrobial activity test. This project was supported by the Chinese Scholarship Council (CSC).

REFERENCES

[1] Robak H. Investigations regarding fungi on Norwegian ground wood pulp and fungal infection at wood pulp mills. Nyt Mag Naturvidenskaberne 1932;71.

[2] Roose-Amsaleg C, Brygoo Y, Harry M. Ascomycete diversity in soil-feeding termite nests and soils from a tropical rainforest. Environ Microbiol 2004;6:462–9. https://doi.org/10.1111/j.1462-2920.2004.00579.x.

[3] Barron GL. New Species and New Records of Oidiodendron. Can J Bot 1962;40:589–607. https://doi.org/10.1139/b62-055.

[4] Morrall RAA. Two new species of Oidiodendron from boreal forest soils . Can J Bot 1968;46:203–6. https://doi.org/10.1139/b68-034.

[5] Calduch M, Gené J, Cano J, Stchigel AM, Guarro J. Three new species of Oidiodendron Robak from Spain. vol. 50. 2004.

[6] Rice A V., Currah RS. Oidiodendron: A survey of the named species and related anamorphs of Myxotrichum. Stud Mycol 2005;53:83–120. https://doi.org/10.3114/sim.53.1.83.

[7] COUTURE M, FORTIN JA, DALPE Y. Oidiodendron Griseum Robak: an Endophyte of Ericoid Mycorrhiza in Vaccinium Spp. New Phytol 1983;95:375–80. https://doi.org/10.1111/j.1469-8137.1983.tb03505.x.

[8] Martino E, Perotto S, Parsons R, Gadd GM. Solubilization of insoluble inorganic zinc compounds by ericoid mycorrhizal fungi derived from heavy metal polluted sites. vol. 35. 2003. https://doi.org/10.1016/S0038-0717(02)00247-X.

[9] De Tommaso G, Salvatore MM, Nicoletti R, DellaGreca M, Vinale F, Bottiglieri A, et al. Bivalent metal-chelating properties of harzianic acid produced by Trichoderma pleuroticola associated to the gastropod Melarhaphe neritoides. Molecules 2020;25. https://doi.org/10.3390/molecules25092147.

[10] Bennett JW, Bentley R. What's in a Name?-Microbial Secondary Metabolism. Adv Appl Microbiol 1989;34:1–28. https://doi.org/10.1016/S0065-2164(08)70316-2.

[11] Vinale F, Manganiello G, Nigro M, Mazzei P, Piccolo A, Pascale A, et al. A novel fungal metabolite with beneficial properties for agricultural applications. Molecules 2014;19:9760–72. https://doi.org/10.3390/molecules19079760.

[12] Keller NP. Fungal secondary metabolism: regulation, function and drug discovery. Nat Rev Microbiol 2019;17:167–80. https://doi.org/10.1038/s41579-018-0121-1.

[13] Hambleton S, Egger KN, Currah RS. The genus Oidiodendron : species delimitation and phylogenetic relationships based on nuclear ribosomal DNA analysis . Mycologia 1998;90:854–68. https://doi.org/10.1080/00275514.1998.12026979.

[14] Sawa R, Mori Y, Iinuma H, Naganawa H, Hamada M, Yoshida S, et al. Harzianic acid, a new antimicrobial antibiotic from a fungus. J Antibiot (Tokyo) 1994;47:731–2. https://doi.org/10.7164/antibiotics.47.731.

[15] Vinale F, Flematti G, Sivasithamparam K, Lorito M, Marra R, Skelton BW, et al. Harzianic acid, an antifungal and plant growth promoting metabolite from Trichoderma harzianum. J Nat Prod 2009;72:2032–5. https://doi.org/10.1021/np900548p.

[16] Kunst F, Ogasawara N, Moszer I, Albertini AM, Alloni G, Azevedo V, et al. The complete genome sequence of the gram-positive bacterium Bacillus subtilis. Nature 1997;390:249–56. https://doi.

org/10.1038/36786.

[17] Zgoda JR, Porter JR. A convenient microdilution method for screening natural products against bacteria and fungi. Pharm Biol 2001;39:221–5. https://doi.org/10.1076/phbi.39.3.221.5934.

[18] Müller A, Wenzel M, Strahl H, Grein F, Saaki TNV, Kohl B, et al. Daptomycin inhibits cell envelope synthesis by interfering with fluid membrane microdomains. Proc Natl Acad Sci U S A 2016;113:E7077–86. https://doi.org/10.1073/pnas.1611173113.

[19] Schindelin J, Arganda-Carreras I, Frise E, Kaynig V, Longair M, Pietzsch T, et al. Fiji: An open-source platform for biological-image analysis. Nat Methods 2012;9:676–82. https://doi.org/10.1038/nmeth.2019.

[20] Lamsa A, Liu WT, Dorrestein PC, Pogliano K. The Bacillus subtilis cannibalism toxin SDP collapses the proton motive force and induces autolysis. Mol Microbiol 2012;84:486–500. https://doi.org/10.1111/j.1365-2958.2012.08038.x.

[21] Chen JL, Steele TWJ, Stuckey DC. Modeling and Application of a Rapid Fluorescence-Based Assay for Biotoxicity in Anaerobic Digestion. Environ Sci Technol 2015;49:13463–71. https://doi.org/10.1021/acs.est.5b03050.

[22] Kepplinger B, Morton-Laing S, Seistrup KH, Marrs ECL, Hopkins AP, Perry JD, et al. Mode of Action and Heterologous Expression of the Natural Product Antibiotic Vancoresmycin. ACS Chem Biol 2018;13:207–14. https://doi.org/10.1021/acschembio.7b00733.

[23] Thakur S, Cattoni DI, Nöllmann M. The fluorescence properties and binding mechanism of SYTOX green, a bright, low photo-damage DNA intercalating agent. Eur Biophys J 2015;44:337–48. https://doi.org/10.1007/s00249-015-1027-8.

[24] Kleijn LHJ, Oppedijk SF, T Hart P, Van Harten RM, Martin-Visscher LA, Kemmink J, et al. Total Synthesis of Laspartomycin C and Characterization of Its Antibacterial Mechanism of Action. J Med Chem 2016;59:3569–74. https://doi.org/10.1021/acs.jmedchem.6b00219.

[25] van der Beek SL, Le Breton Y, Ferenbach AT, Chapman RN, van Aalten DMF, Navratilova I, et al. GacA is essential for Group A Streptococcus and defines a new class of monomeric dTDP-4-dehydrorhamnose reductases (RmlD). Mol Microbiol 2015;98:946–62. https://doi.org/10.1111/mmi.13169.

[26] Schaub R, Dillard J. Digestion of Peptidoglycan and Analysis of Soluble Fragments. Bio-Protocol 2017;7. https://doi.org/10.21769/bioprotoc.2438.

[27] Smith TJ, Foster SJ. Characterization of the involvement of two compensatory autolysins in mother cell lysis during sporulation of Bacillus subtilis 168. vol. 177. 1995. https://doi.org/10.1128/jb.177.13.3855-3862.1995.

[28] Kasianowicz J, Benz R, McLaughlin S. The kinetic mechanism by which CCCP (carbonyl cyanide m-Chlorophenylhydrazone) transports protons across membranes. J Membr Biol 1984;82:179–90. https://doi.org/10.1007/BF01868942.

[29] Prince A, Sandhu P, Kumar P, Dash E, Sharma S, Arakha M, et al. Lipid-II Independent Antimicrobial Mechanism of Nisin Depends on Its Crowding and Degree of Oligomerization. Sci Rep 2016;6:1–15. https://doi.org/10.1038/srep37908.

[30] Boger DL. Vancomycin, teicoplanin, and ramoplanin: Synthetic and mechanistic studies. Med Res Rev 2001;21:356–81. https://doi.org/10.1002/med.1014.

[31] Frindert J, Kahloon MA, Zhang Y, Ahmed YL, Sinning I, Jäschke A. YvcI from Bacillus subtilis has in vitro RNA pyrophosphohydrolase activity. J Biol Chem 2019;294:19967–77. https://doi.

org/10.1074/jbc.RA119.011485.

[32] Walker JE. The ATP synthase: The understood, the uncertain and the unknown. Biochem Soc Trans 2013;41:1–16. https://doi.org/10.1042/BST20110773.

[33] Kim JY, Inaoka T, Hirooka K, Matsuoka H, Murata M, Ohki R, et al. Identification and characterization of a novel multidrug resistance operon, mdtRP (yusOP), of Bacillus subtilis. J Bacteriol 2009;191:3273–81. https://doi.org/10.1128/JB.00151-09.

[34] Chan JM, Guttenplan SB, Kearns DB. Defects in the flagellar motor increase synthesis of poly-γ-glutamate in bacillus subtilis. J Bacteriol 2014;196:740–53. https://doi.org/10.1128/JB.01217-13.

[35] Russell AD. Whither triclosan? J Antimicrob Chemother 2004;53:693–5. https://doi.org/10.1093/jac/dkh171.

[36] Kohanski MA, Dwyer DJ, Wierzbowski J, Cottarel G, Collins JJ. Mistranslation of Membrane Proteins and Two-Component System Activation Trigger Antibiotic-Mediated Cell Death. Cell 2008;135:679–90. https://doi.org/10.1016/j.cell.2008.09.038.

[37] Davis BD, Chen L, Tai PC. Misread protein creates membrane channels: An essential step in the bactericidal action of aminoglycosides. Proc Natl Acad Sci U S A 1986;83:6164–8. https://doi.org/10.1073/pnas.83.16.6164.

[38] Tieleman DP, Leontiadou H, Mark AE, Marrink SJ. Simulation of pore formation in lipid bilayers by mechanical stress and electric fields. J Am Chem Soc 2003;125:6382–3. https://doi.org/10.1021/ja029504i.

[39] Tilley SJ, Saibil HR. The mechanism of pore formation by bacterial toxins. Curr Opin Struct Biol 2006;16:230–6. https://doi.org/10.1016/j.sbi.2006.03.008.

[40] Pontes MH, Groisman EA. Slow growth determines nonheritable antibiotic resistance in Salmonella enterica. Sci Signal 2019;12:3938. https://doi.org/10.1126/scisignal.aax3938.

[41] Berka RM, Hahn J, Albano M, Draskovic I, Persuh M, Cui X, et al. Microarray analysis of the Bacillus subtilis K-state: Genome-wide expression changes dependent on ComK. vol. 43. John Wiley & Sons, Ltd; 2002. https://doi.org/10.1046/j.1365-2958.2002.02833.x.

[42] Susanna KA, Fusetti F, Thunnissen AMWH, Hamoen LW, Kuipers OP. Functional analysis of the competence transcription factor ComK of Bacillus subtilis by characterization of truncation variants. Microbiology 2006;152:473–83. https://doi.org/10.1099/mic.0.28357-0.

SUPPORTING INFORMATION

Table S1. HA MIC on pathogenic bacteria. MICs of HA on different pathogenic bacteria were tested starting at a 400 μg/mL which was then serially diluted with a factor 2. a = Gift from University Medical Center Utrecht; b = ATCC strains.

Strain	Gram	MIC (μg/mL)
Acinetobacter baumannii 1179 [a]	-	> 400
Acinetobacter nosocomialis 14-8211 [a]	-	> 400
Enterobacter cloacae complex MC04842 [a]	-	> 400
Escherichia coli TEM-3 GVJS004 [a]	-	> 400
Klebsiella pneumoniae SHV-18 GVJS006 [a]	-	> 400
Pseudomonas aeruginosa ATCC57853 [b]	-	> 400
Stenotrophomonas maltophilia GV20A226 [a]	-	> 400
Enterococcus faecium VRE GV16D030 [a]	+	100
Enterococcus faecium GV15A623 [a]	+	50
Listeria monocytogenes GV21-4a [a]	+	25
Staphylococcus aureus MSSA 476 GVS0101 [a]	+	50
Staphylococcus aureus MRSA USA300 GVS1474 [a]	+	200
Staphylococcus epidermidis GV08A1071 [a]	+	50
Streptococcus pneumoniae 05A396 [a]	+	25

Table S2. Exogenous Lipid II and its precursors did not affect HA antimicrobial activity. Vancomycin, nisin and HA have an antimicrobial effect on *B. subtilis*. Quenching of this antimicrobial effect was tested by addition of exogenous Lipid II and precursors (10 μM for nisin and vancomycin and either 10 μM or 150 μM for HA; results of both lipid concentrations on antimicrobial effect of HA were similar) prior to the addition of indicated antimicrobials at 1 × or 2 × their MIC as indicated. Bacterial growth was assessed and the assay scored as unaffected (-) or affected (+) by the addition of exogenous lipid.

Antagonist	Vancomycin (2 × MIC)	Nisin (2 × MIC)	HA (2 × MIC)	HA (1 × MIC)
Blank	-	-	-	-
Lipid I	+	+	-	-
Lipid II	+	+	-	-
C55-P	-	+	-	-

Table S3. *B. subtilis* strain M9015 harbors five mutations in four genes. Bioinformatic analysis of the genome sequences of *B. subtilis* strain 168 and M9015 results in 10 possible mutations, five of which are reliable. The position of the mutations is indicated and is based on the reference genome NC_000964.3. The mutations were visualized using Integrated Genomics Viewer and the gene names of the verified reliable mutations are indicated.

# Mutation	Position	WT	M9015	Reliable?	Mutated gene
1	353056	AAGCAGCTGATC GAGCAGCTGA	AAGCAGCTGA	No	/
2	1872540	T	C	Yes	*ymaB*
3	2152047	A	C	No	/
4	2480653	CT	C	No	/
5	2480666	GT	G	No	/
6	2581726	GTTTTTT	GTTTTTTT	No	/
7	3374690	G	GA	Yes	*yusO*
8	3374945	AGAGGAAACGGA	AGAGGAAACGGAGGAAACGGA	Yes	*yusO*
9	3638128	ATTTTTTTT	ATTTTTTT	Yes	*flgL*
10	3786681	G	A	Yes	*atpE*

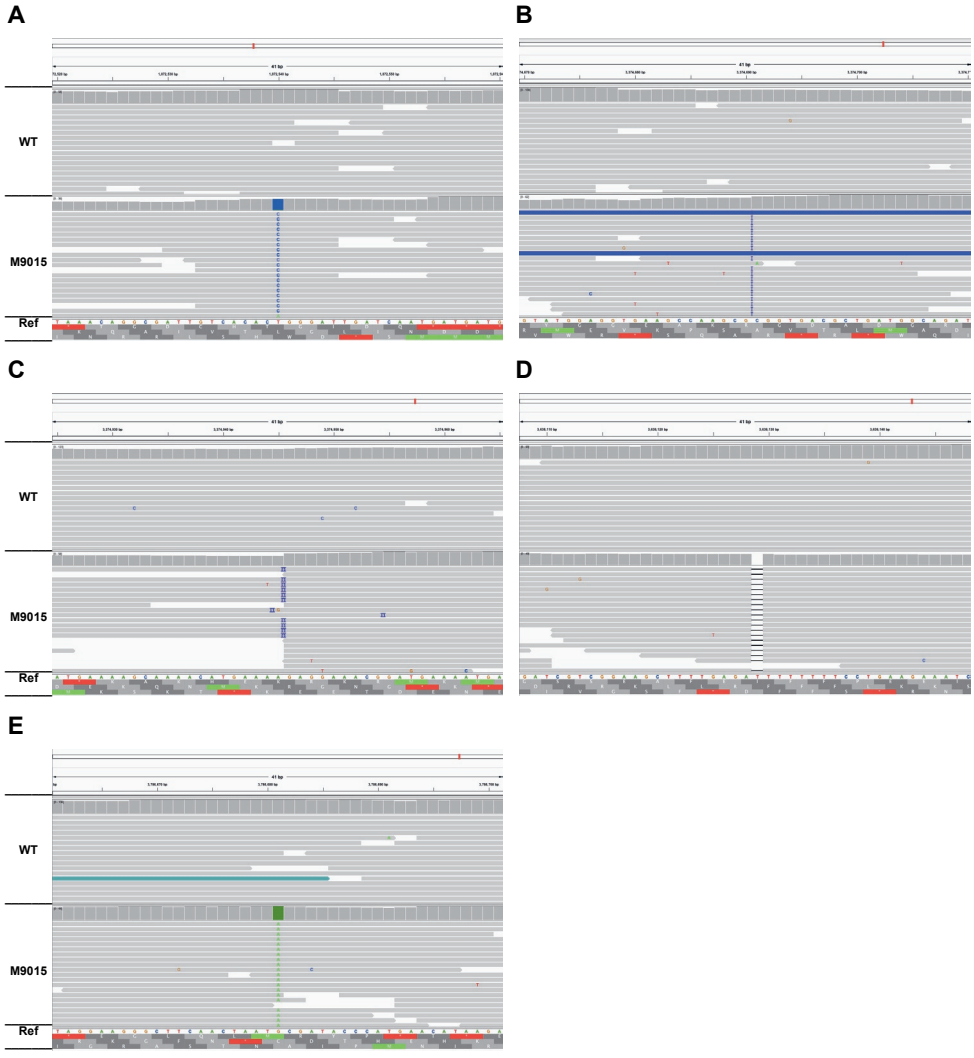

Fig. S1. Viewing gene variations with Integrated Genomics Viewer (I). 10 predicted mutated sites were verified using Integrated Genomics Viewer. Five correctly predicted mutations (Mutation#2, #7-#10) (see Table 2) were listed in (A) to (E). "Ref" indicated the reference genome. Representative reads (around 15) were presented for both WT and M9015.

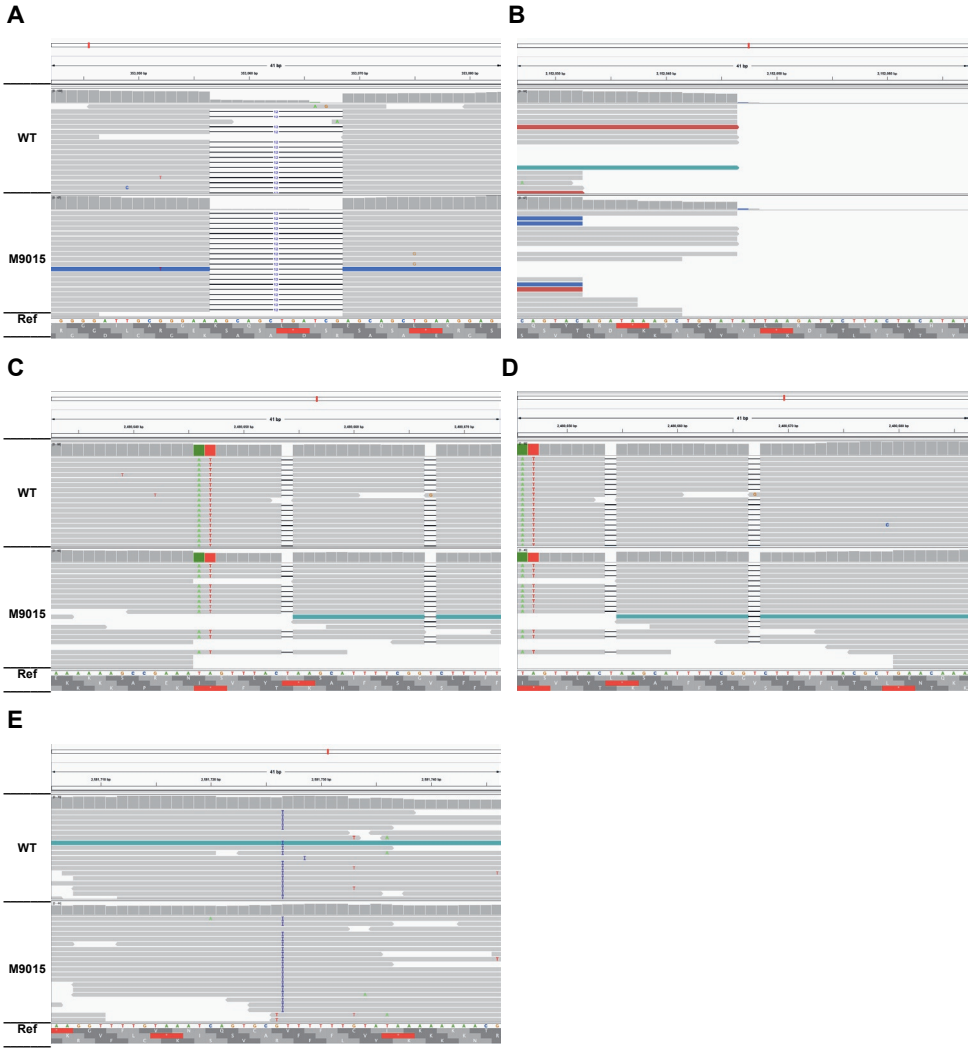

Fig. S2. Viewing gene variations with Integrated Genomics Viewer (II). 10 predicted mutated sites were verified using Integrated Genomics Viewer. Five wrongly predicted mutations (Mutation#1, #3-#6) (see Table 2) were listed in (A) to (E). "Ref" indicated the reference genome. Representative reads (around 15) were presented for both WT and M9015.

Summarizing Discussion

CHAPTER 6

Xudong Ouyang[1,2] and Jeroen den Hertog[1,2]

1. Hubrecht Institute-KNAW and University Medical Center Utrecht, Utrecht, the Netherlands
2. Institute Biology Leiden, Leiden University, Leiden, the Netherlands

Revisited insight into the traditional antimicrobial discovery strategy

Despite all the benefits from antimicrobial therapies, we cannot ignore the issue that these therapies have contributed to antimicrobial resistance [1–4]. In **Chapter 1**, we have introduced this issue briefly. The infections by multidrug resistant "superbugs" are causing higher patient mortality and rising costs, resulting in high pressure on healthcare systems around the world [5,6]. To facilitate lifting this issue, our lab was motivated to establish a project on searching for novel antimicrobials, preferably ones with a new mechanism of action (MoA). We have chosen fungal natural products as the source for this purpose, with one of the reasons being the adjacency to the Westerdijk Fungal Biodiversity Institute, which is one of the biggest fungal collection centers in the world. Additionally, natural products have had long and important applications in medical treatments through history [7,8], although pharmaceutical companies have been less interested in natural antimicrobial discovery recently [9]. We want to attract their attention back to the promising field of fungal natural products by exhibiting some encouraging antimicrobial candidates from our screen.

In **Chapter 3**, we have described our antimicrobial discovery strategy in detail. In spite of the popularity of genomics and bioinformatics in biosynthetic gene cluster screening [10], we have still chosen to take advantage of the traditional cultivation-based screening method, because this method is straightforward and provides direct insight into antimicrobial activity, and genome data were not always available particularly for less studied species, which actually have a high chance to produce novel metabolites. After screening for antimicrobial activity of more than 10,000 fungal species on several pathogenic bacteria, including both Gram-positive strains and Gram-negative strains, the positively scored fungi were then ready for further analysis. Among this fungal library, we have found hundreds of hits, including potent antimicrobial hits that inhibit the growth of multiple pathogenic strains and selective antimicrobial hits that only inhibit one of these bacterial strains. However, only approximately 3% of the fungi scored positive. This might due to the resistance of the tested pathogenic bacteria. Another, perhaps more convincing reason might be the low expression level of antimicrobial gene clusters, which might have led to low amount of antimicrobial activity in the fungal supernatant. Low levels of antimicrobial compounds hampered the downstream identification process as well, but we increased the antimicrobial yield for many strains by changing the culture conditions, e.g. using plate culture. Fungi regulate their secondary metabolite production under different conditions [11–13]. Therefore, to establish a

new fungal library by plate extractions, might be a good future plan to explore the hidden sites of the fungal kingdom. Another promising plan might be to start new screens by activating the silent genes regarding secondary metabolite producing by co-culturing with inhibitors, e.g. suberoylanilide hydroxamic acid or anacardic acid. These inhibitors were also proven to generate new metabolite maps in fungi [14,15]. With increasing sequencing data being available in the future, genomics will certainly become powerful tools regarding fungal metabolite discovery. However, the cultivation-based strategies seem to be promising and readily available tools to explore antimicrobials among fungal natural products at the moment.

Next, to identify the antimicrobial activity from the obtained hits, we chose the model organism of Gram-positive bacteria, *Bacillus subtilis*, for the purpose of re-screening with the following reasons: In **Chapter 1**, we have discussed the distinctive structures between Gram-positive and Gram-negative bacteria, which makes Gram-positive strains to be more sensitive to antimicrobial compounds [16,17]. Thus, using a Gram-positive organism as a read-out might reduce the chance to omit potential antimicrobials. Furthermore, with the development of antibiotic adjuvants [18], such as inhibitors of the efflux pump or outer membrane permeabilizers, it might be possible to apply Gram-positive antimicrobials on Gram-negative pathogens in the future. In addition, treatment of infections with Gram-positive multi-resistant pathogens is also a considerable issue to be resolved. In **Chapter 3**, it was revealed that *B. subtilis* was inhibited by more than 80% of the rescreened fungi, suggesting *B. subtilis* is a well-qualified read-out. Notably, instead of testing the supernatant, we only tested the ethyl acetate extractions on *B. subtilis*, because of the inaccurate results from the test with supernatant according to the unstable compound yield of large-scale cultures. Therefore, the remaining 20% of inactive hits might due to the resistance of *B. subtilis*, or to the invalidation of ethyl acetate extraction of these specific active compounds. For the latter problem, we have not established an easy protocol as an appropriate solution yet. The compounds that are not extractable by ethyl acetate, do not rank high on our priority list currently, but rather may be potential candidates for the future.

In the end, we achieved our goal of successful identification of several antimicrobials, including both well-known and poorly-described ones. This suggests that our screening strategy works for antimicrobial discovery and our fungal collection is a promising source for bioactive compounds.

Rapid prediction of antimicrobial MoA

Identification of antimicrobial targets is one of the vital parts in antimicrobial discovery and development. However, the target candidates in bacterial cells are very broad, making this MoA identification process complex and laborious [19,20]. As discussed in **Chapter 2**, there is no universal method intended for all antimicrobials. Direct approaches (target-based screenings) are able to show direct interactions between antimicrobials and their targets, but these processes are time-consuming and require prerequisite hypotheses. Although these are old approaches that were established several decades ago, they are the only commonly used methods that may provide the direct targets and therefore are still in use today. Improvements of these methods are generally along two avenues. One is the combination of the old strategies with the continuously developing high-end techniques and modernize them into fast and high-throughput approaches, e.g. applying next-generation sequencing onto genetic approaches, or developing a non-selective universal labeling ligand in affinity chromatography. The other avenue is to lower the workload by providing appropriate and accurate hypotheses about the pathways of the antimicrobial targets, which are normally generated by indirect approaches, i.e. the phenotype-based screenings. In this manner, it is important to establish rapid and accurate phenotype-based approaches. Because the time spent and cost involved in the omics-approaches is relatively high, we have developed a simple, cost-effective method for the initial stage of target identification, which is an imaging-based strategy, dynamic bacterial cytological profiling (DBCP).

DBCP is similar to cytological profiling of eukaryotic cells and the details were described in **Chapter 4**. It is an imaging strategy to track the morphological changes of fluorescently labeled bacterial cells in response to antimicrobials for 30 to 60 min using time-lapse imaging and quantitative image analysis. Using this strategy, we successfully distinguished 14 known antimicrobial compounds into five main classes: DNA, RNA, protein, cell membrane and cell wall. The concept of DBCP was established on the basis of bacterial cytological profiling (BCP), a static imaging strategy which has been applied to classify antimicrobials against Gram-negative bacteria since 2013 [21]. We successfully used DBCP on Gram-positive bacteria. In comparison, DBCP provides more information than BCP without extra elaborate preparation. DBCP allows recording of the direct response from single cells to specific antimicrobial agents over time. Hence the differences between treated and untreated are compared from the same cell, which minimizes the chance to compare differences because of changing circumstances. DBCP also provides the first indication of the

timepoints when a certain antimicrobial starts to have effects, cell growth starts to be inhibited and cells are killed. These are also important parameters that distinguish antimicrobial MoA.

To facilitate DBCP, we developed a bacterial time-lapse imaging protocol, which is based on a previously described technique [22]. We included several improvements in the imaging technique that we developed. Our imaging technique is less time-consuming and drugs do not have to be pre-added to bacteria. Our syringe-made agarose pad is robust and can be used within 10 min from preparation. Drugs for experiments may be added to the agarose pad during preparation, or to the top well of the agarose pad at any stage of the imaging process. This proved to be important for time-lapse imaging of drug-treatment of bacteria, because it allowed us to image bacteria before treatment, establish normal growth and then image bacteria during drug treatment. With these improvements, DBCP may be used to rapidly distinguish the MoA class and subclass even without prior knowledge of the antimicrobial. In addition, this time-lapse imaging protocol may also be a promising tool for other studies like antibiotic combination, protein interaction or gene function.

Compared to the omics approaches, DBCP provides reliable MoA information, but with a less tedious workflow and lower amount of compound required. But it also has limitations. This imaging-based strategy results in the 'most similar' signatures, and thereby has an intrinsic danger of false positive matches. Therefore, subsequent validation experiments are fundamental to this approach. Nevertheless, considering the ease of accessibility and the affordability, DBCP is an excellent approach for the initial stage of MoA identification.

Two poorly-described antimicrobials with interesting MoAs

In addition to a range of well-known antimicrobials, two interesting antimicrobials were successfully identified in our screen, which are berkchaetoazaphilone B (BAB, from *Pleurostomophora richardsiae*) and harzianic acid (HA, from *Oidiodendron flavum*). Since there were not much data available regarding their antimicrobial activities yet, we investigated their antimicrobial MoAs as described in this thesis.

The compound structure and MoA identification of BAB was described in **Chapter 3**. BAB was previously identified in 2015 as an anti-cancer agent [23]. However, no following data was available regarding its activities. Our study showed that it also had strong anti-bacterial activity against Gram-positive bacteria including a methicillin-resistant S*taphylococcus aureus* (MRSA). To determine its MoA, we chose several strategies. Initially, we applied a phenotype-based approach, DBCP,

and it suggested BAB not to be classified into one of the five main classes, because it had non-cell-envelope effects but without inducing abnormal nucleoid length: cell length ratio. Next, we performed a series of bioactivity assays and a genetic screening. Screening of the Nebraska Transposon Mutant Library (NTML) led to the identification of 16 candidate genes that may be involved in the antimicrobial activity of BAB. 10 of these genes have a role in metabolism, suggesting that BAB affects energy metabolism in *B. subtilis*. Furthermore, a cell metabolism assay suggested that BAB inhibited mitochondrial metabolism completely in HepG2 cells. BAB caused a rapid burst of glycolysis, which ran out quickly, which indicates that BAB has a role in energy metabolism in eukaryotic cells as well. Future work should focus on target identification using genetic approaches or affinity approaches. Although the cytotoxicity of BAB on human cells precludes its potential to be a clinical antibiotic, it is still interesting to study its targets because it might provide some new targets for novel antibiotic discovery.

The identification of another interesting antimicrobial, HA, was described in **Chapter 4**, together with a rapid prediction of its MoA by DBCP. A more detailed description of its MoA identification procedure was given in **Chapter 5**. HA was first isolated as a novel antimicrobial agent from a fungal strain *Trichoderma harzianum* in 1994 [24]. But surprisingly, subsequent research describes HA as a plant promotor rather than an antimicrobial [25,26]. Recently, one study has described its antibacterial activity against *Staphylococcus pseudintermedius*, but without any detail about its targets [27]. Therefore, we have tried to elaborate HA's MoA in this thesis with a combination of several MoA identification strategies. First, to generate an accurate hypothesis, we applied DBCP and predicted HA to target the cell envelope (**Chapter 4**). Next in **Chapter 5**, with several membrane measurements and developing a resistant mutant, we confirmed this prediction. In addition, we unraveled that HA only targets the cell envelope at high concentration (at least 2-fold minimum inhibitory concentration, MIC). Our results also suggested that the membrane pore formation mechanism was not due to binding certain lipids, making it interesting for further study. Although the mechanism of HA was revealed in more detail, the affected pathway(s) at low concentration remain(s) unclear. The HA-resistant strain, *B. subtilis* M9015, showed cross resistance to rifampin, which might suggest that the RNA synthesis pathway is relevant for HA's MoA. However, this will require more work to elucidate the function of the mutated genes in *B. subtilis* M9015, for instance by directed inactivation of each of these genes as described in the future plans of **Chapter 5**. Overall, HA seems to be an interesting and promising

antimicrobial candidate that might have new targets, and therefore is interesting for further analysis.

Conclusion and future perspectives

Overall in this thesis, we have described a cultivation-based strategy for novel antimicrobial screen in fungi and an imaging-based strategy for antimicrobial MoA identification. Furthermore, we have also elaborated the compound structure and MoA identification of two example antimicrobial agents revealed in our screen. One of them, BAB, was found to affect energy metabolism, whereas another one, HA, was determined as a multi-target antimicrobial agent.

There will undoubtedly be more antimicrobial agents produced by fungi in our library that we did not cover. In addition, there are many options to modify the screen and/or the fungal library. In case a new compound is discovered, it might be classified within one hour based on its MoA using the MoA identification strategy, DBCP, that we developed. DBCP is rapid, accurate and is easy-accessible for most microbiology labs. Taken together, the combination of a collection of natural compounds (mixtures) and DBCP is a highly promising strategy for antimicrobial compound discovery.

REFERENCES

[1] Dcosta VM, King CE, Kalan L, Morar M, Sung WWL, Schwarz C, et al. Antibiotic resistance is ancient. Nature 2011;477:457–61. https://doi.org/10.1038/nature10388.

[2] Ling LL, Schneider T, Peoples AJ, Spoering AL, Engels I, Conlon BP, et al. A new antibiotic kills pathogens without detectable resistance. Nature 2015;517:455–9. https://doi.org/10.1038/nature14098.

[3] Park AJ, Krieger JR, Khursigara CM. Survival proteomes: The emerging proteotype of antimicrobial resistance. FEMS Microbiol Rev 2016;40:323–42. https://doi.org/10.1093/femsre/fuv051.

[4] Holmes AH, Moore LSP, Sundsfjord A, Steinbakk M, Regmi S, Karkey A, et al. Understanding the mechanisms and drivers of antimicrobial resistance. Lancet 2016;387:176–87. https://doi.org/10.1016/S0140-6736(15)00473-0.

[5] Gelband H, Miller-Petrie M, Pant S, Gandra S, Levinson J, Barter D, et al. The state of the world's antibiotics 2015. Wound Heal South Africa 2015;8:30–4.

[6] Butler MS, Buss AD. Natural products - The future scaffolds for novel antibiotics? Biochem Pharmacol 2006;71:919–29. https://doi.org/10.1016/j.bcp.2005.10.012.

[7] Nishimura S, Matsumori N. Chemical diversity and mode of action of natural products targeting lipids in the eukaryotic cell membrane. Nat Prod Rep 2020;37:677–702. https://doi.org/10.1039/c9np00059c.

[8] Harvey AL, Edrada-Ebel R, Quinn RJ. The re-emergence of natural products for drug discovery in the genomics era. Nat Rev Drug Discov 2015;14:111–29. https://doi.org/10.1038/nrd4510.

[9] Wright GD. Opportunities for natural products in 21st century antibiotic discovery. Nat Prod Rep 2017;34:694–701. https://doi.org/10.1039/c7np00019g.

[10] Kück U, Bloemendal S, Teichert I. Putting Fungi to Work: Harvesting a Cornucopia of Drugs, Toxins, and Antibiotics. PLoS Pathog 2014;10:3–6. https://doi.org/10.1371/journal.ppat.1003950.

[11] Yogabaanu U, Weber JFF, Convey P, Rizman-Idid M, Alias SA. Antimicrobial properties and the influence of temperature on secondary metabolite production in cold environment soil fungi. Polar Sci 2017;14:60–7. https://doi.org/10.1016/j.polar.2017.09.005.

[12] Shang Z, Li XM, Li CS, Wang BG. Diverse secondary metabolites produced by marine-derived fungus nigrospora sp. MA75 on various culture media. Chem Biodivers 2012;9:1338–48. https://doi.org/10.1002/cbdv.201100216.

[13] Félix C, Salvatore MM, DellaGreca M, Ferreira V, Duarte AS, Salvatore F, et al. Secondary metabolites produced by grapevine strains of Lasiodiplodia theobromae grown at two different temperatures. Mycologia 2019;111:466–76. https://doi.org/10.1080/00275514.2019.1600342.

[14] Chung YM, El-Shazly M, Chuang DW, Hwang TL, Asai T, Oshima Y, et al. Suberoylanilide hydroxamic acid, a histone deacetylase inhibitor, induces the production of anti-inflammatory cyclodepsipeptides from Beauveria felina. J Nat Prod 2013;76:1260–6. https://doi.org/10.1021/np400143j.

[15] Mafezoli J, Xu Y ming, Hilário F, Freidhof B, Espinosa-Artiles P, dos Santos LC, et al. Modulation of polyketide biosynthetic pathway of the endophytic fungus, Anteaglonium sp. FL0768, by copper (II) and anacardic acid. Phytochem Lett 2018;28:157–63. https://doi.org/10.1016/j.

phytol.2018.10.011.

[16] Exner M, Bhattacharya S, Christiansen B, Gebel J, Goroncy-Bermes P, Hartemann P, et al. Antibiotic resistance: What is so special about multidrug-resistant Gram-negative bacteria? GMS Hyg Infect Control 2017;12:Doc05. https://doi.org/10.3205/dgkh000290.

[17] Miller SI. Antibiotic resistance and regulation of the Gram-negative bacterial outer membrane barrier by host innate immune molecules. MBio 2016;7. https://doi.org/10.1128/mBio.01541-16.

[18] Breijyeh Z, Jubeh B, Karaman R. Resistance of gram-negative bacteria to current antibacterial agents and approaches to resolve it. Molecules 2020;25. https://doi.org/10.3390/molecules25061340.

[19] Schenone M, Dančík V, Wagner BK, Clemons PA. Target identification and mechanism of action in chemical biology and drug discovery. Nat Chem Biol 2013;9:232–40. https://doi.org/10.1038/nchembio.1199.

[20] Muroi M, Futamura Y, Osada H. Integrated profiling methods for identifying the targets of bioactive compounds: MorphoBase and ChemProteoBase. Nat Prod Rep 2016;33:621–5. https://doi.org/10.1039/c5np00106d.

[21] Nonejuie P, Burkart M, Pogliano K, Pogliano J. Bacterial cytological profiling rapidly identifies the cellular pathways targeted by antibacterial molecules. Proc Natl Acad Sci U S A 2013;110:16169–74. https://doi.org/10.1073/pnas.1311066110.

[22] de Jong IG, Beilharz K, Kuipers OP, Veening JW. Live cell imaging of Bacillus subtilis and Streptococcus pneumoniae using automated time-lapse microscopy. J Vis Exp 2011:1–6. https://doi.org/10.3791/3145.

[23] Stierle AA, Stierle DB, Girtsman T, Mou TC, Antczak C, Djaballah H. Azaphilones from an Acid Mine Extremophile Strain of a Pleurostomophora sp. J Nat Prod 2015;78:2917–23. https://doi.org/10.1021/acs.jnatprod.5b00519.

[24] Sawa R, Mori Y, Iinuma H, Naganawa H, Hamada M, Yoshida S, et al. Harzianic acid, a new antimicrobial antibiotic from a fungus. J Antibiot (Tokyo) 1994;47:731–2. https://doi.org/10.7164/antibiotics.47.731.

[25] Vinale F, Flematti G, Sivasithamparam K, Lorito M, Marra R, Skelton BW, et al. Harzianic acid, an antifungal and plant growth promoting metabolite from Trichoderma harzianum. J Nat Prod 2009;72:2032–5. https://doi.org/10.1021/np900548p.

[26] Vinale F, Manganiello G, Nigro M, Mazzei P, Piccolo A, Pascale A, et al. A novel fungal metabolite with beneficial properties for agricultural applications. Molecules 2014;19:9760–72. https://doi.org/10.3390/molecules19079760.

[27] De Filippis A, Nocera FP, Tafuri S, Ciani F, Staropoli A, Comite E, et al. Antimicrobial activity of harzianic acid against Staphylococcus pseudintermedius. Nat Prod Res 2020;0:1–6. https://doi.org/10.1080/14786419.2020.1779714.

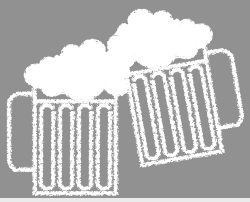

Appendix

SUMMARY

This thesis describes the antimicrobial discovery strategy developed in our group, the den Hertog Group at the Hubrecht Institute. It includes a cultivation-based screening approach for novel antimicrobial agents from the source of fungi, and a bacterial time-lapse imaging approach for antimicrobial mechanism of action (MoA) identification. With this strategy, we have discovered several interesting antimicrobial agents and have demonstrated the detailed antimicrobial property of two of them, berkchaetoazaphilone B (BAB) and harzianic acid (HA).

In **Chapter 1**, we briefly introduce the antimicrobial resistance issue of Gram-positive bacteria. We review information about current status of antimicrobial resistance, which suggests that we have a strong need for novel antimicrobials. Next, we discuss the value of fungal natural products, and their potential for antimicrobial discovery process. We compare the differences between Gram-positive and Gram-negative bacteria, and demonstrate the reasons why we aimed to search for novel antimicrobials against Gram-positive bacteria and why we chose *Bacillus subtilis* as a model for this study. In the end, we provide information on the scope and the outline of this thesis.

In **Chapter 2**, we review the advances in MoA identification strategies that were commonly used over the past 20 years, and provide insight into overcoming this bottleneck step for antimicrobial discovery. We discuss the advantages and disadvantages in both classic and modern approaches. Due to the limitations in almost every single method, the most appropriate strategy has to be selected depending on the expertise of the lab and the properties of the antimicrobial agent.

In **Chapter 3**, we demonstrate the approach that we used to screen fungal natural antimicrobial compounds. We screened for antimicrobial activity using a fungal secondary metabolites library against seven pathogenic bacteria and tried to identify the active compounds using ethyl acetate extraction, HPLC fractionation together with chemical analysis. This approach resulted in 280 antimicrobial hits from 10,207 fungi and the identification of 17 compounds from 26 strains with a re-screening of 56 fungi. The identified metabolites consist of both known antimicrobial compounds as well as relatively unexplored compounds. Among these identified antimicrobials, one compound, BAB is an interesting antimicrobial agent, which was found to affect bacterial energy metabolism.

In **Chapter 4**, we describe a novel antimicrobial MoA identification approach that was developed in our group. This approach is able to rapidly distinguish the effect of anti-Gram-positive bacterial compounds from different classes. To achieve

this, we developed a novel imaging strategy using time-lapse imaging to record dynamic bacterial cytological changes. We improved the imaging protocol to make it simple and functional for bacterial long-term imaging. Using this method, dubbed Dynamic Bacterial Cytological Profiling (DBCP), we observed bacteria over time and established fluorescence intensities qualitatively and quantitatively. It allowed to rapidly distinguish 14 antimicrobials from all of the five main antimicrobial classes. Finally, we used DBCP to establish the MoA of HA, a poorly described secondary metabolite purified from the fungal culture of *Oidiodendron flavum*. We conclude that DBCP is an excellent tool for the first approach of antimicrobial MoA classification.

In **Chapter 5**, we further describe the antimicrobial property of HA on its inhibitory spectrum, MoA and resistance information, discover HA to be a multi-targeting antimicrobial agent against Gram-positive bacteria. It targets the cell membrane, but only at high concentrations. We developed a HA-resistant strain, M9015, and discovered that mutant colonies had a more translucent appearance than wild type, which might be due to reduced cell size. The M9015 strain showed cross resistance to rifampin. However, it remains to be determined whether HA also belongs to the RNA class of antimicrobials. M9015 harbors five mutations in the coding region of four distinct genes. Although further analysis of these genes might still be required to generate more insight into the MoA of HA at low concentrations, the existing data have already revealed the value of HA to be a potential candidate for clinical application.

Finally, we summarize the discussions of this thesis with future perspectives in **Chapter 6**. We have provided a pipeline of antimicrobial discovery with detailed strategies from the upstream of screening fungal natural products to the downstream of MoA identification. This thesis contributes to obtain new insight, valuable for antimicrobial research.

NEDERLANDSE SAMENVATTING

In dit proefschrift wordt de strategie beschreven om antimicrobiële agentia te ontdekken, zoals deze is ontwikkeld in de onderzoeksgroep van den Hertog in het Hubrecht institute. Het omvat een op kweek gebaseerde screeningsbenadering voor nieuwe antimicrobiële moleculen uit schimmels, en een bacteriële time-lapse-beeldvormingsbenadering voor het identificeren van het antimicrobiële werkingsmechanisme. Met behulp van deze twee strategieën, zijn er verschillende interessante antimicrobiële moleculen geïdentificeerd en demonstreren wij de antimicrobiële eigenschappen van berkchaetoazaphilone B (BAB) en harzianic acid (HA).

In **Hoofdstuk 1** geven wij een korte introductie over de antimicrobiële resistentie van grampositieve bacteriën. Hierin wordt de huidige status van antimicrobiële resistentie bekeken en die suggereert dat we een sterke behoefte hebben aan nieuwe antimicrobiële stoffen. Vervolgens beschrijven we de status van natuurproducten van schimmels en hun potentieel voor het ontdekkingsproces van nieuwe antimicrobiële stoffen. Daarnaast vergelijken we de verschillen tussen grampositieve en gramnegatieve bacteriën, en geven we de redenen aan waarom we wilden zoeken naar nieuwe antimicrobiële middelen tegen grampositieve bacteriën en waarom we *Bacillus subtilis* als model voor deze studie kozen. Tenslotte geven we informatie over de reikwijdte en de opzet van dit proefschrift.

In **Hoofdstuk 2** bekijken wij de vooruitgang van werkingsmechanisme identificatie strategieën voor antimicrobiële moleculen die zijn toegepast in de laatste 20 jaar en geven we een overzicht van voordelen en nadelen en bediscussiëren wij de tekortkomingen van deze methodes. Wij suggereren dat de best passende methodes geselecteerd moeten worden op basis van de antimicrobiële eigenschappen van het molecuul.

In **Hoofdstuk 3** beschrijven wij de methodes voor de identificatie van antimicrobiële moleculen uit schimmels. We screenden op antimicrobiële activiteit met behulp van een bibliotheek met secundaire metabolieten van schimmels tegen zeven pathogene bacteriën en probeerden de actieve verbindingen te identificeren met behulp van ethylacetaatextractie, HPLC-fractionering en chemische analyse. Deze aanpak resulteerde in het vinden van 280 antimicrobiële activiteiten onder de 10.207 schimmels en de identificatie van 17 verbindingen uit 26 stammen bij nadere analyse van 56 schimmels. De geïdentificeerde metabolieten bestaan uit zowel bekende antimicrobiële verbindingen als relatief onbekende verbindingen. Van

deze geïdentificeerde antimicrobiële stoffen is een verbinding, BAB, een interessant antimicrobieel middel dat het bacteriële energiemetabolisme blijkt te beïnvloeden.

In **Hoofdstuk 4** beschrijven we een nieuwe antimicrobieel werkingsmechanisme-identificatiemethode die in onze groep is ontwikkeld. Deze benadering is in staat om snel het effect van anti-grampositieve bacteriële verbindingen uit verschillende klassen te onderscheiden. Om dit te bereiken, ontwikkelden we een nieuwe beeldvormingsstrategie met behulp van time-lapse-beeldvorming om dynamische bacteriële cytologische veranderingen vast te leggen. We verbeterden het beeldvormingsprotocol om het eenvoudig en functioneel te maken voor langdurige bacteriële beeldvorming. Met behulp van deze methode, genaamd Dynamic Bacterial Cytological Profiling (DBCP), zijn we in staat om bacteriën in de tijd te observeren en de fluorescentie-intensiteiten kwalitatief en kwantitatief vast te stellen. Het maakt het mogelijk om antimicrobiële stoffen snel te onderscheiden van alle vijf belangrijkste antimicrobiële klassen. Tenslotte gebruiken we DBCP om het antimicrobieel werkingsmechanisme van HA vast te stellen, een secundaire metaboliet, waar weinig van bekend is en die is gezuiverd uit de schimmelcultuur van *Oidiodendron flavum*. Dit bewijst dat DBCP een uitstekend hulpmiddel is voor de eerste benadering van antimicrobieel werkingsmechanisme-classificatie.

In **Hoofdstuk 5** beschrijven we de antimicrobiële eigenschap van HA op het remmende spectrum, antimicrobieel werkingsmechanisme en resistentie-informatie, en dat HA een multi-targeting antimicrobieel middel is tegen grampositieve bacteriën. HA grijpt aan op de celmembraan, maar alleen in hoge concentraties. We hebben een HA-resistente stam, M9015, ontwikkeld en ontdekten dat mutante kolonies een meer doorschijnend uiterlijk hadden dan wildtype, wat te wijten kan zijn aan verminderde celgrootte. De M9015-stam vertoonde kruisresistentie tegen rifampicine. Het moet echter nog vastgesteld worden of HA ook tot de RNA-klasse van antimicrobiële stoffen behoort. M9015 herbergt vijf mutaties in het coderende gebied van vier verschillende genen. Hoewel verdere analyse van deze genen misschien nog nodig is om meer inzicht te krijgen in het antimicrobieel werkingsmechanisme van HA bij lage concentraties, hebben de bestaande gegevens al aangetoond dat HA een potentiële kandidaat is voor klinische toepassing.

Tenslotte vatten we de discussies van dit proefschrift samen met toekomstperspectieven in **Hoofdstuk 6**. We hebben een pijplijn van identificatie van antimicrobiële agentia ontwikkeld met gedetailleerde strategieën variërend van het screenen van natuurlijke schimmelproducten tot de identificatie van antimicrobiële-werkingsmechanisme van verbindingen. Dit proefschrift draagt bij

aan het verkrijgen van nieuwe inzichten, die waardevol zijn voor antimicrobieel onderzoek.

CURRICULUM VITAE

Xudong Ouyang was born on September 18th 1991 in Jinan, China. He grew up in the neighborhood of his hometown. After completing his high school study in Shandong Experimental High School, he received his Bachelor's education of Biotechnology at Shandong Normal University in the years between 2010 to 2014. He received several scholarships from the university during this study and obtained his Bachelor's degree with a thesis on researching the probiotics in fermented Chinese medicine. In the meanwhile, he studied a second major in English and obtained his second Bachelor's degree. Later, he decided to pursue his interest in microbiology and studied for a Master's degree at the State Key Laboratory of Microbial Technology at Shandong University. During this period, he studied the bacteriocins from lactic acid bacteria, which are considered as potential antibiotic alternatives. He gained more interest on antibiotic studies and would like to study further.

In 2017, he completed his Master's study with a thesis and a diploma, received a PhD funding from the Chinese Scholarship Council and moved to the Netherlands for a PhD journey. He worked on his antimicrobial research in the lab of Jeroen den Hertog at the Hubrecht Institute in Utrecht within the Graduate School of Sciences of Leiden University in Leiden. The focus of his PhD was to discover novel antimicrobials and to study their mechanisms of action. The summary of these studies is presented in this thesis.